THE UNIVERSITY OF QUEENSLAND

AUSTRALIA

The Coastal Convective Interactions Experiment

Joshua Stephen Soderholm

BSc (Hons)

A thesis submitted for the degree of Doctor of Philosophy at

The University of Queensland in 2016

School of Geography, Planning and Environmental Management

Abstract

Prediction of convective storm environments relies principally upon the broad-scale meteorology (e.g., synoptic boundaries and air masses) in contrast to local-scale (2 – 20 km) processes within the planetary boundary layer (PBL). Diurnal heating of the Earth's heterogeneous surface at these finer scales forces circulations (e.g., sea breezes, valley winds, urban heat island circulations) which have been related to trends in the meteorological and climatological activity of storms; however, a quantitative understanding of their interactions with deep convection is limited. This is especially true for physical settings which support a variety of PBL circulations that challenge our understanding of storm characteristics and evolution. This thesis presents results from the Coastal Convective Interactions Experiment (CCIE), which incorporates meteorological and climatological analyses to provide a comprehensive understanding of how a complex coastal setting influences the convective storm environment. An 18-year radar-derived storm climatology (July 1997 – June 2015) is developed for Southeast Queensland (SEQ), Australia, supporting the operational planning and findings of Australia's first thunderstorm field campaign. The following thesis presents the experimental design and findings of the CCIE to establish the drivers of storm activity in a coastal setting.

Results from the CCIE climatology confirmed not only the hailstorm hotpots recognised by experienced local forecasters, but also a correlation between the storm frequency and sea breezes. To investigate the meteorology of hailstorm hotspots and interactions with the sea breeze further, climatological results were applied to coordinate a field measurement campaign. Observations of the PBL and convective storms were collected across two consecutive warm-seasons (Nov 2013 to Jan 2014 and Nov 2014 to Jan 2015) using a variety of static (RASS, SODAR, AWSs) and adaptive/mobile (CP-2 research radar, Doppler scanning lidar, polarised X-band radar, aerological soundings) platforms. Significant variability on time scales of minutes of sea breezes and convective storm cold-pools was observed, highlighting the limitations of contemporary concepts for gravity currents. Interaction observed between storm and sea breeze circulations demonstrated the importance of storm inflow thermodynamics for determining updraft intensity, motivating further investigation of the pre-storm environment.

Detailed analysis of the CCIE climatology datasets provided an understanding of SEQ hailstorms across a range of spatiotemporal scales. At the inter-annual time scale, the El-Niño Southern Oscillation (ENSO) was shown to have a statistically significant relationship with both hailstorm and sea breeze frequency in SEQ. Synoptic scale southeasterly changes that were found to couple with sea breezes provide the most favourable environment for hailstorms, particularly for southwest SEQ. At the mesoscale, hail development within convective cells was found to be most frequent within the inland limb of maritime air masses on sea breeze days. It was concluded, that the maritime sea breeze air is potentially favourable for convection after modification through inland propagation and the associated entrainment of sensible heat.

Investigation of the CCIE field campaign datasets show that diurnal modification of the coastal PBL by near-surface and boundary layer processes provide favourable preconditioning for convective storms. This includes: (1) early sea breeze onset for the city of Brisbane due an urban heat island enhanced land-sea thermal contrast, (2) significant afternoon warming and moistening above the sea breeze attributed to the advection of the inland convective boundary layer coastward under prevailing westerly flow, and (3) substantial variations in near-surface moisture likely associated with topography and land-use. For the 27 November 2014 Brisbane case study hailstorm event, which caused damages exceeding $1.5 billion AUD, these diurnal preconditioning processes are shown to be favourable for the development of a mesoscale convective environment capable of supporting large hailstone growth. The multicell-HP supercell storm mode identified for this event and previous similar events in SEQ is hypothesised to be more sensitive to variations in near-surface and boundary layer instability. This is in contrast to contemporary supercell storms, highlighting the importance of PBL observations for developing an understanding of convective storms in subtropical coastal environments.

In summary, this thesis provides a substantial and original contribution towards understanding of subtropical coastal storm environments. The integration of meteorological and climatological datasets from the CCIE provided a wealth of evidence highlighting the importance of mesoscale processes for storm evolution across a range of spatiotemporal scales. Long-term statistics show the influence of sea breeze activity upon climatological storm trends, in additional to the overall forcing by synoptic and background climate states. Observations provided a physical understanding of the favourable

preconditioning mechanisms for the development and intensification of convective storms within the typically stable coastal boundary layer. Importantly, the thesis also conveys the benefits of integrating meteorological and climatological analysis to develop a comprehensive understanding of convective storm environments.

Declaration by author

This thesis **is composed of my original work, and contains** no material previously published or written by another person except where due reference has been made in the text. I have clearly stated the contribution by others to jointly-authored works that I have included in my thesis.

I have clearly stated the contribution of others to my thesis as a whole, including statistical assistance, survey design, data analysis, significant technical procedures, professional editorial advice, and any other original research work used or reported in my thesis. The content of my thesis is the result of work I have carried out since the commencement of my research higher degree candidature and does not include a substantial part of work that has been submitted **to qualify for the award of any** other degree or diploma in any university or other tertiary institution. I have clearly stated which parts of my thesis, if any, have been submitted to qualify for another award.

I acknowledge that an electronic copy of my thesis must be lodged with the University Library and, subject to the policy and procedures of The University of Queensland, the thesis be made available for research and study in accordance with the Copyright Act 1968 unless a period of embargo has been approved by the Dean of the Graduate School.

I acknowledge that copyright of all material contained in my thesis resides with the copyright holder(s) of that material. Where appropriate I have obtained copyright permission from the copyright holder to reproduce material in this thesis.

Publications during candidature

Peer-reviewed papers Accepted

Soderholm J, McGowan HA, Richter H, Walsh K, Weckwerth T, Coleman M. 2015: The Coastal Convective Interactions Experiment (CCIE): Understanding the role of sea breezes for hailstorm hotspots in Eastern Australia. *Bulletin of the American Meteorological Society* doi:10.1175/BAMS-D-14-00212.1

Soderholm J, McGowan HA, Richter H, Walsh K, Weckwerth T, Coleman M. 2016a: Long-term trends and drivers of hailstorm variability in Southeast Queensland, Australia. *Quarterly Journal of the Royal Meteorological Society*. Accepted with minor revisions (8 June 2016)

Conference Abstracts

Soderholm JS, McGowan HA, Richter HX, Walsh K, Weckwerth T, Coleman M. 2015: Coastal Convective Interactions Experiment. *Australian Meterological and Oceangraphic Society, National Conference*, 15-17 July 2015, Brisbane, Queensland, Australia

Soderholm JS, McGowan HA, Richter HX, Walsh K, Weckwerth T, Coleman M. 2015: Coastal Convective Interactions Experiment. *American Meteorological Society, 37th Conference on Radar Meteorology,* 14-18 September 2015, Norman, Oklahoma, United States

Publications included in this thesis

Soderholm J, McGowan HA, Richter H, Walsh K, Weckwerth T, Coleman M. 2015: The Coastal Convective Interactions Experiment (CCIE): Understanding the role of sea breezes for hailstorm hotspots in Eastern Australia. ***Bulletin of the American Meteorological Society*** doi:10.1175/BAMS-D-14-00212.1 – incorporated as Chapter 3.

Contributor	**Statement of contribution**
Joshua Soderholm (Candidate)	Designed experiments (90%) Wrote the paper (100%)
Hamish McGowan	Designed experiments (5%) Paper Review
Harald Richter	Paper Review
Kevin Walsh	Paper Review
Tammy Weckwerth	Designed experiments (5%) Paper Review
Matthew Coleman	Project Funding

Soderholm J, McGowan HA, Richter H, Walsh K, Weckwerth T, Coleman M. 2016: Long-term trends and drivers of hailstorm variability in Southeast Queensland, Australia. ***Quarterly Journal of the Royal Meteorological Society*** Accepted with minor revisions (8 June 2016) – incorporated as Chapter 4.

Contributor	**Statement of contribution**
Joshua Soderholm (Candidate)	Designed experiments (100%) Wrote the paper (100%)
Hamish McGowan	Paper Review
Harald Richter	Paper Review
Kevin Walsh	Paper Review
Tammy Weckwerth	Paper Review
Matthew Coleman	Project Funding

Contributions by others to the thesis

No contributions by others.

Statement of parts of the thesis submitted to qualify for the award of another degree

None

Acknowledgements

The Coastal Convective Interactions Experiment (CCIE) represents the most rewarding 4 years of my life so far, and the culmination of more than 8 years of research, planning and persistence to unlock the mysteries of thunderstorms in Southeast Queensland (SEQ). This journey would not have been possible without the significant intellectual, financial and moral support from so many people.

Firstly, my thanks to Professor Hamish McGowan who in early 2008 encouraged the grand (and expensive) aspirations of an unknown undergraduate student for storm-chasing experiments with mobile radars and lidars. The infrastructure, collaborations and funding Hamish has established in support of my work has been nothing short of incredible, serving as a testament to his perseverance and passion for meteorology. Starting from little more than radiosonde pilot study, The University of Queensland (UQ) now operates Australia's first mobile polarised weather radar, and the sky's the limit. At home in the field, Hamish also holds the record for the most storm intercepts, with 12 events across 11 CCIE IOPs. A storm was never far away with Hamish at the wheel.

During the early stages of my research career I was also fortunate enough to work under the supervision of Jeff Callaghan, a senior forecaster from the Bureau of Meteorology (BoM) Queensland Regional Office. Preliminary research conducted by Jeff and his intuitive understanding of SEQ thunderstorms fostered the questions I sought to answer throughout this thesis. Ongoing support from the Regional BoM Office through the provision of IOP forecasts and adaptive radiosonde releases has been essential to the success of the CCIE. Furthermore, I am grateful to Tony Wedd and Peter Otto for ensuring my research questions were grounded by the realities faced by forecasters. I hope the concepts delivered by this thesis can assist in forecasting the next "big one".

A majority of my PhD was spent at the BoM head-office in Melbourne under the supervisor of the Dr. Harald Richter. There would be large gaps in our understanding of SEQ thunderstorms without Harald's invaluable wisdom and guidance, for which I am especially grateful. To Beth Ebert and Peter May from BoM R&D for the in-kind and financial support, and in particular, usage CP-2 during IOPs with the vigilant assistance of Ken Glasson. As the last scientist to use CP-2, it was truly a humbling experience to be part of its 40 year

history. Thank you also to my University of Melbourne supervisor, Kevin Walsh for your reviews and statistics support.

The CCIE field campaign would not have been possible without the significant financial and in-kind backing by Matthew Coleman from Fugro Spatial Solutions Pty Ltd. Working with Matt and the ROAMES team prior to my PhD drove the refinement of the climatology software at the heart of this project. I acknowledge the generous industry support by Leosphere and Furuno Electric Co Ltd for facilitating the mobile observation platforms deployed during CCIE, allowing us to push their technology to the limit. I hope the new applications and insights offered by the CCIE further drives the development of mobile radars and lidars. During my PhD I was fortunate to collaborate with two of the most inspirational and respected meteorologists in my field: Dr Tammy Weckwerth and Jim Wilson from NCAR in Boulder, Colorado. Their wealth of knowledge regarding field campaigns, radars, thunderstorms and clear-air processes enriched the CCIE immensely.

The 30 IOPs during CCIE would have been inconceivable without the hundreds of hours provided by volunteers. In no particular order this includes: Michael Gray, Michael Hewson, Hamish McGowan, Nicholas McCarthy, Malcolm Nunn, Sophie Thomas, Chris Chambers, Stephen Soderholm, Lev Susany, Anthony Lumsden, Emily Field, Harald Richter, Sabrina Wu, Nik Callow, Andrew Lowry, Michael Tobe, Tom Kavanagh, Jordan Brook, Lauren Ravizzotti, Lydia McKenzie, Tegan Hall, Annie Nguyen and Dean Narramore. I apologise to those who weren't rewarded with a storm! Secure sites for CCIE weather stations were kindly provided by Russell & Jenny Jenner (Kalbar), Andrew Wills (Tarome) and Janene Cornelius (Grandchester). Thanks also to Michael, Genna, Suhan and the professional staff at GPEM who effortlessly managed my unceasing purchasing and travel. And to Anthony Cornelius from WeatherWatch, for his invaluable IOP forecasts, chasing advice and knowledge of the SEQ storm environment.

Finally, I wish to acknowledge the support of my friends in Brisbane and Melbourne, my family in Brisbane and Annie who encouraged, supported and tolerated me over the past 4 years. This journey wouldn't be complete without you.

Keywords

field experiment, radar climatology, boundary layer meteorology, hail, thunderstorm, coastal environment, Brisbane

Australian and New Zealand Standard Research Classifications (ANZSRC)

ANZSRC code: 040107, Meteorology, 50%

ANZSRC code: 040105, Climatology, 50%

Fields of Research (FoR) Classification

FoR code: 0401, Atmospheric Science, 100%

Table of Contents

List of Figures & Tables

Figures

Tables

List of Abbreviations

- AWS: Automatic Weather Station
- BL: Boundary Layer
- BoM: Bureau of Meteorology
- CBL: Convective Boundary Layer
- CCIE: Coastal Convective Interactions Experiment
- CIN: Convective Inhibition
- EPH: Department of Environment and Heritage Protection
- ENSO: El Niño Southern Oscillation
- θ_e: Equivalent Potential Temperature
- HCI: Hailstorm Convective Initiation
- HD: Hailstorm Development
- HP: High Precipitation
- IPO: Inter-decadal Pacific Oscillation
- LFC: Level of Free Convection
- MATLAB: MATrix LABratory
- NCAR: National Center for Atmospheric Research
- PBL: Planetary Boundary Layer

- PDF: Probability Distribution Function
- PGF: Pressure Gradient Force
- PPI: Plan Position Indicator
- RASS: Radio Acoustic Sounding System
- RHI: Range Height Indicator
- SBCAPE: Surface Based Convective Available Potential Energy
- SEQ: Southeast Queensland
- SOI: Southern Oscillation Index
- SODAR: Sonic Detection and Ranging
- TITAN: Thunderstorm Identification, Tracking, Analysis and Nowcasting
- TN: True North
- TST: Thunderstorm Synoptic Type
- UBL: Urban Boundary Layer
- UQ-XPOL: University of Queensland X band Polarimetric Radar
- UHI: Urban Heat Island
- UTC: Coordinated Universal Time
- WDSS-II: Weather Decision Support System – Integrated Information

Chapter 1. Introduction

This thesis presents an observational study of the climatological and meteorological process driving convective storms in the coastal setting of South East Queensland (SEQ), Australia. Long term observational datasets (July 1997 - June 2015) and field campaign datasets from the Coastal Convective Interactions Experiment (CCIE; November 2013 – January 2014 and November 2013 – January 2015) are applied throughout. This chapter presents an introduction to convective storms and coastal atmosphere processes (1.1) and the rationale for the CCIE (1.2). The research aim and objectives are presented in section 1.3, followed by an overview of the thesis structure (1.4).

1.1 Convective Storms and Coastal Environments

Convective storms occur across every continent when atmospheric potential instability is realised through the development of deep convective updrafts, and the subsequent growth of cumulonimbus clouds. An estimated 16 million convective storms develop each year, particularly in warmer mid and lower latitude climates where moisture rich air is readily available (The National Severe Storms Laboratory 2015). Such storms are often beneficial, providing a significant component of warm season precipitation for many regions (Changnon 2001); however a small percentage also produce surface weather that is classified as severe (e.g., large hail, strong winds, flash flooding and tornadoes). Severe storms continue to result in significant economic losses (e.g.; $1.4B AUD from the 27 November 2014, Brisbane hailstorm; Insurance Council of Australia 2015) through damage to infrastructure, agriculture and other assets, and fatalities, in spite of the vast improvements in predictive and warning capabilities over the past several decades.

The initiation and evolution of storms is primarily determined by the atmospheric environment from which they develop. On larger scales, synoptic scale processes regularly provide preconditioning for convection (e.g., moisture advection, upper level instability), and a trigger mechanism for initiation (e.g., cold fronts, troughs; (Johnson and Mapes 2001). Concepts governing these large-scale processes are often independent of physical setting, particularly those within the mid to upper troposphere, allowing for the application irrespective of region. Variability forced by the physical setting is most evident when storm updrafts and downdrafts interact with the planetary boundary layer (PBL). A diverse range of processes can influence the buoyancy and shear of the PBL, including

diurnally forced circulations (sea breezes, land breezes, thermotopographic flows), dynamic processes (e.g., surface friction, topographic channelling/blocking) and surface types (e.g., agriculture, native, urban), which can result in changes to storm intensity (e.g., (Banta and Schaaf 1987; Kingsmill 1995; Weckwerth et al. 2004)

The Great Plains of the United States of America has remained the centre of international severe storm research (both field campaigns and numerical simulations) since the late 1940's, owing to the frequent tornado occurrence. Concepts developed from this relatively homogeneous physical setting (e.g., grassland plains and prairie) have provided the foundation for predicting and warning of convective storms globally. However, this region remains sparsely populated in contrast to coastal regions, where approximately 44% of the global population reside within 150 km from the coast (United Nations 2010). In contrast to the Great Plains, the physical setting of coastal regions is considerably diverse, leading to the development of complex PBL circulations (e.g., Banta 1995; Novak and Colle 2006; Chemel and Sokhi 2012). For the low-lying Florida peninsula, the sea-breeze is recognised as a primary mechanism for convective storm initiation and maintenance (Wakimoto and Atkins 1994; Wilson and Megenhardt 1997). Furthermore, atmospheric processes associated with topography (e.g., Banta and Schaaf 1987; Weisman 1990a; Weckwerth et al. 2011), urban landscapes (e.g., Chen et al. 2007; Niyogi et al. 2011; Haberlie et al. 2015b) and reservoirs (Haberlie et al. 2015) influence the development of convective storms. Therefore, to develop a clear understanding of the convective environment in complex physical settings such as coastal regions, contemporary storm concepts must be incorporated with a comprehensive understanding of the PBL.

1.2 Rationale

Reoccurrences of severe convective storms on yearly to decadal time-scales quickly become part of "local knowledge" through their long-lasting social (Riebsame et al. 1986; Trainor et al. 2015) and economic impacts (Doswell 2003). The South East Queensland (SEQ) region of Australia is well-known for frequent warm-season convective storms (Dowdy and Kuleshov 2014; Allen and Allen 2016), thus it is not unexpected to find that forecasters and the public recognise the existence of "hotspots", where storm activity is exceptionally frequent. In spite of the accumulating experience built from several decades of observational studies, idealised simulations and full-physics modelling, a deeper understanding regarding the presence and drivers of these hotspots on the meso-gamma

scale (2 - 20 km) is comparatively lacking (Orlanski 1975). In part, this limitation arises from the scarcity of storm-resolving and PBL observational datasets that extend over a sufficient period to provide a robust dataset (Fabry et al. 2013). From the perspective of community safety and economic interests, a climatological understanding of convective storm frequency on a local scale has immediate applications in minimising vulnerability and refining disaster preparedness. Within Australia, severe storms alone account for the greatest insured losses among all natural disasters, where damages from individual events often exceed $1 billion AUD (Australian Emergency Management Institute 2014).

For a regional forecaster, an awareness of the atmospheric processes that favour convective storms has significant potential to improve skill and lead time. The importance of such knowledge was highlighted by Sills et al. (2004) following the analysis of a tornadic supercell over an urbanised region of Sydney; "*Improved warning lead time and accuracy for such events requires better knowledge of the relationship between boundaries and severe weather*". The diversity of preconditioning and trigger processes, especially in regions of significant topography or complex coastlines, limits the applicability of a case study approach for conceptually understanding climatological hotspots. At the other end of the spectrum, previous climatological studies often lack a sufficiently long duration and spatial resolution to quantify storm frequency at scales required to analyse local triggering and conditioning processes. The following study integrates these two approaches into a single methodology in an effort to understand the climatological and meteorological drivers of frequent convective storms activity in a continental coastline environment. The application of concepts developed by the CCIE extends beyond SEQ to comparable coastal settings globally prone to warm season storms, including southern and southeastern United States (Blanchard and López 1985; Cintineo et al. 2012), Brazil/Argentina (Pinto et al. 2013), Spain (Azorin-Molina et al. 2014b) and Italy (Baldi et al. 2014).

1.3 Aim and Objectives

The following study seeks to understand the meteorological and climatological processes which favour convective storms in SEQ, Australia, thereby filling significant knowledge gaps regarding coastal convective storm environments. This primary aim addresses the overarching research question: What is the contribution of atmospheric processes within the coastal setting, in particular the sea breeze, for the intensification of convective

storms? To address this question, three primary objectives and sub-objectives were formulated.

Objective 1: Develop a methodology for quantifying the drivers of frequent convective storm activity at climatological and meteorological scales for the SEQ region using observational datasets.

- Construct a long-term radar-derived climatology of spatial hailstorm occurrence for SEQ to quantify anecdotal “hot-spots” known by regional forecasters

- Implement a robust sea breeze detection strategy specific to the South East Queensland region using an observational approach.

- Design and coordinate a field campaign to strategically target hailstorm hotspots and the sea breeze using a variety of specialised mobile (UQ-XPOL, weather stations, soundings) and fixed (CP-2, weather stations) instrumentation.

Objective 2: Investigate the long-term climatologies of SEQ sea-breeze and convective storm activity for evidence of forcing on spatial scales ranging from local (< 10 km) to climate teleconnections.

- On inter-annual time scales, statistically verify the influence of the ENSO upon hailstorms and the sea breeze.
- On synoptic scales, identify the dominant synoptic types for hailstorm and sea breeze activity, and investigate associated changes in frequency and spatial distribution.

- On the local scale, explore the spatiotemporal occurrence of hailstorm initiation and intensification in relation to sea breeze proximity across the climatology for statistical evidence of sea breeze interactions.

Objective 3: Explore the influence of local processes upon the preconditioning and the evolution of convective storms through observations obtained by the CCIE.

- Determine the influence of land surface characteristics (e.g., agriculture, urban areas) upon evolution of the surface meteorology (e.g., temperature, moisture, wind fields) in relation to the climatological distribution of convective storms in SEQ.

- Examine how the PBL circulations (e.g., sea breeze) influence the preconditioning of the convective storm environment.

- Explore the influence of the near-surface and PBL characteristics upon the evolution of a high-end storm event observed by the CCIE.

1.4 Thesis Structure

This thesis contains three chapters that address the three research objectives. Fig. 1.1 presents a flow chart that illustrates the linkage between the research objectives and the three core chapters (3,4,5). To provide context for this study, a comprehensive review of coastal convective storm environments and historical events in SEQ is provided in chapter 2. Chapter 3 develops the climatological methods for quantifying convective storm and sea breeze variability. A field campaign strategy for the CCIE is introduced to target regions of frequent storm activity evident from the climatological analysis and preliminary results presented. Chapter 4 further investigates the climatology datasets presented in chapter 3 in relation to forcing on global, synoptic and local scales. In chapter 5, the local scale forcing of convective storms (e.g., sea breezes) identified by chapter 3 and expanded upon in chapter 5 is explored further using the observational dataset from the CCIE field campaign. A synthesis of research outcomes and overall conclusions are presented in chapter 6.

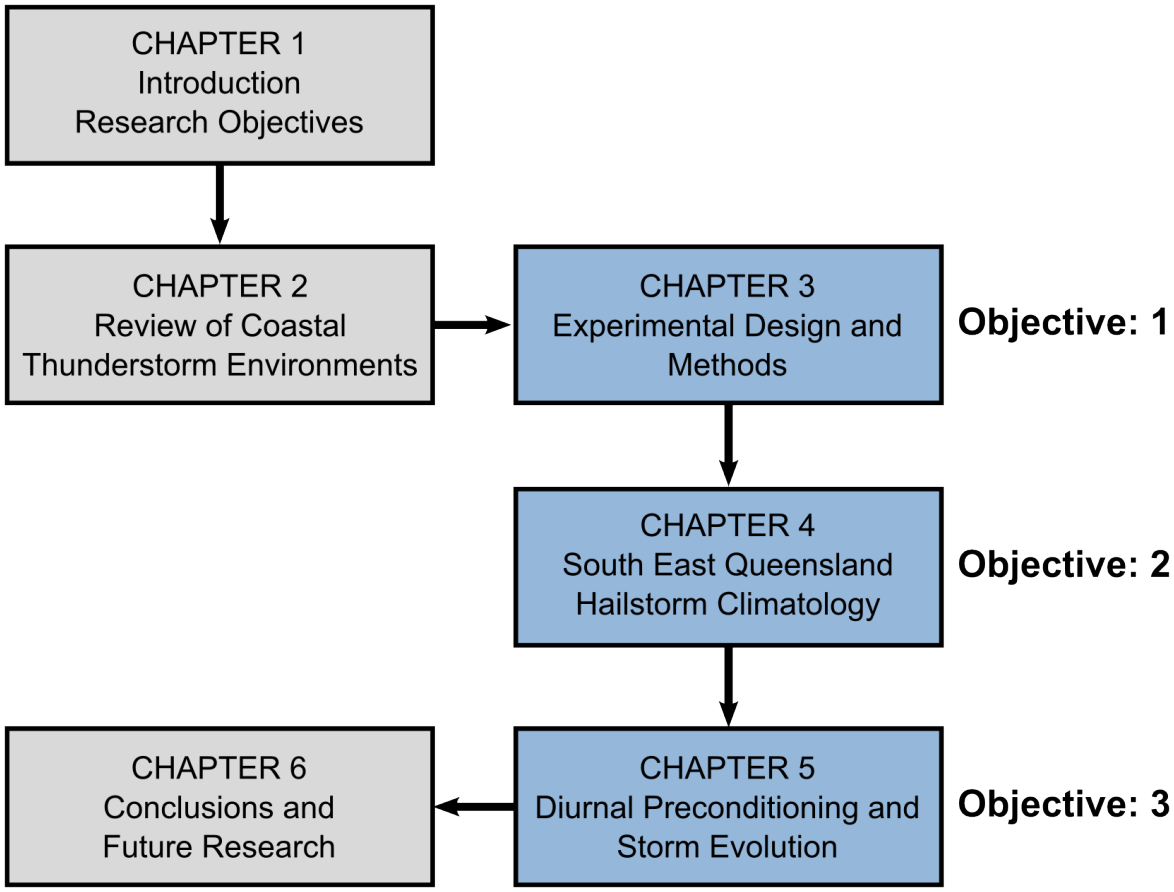

Figure 1.1: Thesis structure and flow chart

Chapter 2. Review of Coastal Convective Environments and Storms

The following chapter reviews the atmospheric processes which influence convective storm development in the context the coastal environments, and highlights key knowledge gaps which require attention. It also examines the physical setting of SEQ in relation to PBL processes and presents a brief history of severe storm events which motivated this study.

2.1 Meteorology of Coastal Convective Storm Environments

2.1.1 Surface Effects

Characteristics of planetary surface type (e.g.; water, ice, land), anthropogenic usage (e.g.; urban, agriculture, pastoral) and elevation are closely coupled to the thermodynamic and kinematic characteristics of the near-surface atmosphere in response to surface heat fluxes (latent and sensible) and frictional effects. Furthermore, heterogeneous surfaces induce variability within the PBL, which contribute significantly to the regional and local climate and meteorology. For convective storms, subtle variations in moisture, temperature and convergence are considered important factors for both initiation (e.g., Weckwerth 2000; Wakimoto and Murphey 2009; Frye and Mote 2010) and intensification (e.g., Smith et al. 2000; Mona et al. 2016). Crook (1996) summarised the thermodynamic sensitivity of convection using the results of an analytical study; *"It is found that variations in boundary layer temperature and moisture that are within typical observational variability (1ºC and 1 g kg^{-1}, respectively) can make the difference between no initiation and intense convection"*. Such variations are common during the diurnal evolution of the PBL, and in particular, for complex physical settings (e.g., coastal environments).

Changes in surface properties due to mountainous terrain can have substantial effects upon convection. Banta et al. (1990) identified three distinct processes: (1) mechanical lifting of air to the LFC, (2) development of thermally forced circulations, and (3) dynamical effects including channelling and blocking. Under settled synoptic conditions, thermally forced circulations dominate mountain meteorology. Lower static stability of warming elevated surfaces coupled with the development of upslope flow leads to the formation of convergence zones along mountain ridgelines, acting as a trigger for convection (Banta

1984). As a result, clouds often develop first over mountainous regions, in contrast to neighbouring to valleys and plains. This process can be seen across a diverse number of environments, including the European Alps (Weckwerth et al. 2011; Nisi et al. 2016), Colorado Rocky Mountains (Banta and Schaaf 1987; Cintineo et al. 2012), Appalachian Mountains of eastern North American (Weisman 1990b), Andes Mountains of South America (Mezher et al. 2012), Prebetic Ranges of the Iberian Peninsula (Azorin-Molina et al. 2014a), and the Great Dividing Range of Australia (Potts et al. 2000; Soderholm et al. 2016)

Convective storm environments are also influenced by the surface properties (e.g., albedo, heat capacity, moisture content). Wet landscapes increase near-surface humidity, potentially leading to great parcel instability (Segal et al. 1995) and increased convective storm activity (Brimelow et al. 2011). Furthermore, anthropogenic land use has led to increasingly heterogeneous surface properties, particularly for the more densely populated regions (e.g., coastal cities), impacting near-surface heating and moisture. For example, naturally dry settings (e.g., prairie, semi-arid landscapes) that are irrigated for agriculture can experience an increase in near-surface moisture and therefore parcel bouyancy (Pielke and Zeng 1989). Metropolitan areas often experience significantly warmer temperatures than surrounding rural regions (urban heat islands) in response to their higher heat capacity and lower albedo of paved surfaces and urban canyons (Gartland 2011), leading to changes in storm frequency and distribution (Chen et al. 2007; Niyogi et al. 2011; Haberlie et al. 2014). More recently, Haberlie et al. (2015a) showed that artificial reservoirs affect the climatological frequency of convective initiation. Quantifying this fine-scale variability remains difficult without extensive surface instrumentation (e.g.; Weckwerth et al. 2004) or specialised remote-sensing techniques (e.g.; radar refractivity gradients; Feng et al. 2016). The availability of this information for near surface thermodynamic conditions benefits both the nowcasting of convective initiation (Wilson et al. 1998) and initialisation of numerical weather prediction models (Gasperoni et al. 2013; Crook 1996).

2.1.2 Planetary Boundary Layer Circulations and Convergence Zones

The importance of convergence zones for the initiation and development of convection was first noted by Byers & Braham (1949). Research throughout the past sixty years has

continued to emphasise their importance for convection storm evolution, despite the inherent difficultly of quantifying what is a predominantly clear air process. Wilson & Schreiber (1986) pioneering application of Doppler radar to observe clear air circulations provided the first insight into how to overcome this obstacle. Through an analysis of 653 convective storms in the Denver region, USA, it was shown that convergence zones were in proximity to the initiation of 80% of storms. This study and subsequent research has proven the apparent randomness of convective initiation and evolution closely resembles a deterministic process when sufficient knowledge of the planetary boundary layer environment is available (Jorgensen and Weckwerth 2003).

The PBL represents the surface boundary layer of the troposphere under the influence of the surface environment. On the smallest scale, thermal columns arising from uneven surface heating force the development of a CBL within the PBL, through the vertical mixing of buoyant parcels. In the presence of vertical wind speed shear, thermal circulations are often organised into horizontal convective rolls (HCRs; Weckwerth 1997). HCRs have been associated with significant moisture variability in the CBL (Weckwerth et al. 1996) and the development of convergence zones between ascending rolls branches (Fig. 2.1), thereby providing a potential trigger for convective storms (Wilson et al. 1992; Kingsmill 1995). Under light winds, CBL thermals have been documented as organised as open-cell convection (Bennett et al. 2010).

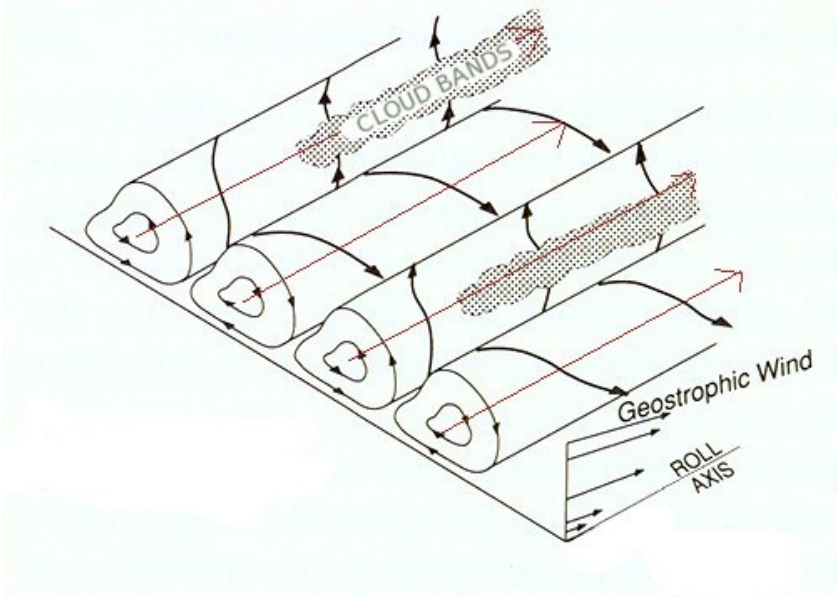

Figure 2.1: Schematic diagram of horizontal convective rolls. Adapted from (Brown 1980)

Diurnal heating and cooling across heterogeneous surface regimes (e.g., water, agricultural, urban and natural landscapes) and topography also forces a variety of predominantly horizontal mesoscale circulations, and associated convergence zones within the PBL. Under settled synoptic conditions, the daytime development of the coastal PBL is predominately influenced by the sea breeze (Fig. 2.2; Miller 2003). The boundary convergence zone along the inland limb of the sea breeze also provides an important trigger for convective initiation (Kingsmill 1995; May et al. 2002; Azorin-Molina et al. 2014a); however the influence of the sea breeze air mass upon deep convection is less clear within the literature.

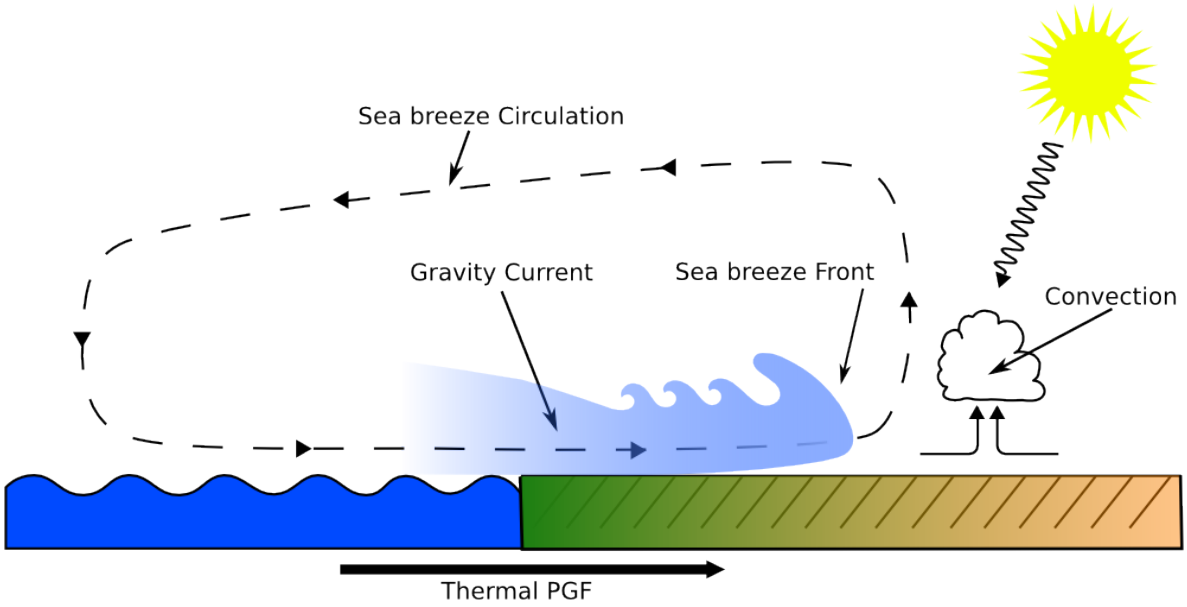

Figure 2.2: Schematic of sea-breeze system. Selected elements of the system are annotated. Adapted from Miller and Keim (2003)

Entrainment of warming land surface parcels as the sea breeze moves inland erodes the maritime inversion (Simpson et al. 1977), particularly for urban environments of enhanced friction and heating (Lemonsu et al. 2006a; Novak and Colle 2006; Dandou et al. 2009). Consideration of this enhanced sea breeze buoyancy is likely critical for understanding the suppression or development of pre-existing convective storms; however, it remains a significant knowledge gap. Furthermore, the sea breeze current increases wind speed shear within the near-surface environment, potentially increasing favourable storm-relative inflow (Coniglio et al. 2011). Coastal settings with substantial relief can also interact and modify the inland propagation of the sea breeze. Topographical channelling leading to an acceleration of the sea breeze front has been observed in the Durance Valley, France

(Bastin et al. 2005); however; this resulted in an overall weakening of the sea breeze circulation. Simulations for the mountainous Monterey Bay region of California indicate valley-wind circulations also interact with the sea breeze, enhancing inland propagation (Darby et al. 2002).

The sea breezes of the Florida peninsula are the most extensively studied of any region, owing to the frequent and explosive convective initiation that occurs between the collision of opposing sea-breezes over land (Byers and Rodebush 1948; Pielke 1974; Blanchard and López 1985; Wilson et al. 1992; Wakimoto and Atkins 1994). In contrast, studies of convective interactions with a continental sea breeze are comparatively lacking from the literature despite this setting occurring over a vast majority of coastlines globally. One of the few comprehensive analysis for a single sea breeze environment was compiled by Koch & Ray (1997) which showed that sea breeze fronts in eastern North Carolina were the second most common convergence zone and the most convectively active, with 74% of fronts initiating convection and 88% of boundary collisions resulting in new convection.

Analogous to sea breezes, thermal gradients from an UHI trigger the development of a local circulation, promoting vertical mixing (Fig. 2.3), while enhancing surface convergence at the periphery of the urban boundary layer (Kanda 2007). For coastal environments, the enhanced UHI thermal gradient has been associated with the earlier onset of the sea breeze, followed by stagnation over the urban environment as the sea breeze is perturbed by the UHI circulation (Melas et al. 2000; Khan and Simpson 2001; Lemonsu et al. 2006b; Freitas et al. 2007). Furthermore, enhanced convergence, vertical motion and aerosols concentrations from the UHI has been documented in association with increased cloud formation (Tsunematsu and Kai 2004; Schatz and Kucharik 2014), convective precipitation rates (Dixon and Mote 2003; Ryu et al. 2015) and storm initiation (Rozoff et al. 2003; Shem and Shepherd 2009). Continuing growth of the near-coastal urban landscape (Small and Nicolls 2003) highlights that UHI processes are increasingly a significant component of the coastal PBL.

Understanding and quantifying the influence of PBL processes upon convective storms is a significant challenge for the meteorological community, and remains the focus of both numerical modelling (Clark et al. 2012; Sun et al. 2014) , observational (Weckwerth et al. 2004; Geerts et al. 2013) and combined efforts (Weisman et al. 2015). PBL circulations

predominantly exist as clear air processes (lacking moist convection) at fine scales ranging from mesoscale (2 km - 200 km) to microscale (< 1 km). Analogous to surface properties, this variability within the PBL is difficult to measure observationally, particularly above the surface. The use of mobile serial soundings (Bryan and Parker 2010; Weisman et al. 2015), static profilers (Puygrenier et al. 2005; Taylor et al. 2011) and lidar (Banta et al. 1993; Muppa et al. 2015) are effective for monitoring the vertical properties of the PBL; however, offer limited or no horizontal coverage. Therefore, a preliminary understanding of the regional PBL environment is required to strategically coordinate the deployment specialised instrumentation during experimental campaigns.

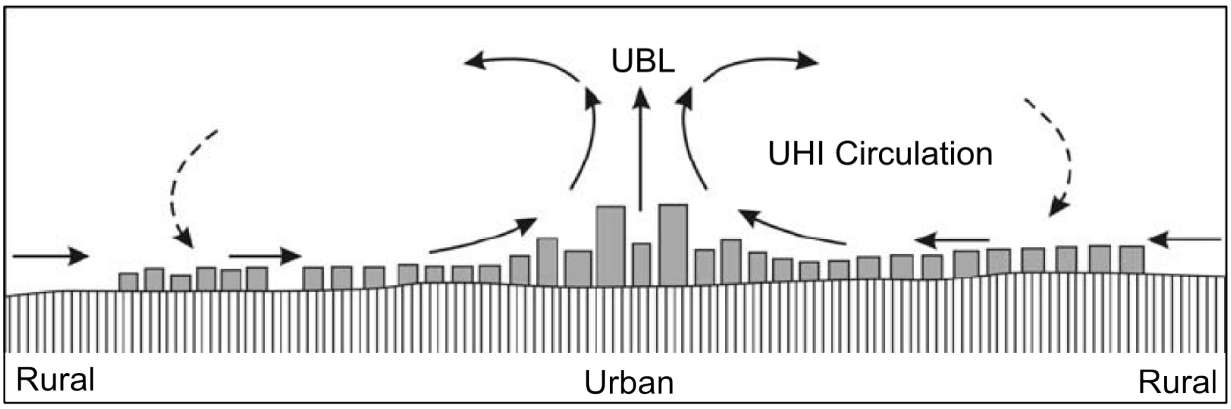

Figure 2.3: Schematic of the UHI Circulation. Adapted from Gal and Sumeghi (2007)

2.2 Convective Storms

Convective clouds are the result of buoyant air parcels lifted above the level of free convection. When this process extends throughout a significant portion of the troposphere, it is referred to as a cumulonimbus cloud or convective storm, regardless of electrification. A single convective storm “cell” forms the building block for a broad spectrum of storm modes. The structure, evolution and associated severe weather of a convective storm is dependent on the favourability of both the storm environment (e.g., PBL sourced parcels) and resultant storm-generated effects.

2.2.1 Structure and Evolution

Prior studies have highlighted the importance of environmental buoyancy and shear for determining the mode of convective storms (Weisman and Klemp 1982, 1984; McCaul and Weisman 2001). The most widely used set of indices for evaluating environment buoyancy

and shear is the Convective Available Potential Energy (CAPE) and 0-6 km vertical wind shear respectively. This dependency results in a spectrum of convective systems that are broadly classified into multicells and supercells (Cotton et al. 2011). More recent studies have highlighted that this morphology is most closely related to the product of storm and shear (Brooks 2009), rather than the quotient relationship originally described by Weisman and Klemp (1982). For environments with minimal shear and buoyancy, individual cell evolution within a storm is characterised by a short lifecycle. Two distinct flows develop, an initial updraft forced by latent heating and environmental instability, and a diabatically cooled downdraft, in response to increasing water and ice loading within the updraft (Doswell 2001). The sub-cloud layer of established, mature cells is characterised by the downdraft diverging horizontally, forming a high-pressure cold pool air mass (Byers and Braham 1949).The surrounding environmental air is lifted by the denser, diverging cold pool, modifying the updraft inflow and potentially triggering new cells through mechanical lifting (Cotton et al. 2011).

The convergence zone at the edge of a cold pool can trigger new cells, leading to the development of a multicell storm composed of many cells at various stages of development (Browning 1977). Multicells can produce severe weather, however severity is limited by the relatively short updraft lifecycle of individual cells. Under deep layer shear, an individual cell may persist through the downshear separation of the precipitation from the updraft (Doswell 2001). Furthermore, rotation within the updraft through the tilting into the vertical and stretching of ambient horizontal vorticity within the PBL can also induce dynamical perturbation pressure (Lemon and Doswell 1979; Weisman and Klemp 1984). This region of dynamically forced low pressure within an updraft supplements buoyancy forced lifting of inflow parcels, increasing the longevity of an individual cell and increasing the potential for severe weather.

2.2.2 Storm-Generated Effects

In the presence of convective storms, the mesoscale environment is modified by a host of storm-generated processes, some of which can be beneficial, while others act to weaken deep convection. Furthermore, storm-generated effects interact with PBL circulations and synoptic scale features, necessitating careful analysis when attributing respective contributions to convective storm evolution.

The simplest storm-generated effect is produced by cloud shading of the surface by cirrus advected ahead of the convective storm, reducing the buoyancy of the inflow environment and generating baroclinic zones which may provide beneficial horizontal vorticity to a storm (Johnson and Mapes 2001; Frame and Markowski 2013). At the surface, cold pools from active and dissipated storms substantially modify the PBL through increased lifting, cooling and wind shear. Acting as a density current, cold pools lift the more buoyant surface airmass ahead of the convective storm, while stabilising the surface environment and suppressing subsequent convection. The depth of the outflow is critical for regenerating multicell convective storms as a rapidly spreading cold pool may no longer have sufficient depth to lift parcels to their LFC. Cold pools can also generate considerable low-level shear in the sub-cloud layer (Browning 1977). The balance between opposing circulation tendencies generated by cold pool (through thermal gradients and vertical shear) and the ambient environment can favour the development of deeper updrafts (Rotunno et al. 1988; Bryan et al. 2004). Rotunno et al. (1988) argued that without low-level ambient shear, cold pool lifted air parcels accelerate horizontally, inhibiting vertical development, providing an important lifting mechanism for linear convection. However, (Stensrud et al. 2005) showed that this balance concept did not compare favourably with observations or numerically simulations of linear systems, limiting its applications for convective storm forecasting.

Observational evidence of the generally favourable effect of low-level shear upon storm updraft intensity was noted by Wilson & Megenhardt (1997), however consideration of boundary relative motion was also necessary to account for convective storm evolution. The principles of boundary relative storm motion were first introduced through numerical studies by Moncrieff & Miller (1976) and later extended by Weisman & Klemp (1986). The importance of this concept was highlighted by Wilson & Megenhardt 1997; *“Storm merger, organization, and lifetime were greatly enhanced when the clouds were moving at a velocity similar to that of the convergence line”*. Sub-tropical coastal settings such as SEQ are recognised for weak ambient shear (Callaghan 1996), suggesting the dominant cold-pool shear would likely favour the multicell storm mode without an additional mechanism for wind shear or convergence within the mesoscale environment (e.g., sea breeze, low level jet).

The storm-generated boundary separating the cold pool air mass from the surrounding air is commonly referred to as a gust front. Figure 2.4 shows an idealised schematic of a gust front extending horizontally away from the source downdraft. Wakimoto (1982) provided the first comprehensive study of the gust front lifecycle using Doppler radar, surface observations and rawinsondes data collected by the North Illinois Meteorological Research on Downburst (NIMROD) project. The evolution of a gust front triggered by an outflow dominant convective cell can be divided into four stages, ending with the complete separation from the parent storm, resulting in its dissipation. Previously documented similarities between the gust-front and theoretical gravity currents was also concluded by Wakimoto. More recent studies have confirmed that detached gust fronts continue propagating long after the parent cell dissipates and are critically important for understanding the initiation of new cells through the lifting of boundary layer air (Goff 1975; Nicholls et al. 1991; Wakimoto and Murphey 2009) and interactions with PBL circulations (Kingsmill 1995; Wilson and Megenhardt 1997). Simulations of multicell storms by (Fovell and Ogura 1989) showed a systemic relationship between gust front propagation speed and increasing environment shear, with the rear inflow jet contributing to colder subcloud layers and faster propagation.

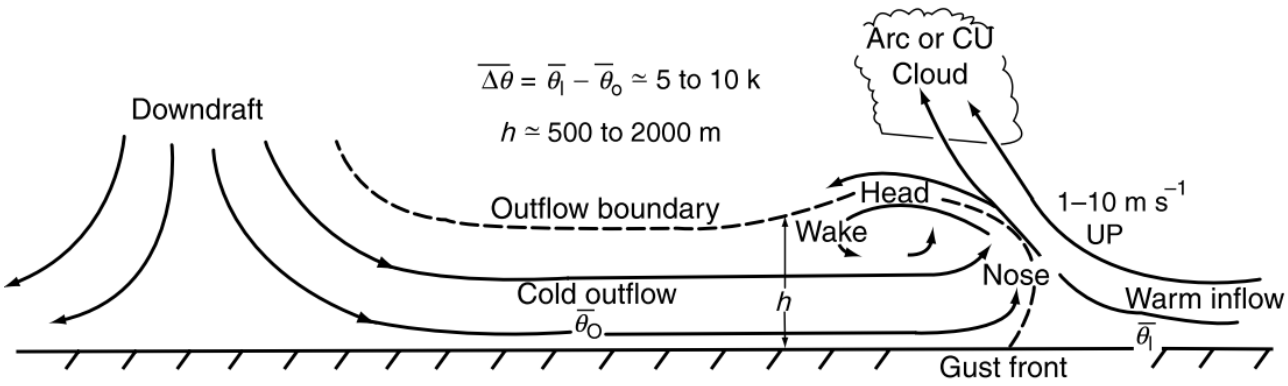

Figure 2.4: Schematic structure of a gust front. Adapted from Goff (1975); Fankhauser (1982); Wakimoto (1982)

Tilting and stretching of ambient horizontal vorticity lifted within the updraft is an important mechanism for the development of supercells (Doswell 1996). Dynamical lowering of mid-level pressure within vertical vorticity couplets which develop along the flanks of the updraft supplements buoyant lifting (Klemp 1987). This mechanism promotes the long-lived updrafts of supercells which are able to transition to more stable inflow environments

which would otherwise weaken multicell storms (Ziegler et al. 2010). In the absence of ambient horizontal vorticity within the convective environment, parcels sourced from more sheared low-level boundaries and local circulations can provide sufficient horizontal vorticity to promote supercell growth (Markowski et al. 1998; Atkins et al. 1999). Examples of these processes can be found throughout the literature. Sills et al. (2004) showed that the sea breeze boundary was central to the development of a tornadic supercell in Sydney, Australia, while on climatological scales, King et al. (2003) showed a relationship between lake breeze convergence zones and a tornado occurrence in Southern Ontario, Canada.

Storm generated processes influence both the clear-air environment surrounding a storm and precipitation-loaded atmosphere within the storm, limiting the effectiveness of a single instrument approach. To overcome this limitation, Bluestein et al. (2014) demonstrated the application of simultaneous observations from collocated X-band radar and pulsed Doppler lidar platforms for observing tornadic storms. Observing storm generated processes has remained an ongoing goal for the VORTEX projects over the past 20 years in an effort to understand tornadogenesis, including the current campaign in southeast United States (VORTEX SE).

2.3 Climatological Studies of Australian Convective Storms

The sporadic nature of convective storm events presents a considerable challenge when constructing a meaningful climatological analysis, particularly at sub-storm scales (e.g., 1 km). The longest available dataset for the study of Australian convective storms is the Bureau of Meteorology Severe Storms Archive, compiled from observer reports. Although this archive extends back to the 19th Century, its lack of completeness and consistency limits the usefulness for direct climatological applications (Allen et al. 2011). Remotely sensed information of hydrometers or lightning associated with convective storms negates the sampling issues found in archived reports, however the comparatively short length of record can limit confidence, particularly for regions of sparse storm activity.

The longest remotely sensed study (25 years) of Australian convective storms is based on an omnidirectional lightning flash counter network (Bates et al. 2015); however this dataset provides no spatial information for discerning hotspot activity. Dowdy and Kuleshov (2014) and Dowdy (2016) applied an 18-year climatology of satellite observed lightning ground flash densities for Australia and globally (35° N to 35° S) respectively. The length of this

dataset not only reduced the effects of short-term spatiotemporal variability, but also improved confidence when evaluating the influence of large-scale modes of variability such as the ENSO. Furthermore, Dowdy (2016) demonstrated that the strong relationship found between ENSO and seasonal lightning activity at numerous locations globally can potentially be applied for accurately predicting convective storms activity multiple seasons ahead.

In the absence of consistent multi-decadal observational datasets, Allen and Karoly (2013) showed that reanalysis proximity soundings from ERA-Interim provide a robust indicator of severe convective storm environments, allowing the authors to construct a 33 year-long environmental climatology (1979-2011). Both Allen and Karoly (2013), and Dowdy and Kuleshov (2014) noted a local maximum of Australian lightning frequency for the SEQ and the adjacent northern New South Wales regions. However, local-scale analysis (<10 km) of hotspot activity was limited due to the coarser spatial resolution of the datasets applied in the studies (1.5° and 7.5° degree, respectively). Climatological analysis of observational soundings can also be applied to investigate environments supportive of storms (Wilson et al. 2013; Peter et al. 2015). While this approach is useful for identifying large-scale regimes associated with convection, spatial identification of boundaries at synoptic scales (e.g., fronts, troughs) and mesoscale (e.g., sea breeze, gust fronts), is absent.

The continual growth of weather radar archives and computing capabilities provides the opportunity to develop a climatological analysis on much finer spatial (1 km or less) and temporal (6 – 10 minutes) scales than possible with other reanalysis, or other observational datasets (Cintineo et al. 2012; Fabry et al. 2013; Nisi et al. 2016). At these scales, the lifecycle of individual convective cells can be examined in addition to the influence of PBL convergence zones, including sea breezes (e.g., Wakimoto and Atkins 1994; Wilson and Megenhardt 1997), gust fronts (e.g., Weckwerth and Wakimoto 1992; Kingsmill 1995; May 1999), orographic effects (e.g., Weckwerth et al. 2011; Nisi et al. 2016) and urban landscapes (e.g., Niyogi et al. 2011; Haberlie et al. 2015b).

From a climatological perspective, the spatially and temporally variable nature of both convergence zones and convective storms presents a considerable challenge for understanding long-term trends in behaviour. The most comprehensive reconstructions are derived from remotely sensed products, including geostationary satellite images of the

cloud field (e.g., King et al. 2003; Azorin-Molina et al. 2009), clear air retrievals from weather radar (e.g., Wilson and Schreiber 1986; Wilson et al. 1994), and radar refractivity (Wakimoto and Murphey 2009). Given the significant processing difficulties and limited availability of these datasets across multi-years, the most robust long-term sea breeze climatologies are still developed using weather station sites through the automated detection of changes associated with the arrival of the maritime air mass (Biggs and Graves 1962; Simpson et al. 1977; Azorin-Molina et al. 2011). Applying this methodology to a transect of stations can also provide a climatological analysis of sea breeze characteristics, including the propagation speed and inland arrival times.

2.4 Regional Setting

The coastal setting of SEQ hosts a range of landscapes (Fig. 2.5). Anthropogenic land use across SEQ is split into rural and agriculture in the western inland region, and a rapidly growing urban population of approximately 3.4 million across the coastal plains in the east, centred on the capital city of Brisbane (Australian Bureau of Statistics 2013). Bordering the western and southern limits of SEQ are mountain ranges with sub-tropical rainforest and wet sclerophyll forest above an altitude of 500 m, while a complex coastline of large sand islands (Moreton and North Stradbroke), and bays extend along the eastern periphery. This diverse setting of SEQ supports topographical, sea breeze and UHI circulations (Physick 1993; Khan and Simpson 2001), which have been shown to interact with convective storms (Callaghan 1996; Richter et al. 2014). Climatologically, SEQ and adjacent northeast NSW experience more severe storm environments than other region in Australia (Allen and Karoly 2014), and the highest lightning frequency outside the tropical region (Dowdy and Kuleshov 2014).

2.4.1 Local Forcing

The initiation of convective storms in SEQ is commonly associated with elevated triggering along the ranges bordering the south and west. The importance of this mechanism was first highlighted in a review of severe storm events by Callaghan (1996), and later confirmed through a 6 year radar climatology of convective storms (Peter et al. 2015). Prevailing westerly flow above the PBL indicates a leeward convergence zone is favoured on the coastal side of the ranges; however, results from previous studies are too coarse to identify this potential trigger. Furthermore, preservation of the native mountain vegetation

supports large areas of sub-tropical rainforest, particularly across the Scenic Rim, indicating favourable high moisture parcels for convective storm development (Brooks and Dotzek 2008).

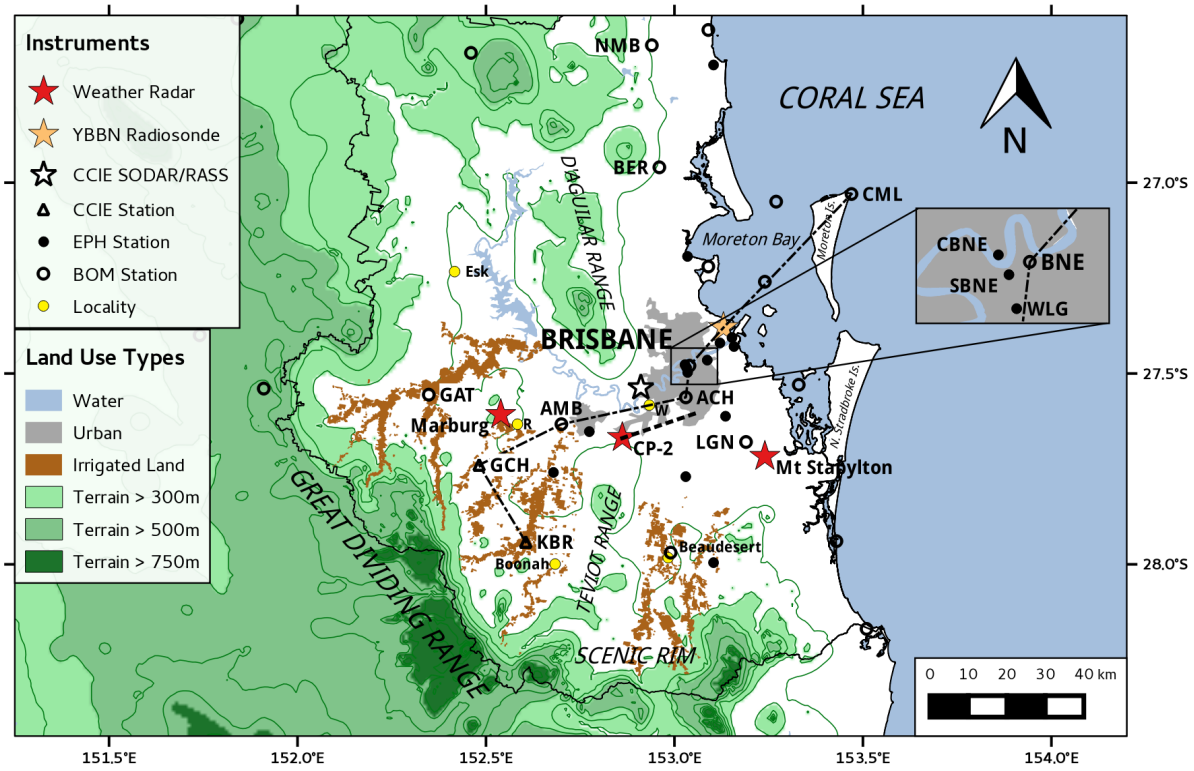

Figure 2.5: The Southeast Queensland region of Australia. Locations of CCIE, BoM and EPH instruments are shown. Weather stations referenced thought text and figures are labelled. More densely populated urban areas are shaded grey and areas of irrigated agriculture are shaded brown. Terrain is contoured at 200 m intervals from 200 m ASL, with light, moderate and dark green shading for areas above 300 m, 500 m and 750 m respectively. Towns of Wacol and Rosewood marked with a "W" and "R", respectively. Referenced throughout the text.

Under ambient conditions that support diurnal heating, sea breeze conditions prevail over SEQ. Early studies of air pollution transport mechanisms for SEQ indicate the sea breeze regularly interacts with the elevated landscape bordering the coastal plains through coupling with upslope flow and channelling (Abbs and Physick 1992). These interactions lead to an acceleration of the sea breeze front between the D'Aguilar and Teviot Ranges into the southwestern region of SEQ. Callaghan (1996) documented the presence of the sea breeze in association with convective storm intensification, resulting in the most

significant events to impact SEQ over the past 50 years. The mechanism for intensification remained unresolved by the author; noting that *"The challenge again here was whether to forecast major development in the storm complex when it reached the [sea breeze] convergence zone".* Simulations of the SEQ sea breeze indicate it provides a 3-4 °C of cooling at 10 m over coastal regions, with the effect diminishing as the airmass advects further inland . Observational and modelling evidence indicate that the urban landscape of Brisbane generates an UHI, leading to a temperature increase of between 1 to 6 °C compared to rural areas (Khan and Simpson 2001). Comparable UHI intensities have been documented for coastal cities globally (Santamouris 2015). Numerical simulations of the Brisbane UHI indicates the locally enhanced land-sea temperature gradients modifies the sea breeze and land breeze onset times, and development of nocturnal drainage flow from the inland ranges. In particular, sea breeze flow over the city was accelerated by several hours across the northeast suburbs of Brisbane, displacing the UHI and associated convergence to the southwest. Sea breezes modified by the UHI have also been simulated for coastal cities internationally (Freitas et al. 2007; Dandou et al. 2009); however, no observational studies exist to support this process.

2.4.2 Larger Scale Drivers

In addition to the sea breeze, (Callaghan 1996) noted that weak cold fronts, commonly referred to as southeasterly changes, are associated with some of the most significant severe storms in SEQ. Under this environment, storms often propagate with the front, suggesting updrafts couple with favourable horizontal shear and convergence assisted parcel lift (Johnson and Mapes 2001; Sills et al. 2004). Climatological investigation of southeasterly changes for SEQ storm environments is absent in spite of the case study evidence. In addition, drylines and upper level troughs are recognised as important synoptic features for the preconditoning and triggering of storms in SEQ (Callaghan 1996).

Climatological analyses exceeding one decade in length also provides the opportunity to investigate inter-annual variability of SEQ convective storm environments, including the relationship with ENSO. Using the BoM severe storms archive, Yeo (2005) found that reports of severe storms days were 60% (30%) more likely during the neutral (El Niño) phase of ENSO than La Niña. Furthermore, Yeo noted than this correlation increased further when only the negative phase of the IPO (pre-1977) was considered, suggesting a

coupling with multi-decdal processes. More recent work by Allen and Karoly (2013) applying calibrated convective indices of severe storm environments derived ERA-Interim reanalysis dataset showed a less certain relationship with ENSO for SEQ and across Australia. Contrasting conclusions between these studies is possibly related to the limitation of the underlying datasets discussed in section 2.3.

2.4.3 Historical Context

The socio-economic impact of frequent convective storm activity in SEQ is recognised through ongoing efforts to understanding the drivers of convective storm activity (Callaghan 1996; Richter et al. 2014; Peter et al. 2015). Hail, in particular, poses the greatest threat to agriculture and property, where losses from multiple events have each exceeded $1 billion AUD (Insurance Council of Australia 2015).The combination of a southeasterly change and sea breeze boundaries have been documented in association with the most significant severe storm events in SEQ: the 1973 tornadic storm through Brisbane (Holcombe, G and Moynihan 1978), a severe hailstorm in 1985 (Callaghan 1996) which resulted in normalised insured losses of $2.1 billion AUD (Insurance Council of Australia 2015), the 1989 Northern suburbs tornado (Callaghan 1996), a particularly intense wind storm event through the northwest suburbs of Brisbane in 2008 (Richter et al. 2014), and again in 2014 for a convective storm which produced giant hail (8 - 9 cm) through Brisbane and the inner suburbs (Parackal et al. 2015), resulting an insured losses exceeding $1.4 billion AUD. Despite the seemingly erratic nature of individual events, experienced forecasters have accumulated an awareness of convective storm hotspots in parts of SEQ (Tony Wedd, personal communication, April 15 2010). This anecdotal evidence of hotspots activity and the repeated occurrence of the southeasterly change – sea breeze environment in case study literature merits further a comprehensive study of the climatological and meteorological processes which favour convective storms activity in SEQ.

CHAPTER 3

EXPERIMENTAL METHODS AND DESIGN

Post-storm rainbow at Marburg on the 3 January 2014 (Anthony Lumsden)

Chapter 3 is based upon the following published article

Soderholm J, McGowan HA, Richter H, Walsh K, Weckwerth T, Coleman M. 2015: The Coastal Convective Interactions Experiment (CCIE): Understanding the role of sea breezes for hailstorm hotspots in Eastern Australia. ***Bulletin of the American Meteorological Society*** doi:10.1175/BAMS-D-14-00212.1.

Chapter 3. Experimental Methods and Design

3.1 Introduction

The purpose of this chapter is twofold. First, it is to demonstrate that significant variability in spatial convective storm frequency exists on the 2-20 km scale in the study area SEQ, Australia. Second, it is to introduce the CCIE design and discuss the underlying meteorological processes observed in an effort to improve the concepts and tools applied for short-term convective storm warnings and forecasts.

3.2 Methods

3.2.1 Radar Derived Climatology of Hailstorms

For the CCIE climatological analysis, a continuous eighteen year (July 1997 to June 2015) volumetric reflectivity radar dataset was sourced from the 1.9-degree S-band weather radar located at Marburg, 50 km west of Brisbane (Fig. 2.5). In Australia, the Marburg dataset is of unprecedented length, providing a unique opportunity to explore long-term convective storm frequency within the region. Regular calibration of the Marburg radar transmitter at intervals of 3-6 months ensures a consistent long-term record. Due to its central location, this radar provides good coverage across SEQ, including the city of Brisbane. Observations within a 16 km radius of this radar were excluded from the analysis due the absence of overhead scanning, while data beyond 100 km in range were excluded due to poor spatial resolution and increasing height of the low-level beam above the surface. A cell-based analysis of this archive was performed using a MATLAB implementation of the identification, tracking and selected analysis algorithms from the WDSS-II (Lakshmanan and Smith 2007). The WDSS-II algorithms were selected for their adaptability during cell detection and consistent cell tracking under a variety of storm modes (e.g., linear systems; supercells). Convective storm cells were detected using the watershed method proposed by Lakshmanan et al. (2009) using a minimum reflectivity threshold of 35 dBZ over a depth of at least 3 km across a minimum aerial extent of 15 km^2. Association of cells between consecutive radar volumes to form storm tracks were computed using the hybrid approach developed by Lakshmanan and Smith (2010).

To provide a proxy for actual hail severity, one kilometre Maximum Expected Size of Hail (MESH) grids (Cintineo et al. 2012) were computed for each storm cell instance and automatically merged for the associated storm track into continuous swaths, comparable to the method developed by Basara et al. (2007). To derive MESH, first the hail kinetic energy (Ė) is derived using weighting function for precipitation types using equation 3.1 (Witt et al. 1998).

$$\dot{E} = 5\,X\,10^{-6}\,X\,10^{0.0854\,Z}\,W(Z)$$

where

$$W(Z) = \begin{cases} 0 & for\ Z \le Z_L \\ \dfrac{Z - Z_L}{Z_U - Z_L} & for\ Z_L < Z < Z_U \\ 1 & for\ Z \ge Z_U \end{cases} \qquad (3.1)$$

where Z is reflectivity in dBZ, W(Z) is the weighting function used to define a transition zones between rain and hail reflectivity where Z_L = 40 dBZ and Z_U = 50dBZ. This parameter allows for the calculation of the severe hail index (SHI) in equation 3.2.

$$SHI = 0.1 \int_{H_T}^{H_0} W_T(H)\,\dot{E}\,dh$$

where

$$W_T(H) = \begin{cases} 0 & for\ H \le H_0 \\ \dfrac{H - H_0}{H_{m20} - H_0} & for\ H_0 < H < H_{m20} \\ 1 & for\ H \ge H_{m20} \end{cases} \qquad (3.2)$$

Here H_0 is the height of the storm base, H_T is the height of the storm top, H_{m20} is the height of the -20°C level, H_0 is the height of the 0°C level and W(Z) is the weighting function used to define a transition zones between rain and hail reflectivity. Finally, MESH can be calculated by equation 3.3.

$$MESH = 2.54\,(SHI)^{0.5} \qquad (3.3)$$

The thermal weighting of MESH is constructed from the physical understanding that most hail stone growth likely occurs between -10 °C and -30 °C (Knight and Knight 2001). Despite the over-forecasting bias of hail size by MESH (Wilson et al. 2009), Cintineo et al. (2012) indicated that it can provide a useful discriminator for the presence of hail using a lower MESH threshold of 21 mm. This threshold is applied for the purpose of this study to provide the largest possible sample size of hailstorms.

The 10-minute interval of the Marburg radar volumes creates significant spatial discontinuities between MESH grids from an individual storm. To reduce this effect, MESH grids are converted into binary grids using a threshold filter set at the minimum value (21 mm) and sequential binary regions along a track are merged (using a convex hull approach) to produce a continuous swath, thus alleviating the discontinuities. By applying the above technique across the entire processed dataset, a spatial climatology of hailstorm frequency can be produced for SEQ. Fig. 3.1a shows local maxima of enhanced hailstorm activity in SEQ. The first region extends from the southwest valleys around the township of Boonah (the Scenic Rim region; see Fig. 2.5) to the north-northeast onto the southern suburbs of Brisbane. A second local maximum in hailstorm frequency occurs on the northern valleys near the town of Esk. Both hotspots are well known to experienced local forecasters as the primary regions for hailstorm activity in SEQ. Initial explanatory hypotheses provided by local forecasters for the more significant Boonah region hotspot centred on the arrival of the sea breeze front in western SEQ, coinciding with the development of convective storms on the southern and western ranges, and increasing boundary layer favourability for deep convection across this region.

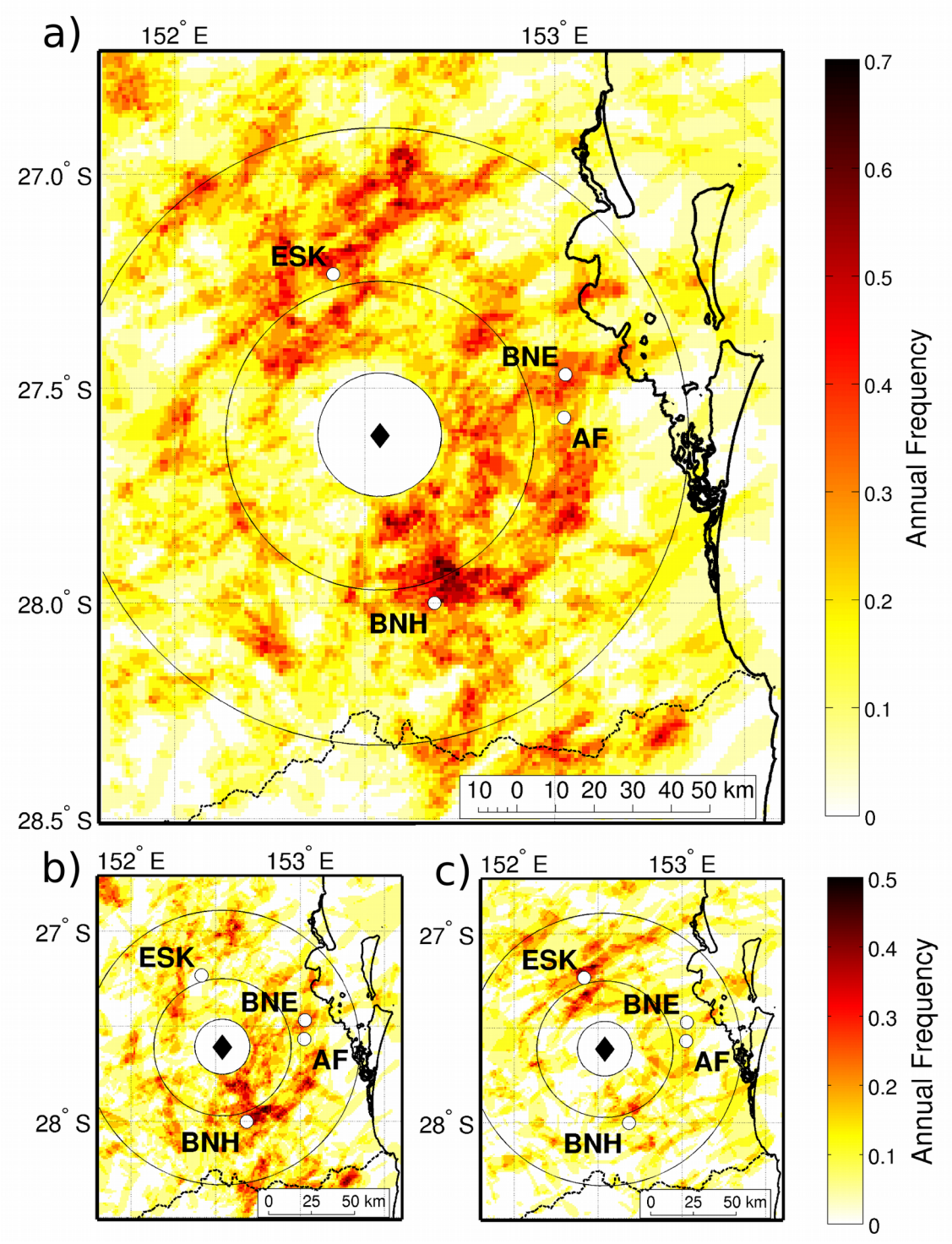

Figure 3.1: Annual cumulative MESH swaths (sum of all MESH values averaged by the number of years in the climatology) for 21 mm threshold for (a) all days. (b) Sea breeze days (c) Non-sea breeze days. Towns marked include Brisbane (BNE), Archerfield (AF), Boonah (BNH) and Esk (ESK). Marburg radar location marked with black diamond and range rings shown at 16 km, 40 km and 80 km.

3.2.2 Sea Breeze Detection

To explore the sea breeze influence upon hailstorms in SEQ, an automated filter-based algorithm was implemented to identify sea breeze days using surface weather station observations (Azorin-Molina et al. 2011). The Archerfield weather station was selected for this climatology due to its location in the western suburbs of Brisbane, guaranteeing that the sea breeze front had propagated at least 25 km inland from the coastline (Fig. 2.5, 3.1). Direct detection of the sea breeze in proximity to the Boonah and Esk regions was not achievable due to the absence of surface weather stations. In comparison to coastal weather stations, the commonly expected temperature drop associated with the passage of the sea breeze front was often absent for the Archerfield site, presumably due to enhanced mixing of near-surface air as it propagates onshore (Novak and Colle 2006). Consequently, the filtering process relies on identifying a series of kinematic, moisture and temporal characteristics of the sea breeze (Fig. 3.2). A verification contingency table (Table 3.1) estimates that the probability of detection (POD) for this method is 81%, with the false alarm ratio (FAR) of 19% (equation 3.4). These scores are comparable to the performance of the Azorin-Molina et al. (2011) implementation, indicating that the detection methodology is suitable for SEQ.

$$POD = \frac{number\ of\ days\ when\ sea\ breezes\ were\ predicted\ \text{and}\ observed}{total\ number\ of\ days\ observed}$$

$$FAR = \frac{number\ of\ days\ when\ sea\ breezes\ were\ predicted\ but\ not\ observed}{total\ number\ of\ days\ predicted} \qquad (3.4)$$

Following the detection of 1,893 sea breeze days (4,316 other days) across the eighteen year period, the hailstorm climatology was divided accordingly. A clear change in the spatial hailstorm frequency is apparent where hailstorms in the Boonah region are more frequent on sea breeze days and suppressed on non-sea breeze days (Fig. 3.1b,c). In contrast, hailstorms within the Esk region remain relatively unaffected by the presence of sea breeze activity due to the coastal ranges east of this site. For example, the Froude number of a 500 m deep sea breeze front moving at 5 m s^{-1} for the 700-800 m high D'Aguilar Ranges (see Fig. 2.5 for location) remains << 1, indicating topographic blocking would occur of onshore flow into the Esk region. In contrast, no significant topography impedes the propagation of the sea breeze into the Boonah region from the northeast.

This preliminary analysis suggests that the sea breeze circulation and associated large-scale conditions influence the spatial distribution of hailstorms over SEQ.

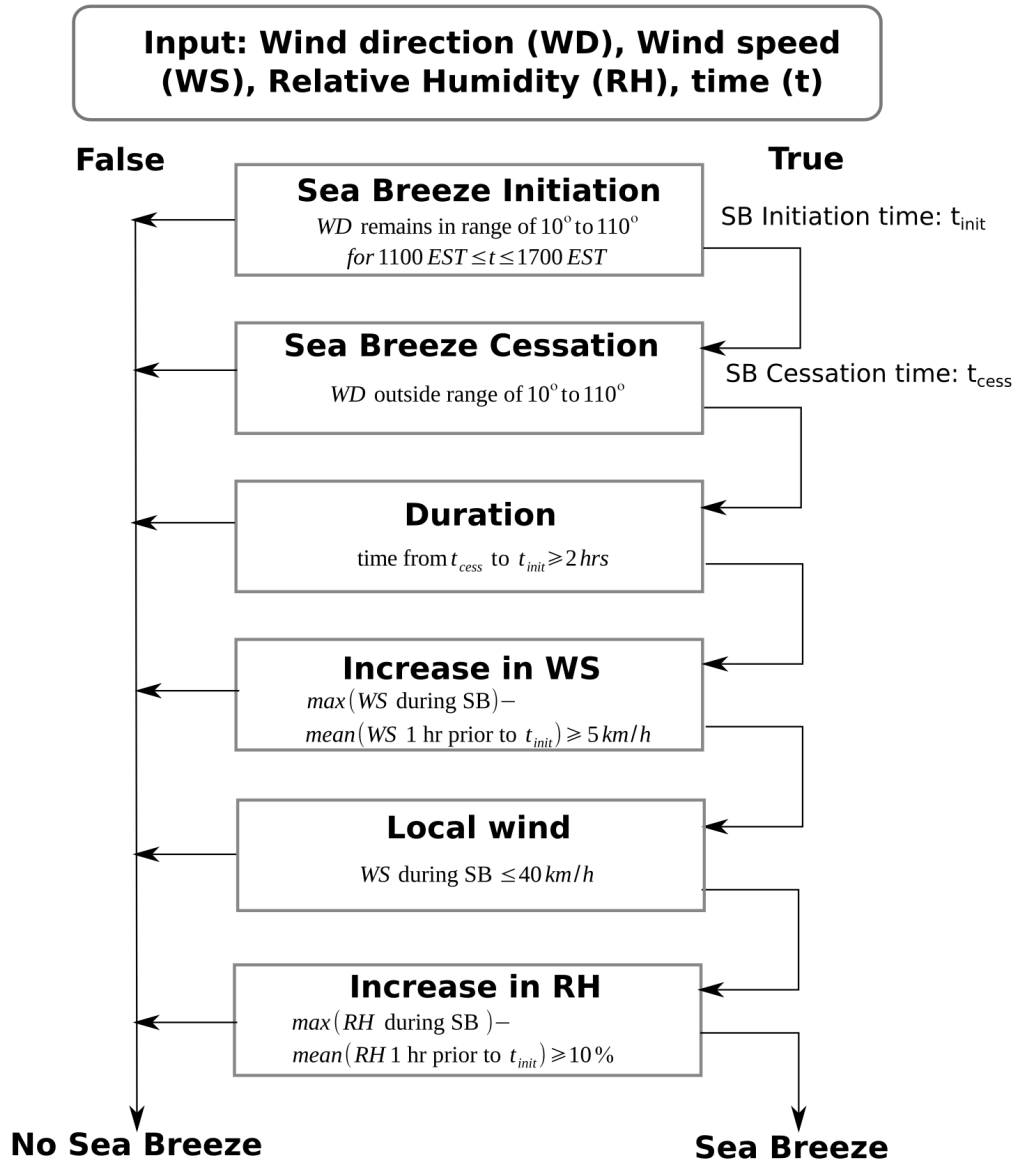

Figure 3.2: Flow diagram showing filters applied to identify sea breeze days based on a single surface weather station dataset at Archerfield across the 17 year period from 1997 to 2014.

Table 3.1: Contingency table for sea breeze detection method verification

	Observed Sea Breeze		
Predicted Sea Breeze	*TRUE*	*FALSE*	*TOTAL*
TRUE	170	41	211
FALSE	40	499	539
TOTAL	210	540	750
Probability of Sea Breeze Detection	0.81		
Probability of non-Sea Breeze Detection	0.92		

3.3 Experiment Motivation and Strategy

The initiation of deep convection along the sea breeze front convergence zone is a well-documented phenomenon (e.g., Miller 2003; Fovell 2005). Florida, in particular, has hosted extensive field programs to investigate this process (e.g., Atkins et al. 1995; Kingsmill 1995; Wilson and Megenhardt 1997), of which some cases have been simulated numerically (e.g., Nicholls et al. 1991; Fovell and Dailey 1999); however, concepts developed for this low-lying peninsula, which commonly produces converging sea breezes from the west and east coasts, have limited application for continental coastlines such as SEQ with significant inland topography. The physical setting found along much of eastern Australia is such that deep convection is most frequently initiated by the Great Dividing Range and lesser coastal ranges (see Fig. 2.5 for location). Under prevailing upper-level westerly steering flow, these storms then move onto the coastal plains, where they often interact with the sea breeze front and post-frontal air mass, in contrast to storms initiating along the sea breeze front. Numerous reports over the past 30 years have documented this mode of interaction in association with the highest impact storm events for the Sydney and Brisbane regions, which resulted in cumulative insured losses exceeding $10 billion AUD (Holcombe, G and Moynihan 1978; Callaghan 1996; Harper and Callaghan 1998; Australian Emergency Management Insitute 2014; Richter et al. 2014). Despite the historical significance of sea breeze – cold pool interactions for eastern Australia, research remains limited to a small body of anecdotal case studies.

To understand how the sea breeze interaction can modify existing convective storms, it must be considered with respect to the fundamental ingredients for deep convection, namely the role of buoyancy and shear (e.g., Doswell 2001). Relative to the western continental air mass (in SEQ), the sea breeze is generally considered as cool, moist and stable. However, modification of the sea breeze via entrainment of warming near-surface air during overland flow promotes increased buoyancy (Simpson et al. 1977). Subtle changes in boundary layer stability are known to have significant effects upon the likelihood of initiating convective storms (Weckwerth 2000; Weckwerth et al. 2008). In addition to modifying buoyancy, the sea breeze generally augments the magnitude of near-surface vertical shear normal to the coastline (east to north easterlies), typically opposing in direction to shear generated by the cold pool forward flank (eastern edge) for convective storms moving under prevailing ambient westerly to south-westerly steering

flow. The net tendency from these opposing shear profiles potentially promotes deeper lift along the cold pool interface, particularly for environments lacking strong ambient low-level environmental shear (e.g., Thorpe et al. 1982; Rotunno et al. 1988). Furthermore, enhanced convection has also been documented observationally for colliding gravity currents (e.g., Wilson and Megenhardt 1997; May 1999; Karan and Knupp 2009). The hypothesised kinematic and thermodynamic processes that take place during an interaction reside at spatial scales that are difficult to accurately initialise or reproduce in numerical models for individual events; therefore an intensive observational approach was considered necessary.

The field campaign phase of the CCIE was designed to capture both the properties of the convective storm and the local environment prior to, and following an interaction with the sea breeze. Field work was conducted across two warm seasons, the first extending from 20 November 2013 until 31 January 2014, while the second period from 15 October 2014 to 31 January 2015. The network of BoM operated radars, automatic weather stations and a radiosonde facility in SEQ formed the backbone of the CCIE. Furthermore, the radars included the polarimetric dual-wavelength (S- and X-band) CP-2 radar and the operational Mt Staplyton S-Band Doppler radar (Fig. 2.5). The proximity of CP-2 to the storm hotspots identified in SEQ, and its exemption from operational surveillance duties, prioritises the radar as a core instrument for the experiment. Building upon the existing BoM network, additional instrumentation was deployed in mobile and static configurations. To complement the Brisbane Airport radiosonde profiles of the sea breeze close to the coast, a SODAR wind profiler and RASS array were deployed on the western fringe of Brisbane, 30 km inland (Table 3.2, Fig. 2.5). A lack of BoM automatic weather stations throughout the Boonah convective storm hotspot prompted the deployment of three additional stations in this region to improve monitoring of sea breeze penetration and inland air mass characteristics.

In comparison to a sea breeze, the propagation and geographic regularity of convective storms is considerably less predictable, presenting a significant challenge for in-situ observations. Over the last two decades, the international community has met this challenge through the use of mobile instrumentation, in particular the use of mobile weather radar (e.g., Weckwerth et al. 2004; Wurman et al. 2012). In an Australian first, a mobile pulsed Doppler lidar was deployed for the 2013/2014 field campaign and a mobile

polarimetric X-band radar (UQ-XPOL) was operated for the 2014/2015 campaign (Fig. 3.3, Table 3.2).

Table 3.2: Summary of Instruments and sensors for the CCIE

Platform	Operator	Instrument	Sampling strategy	Season
Doppler scanning lidar	UQ	Leosphere WL100S	Targeted RHI	1
Mobile X-band radar	UQ	Furuno WR2100	Targeted RHI	2
CP-2	BoM	NCAR (X & S band)	Sequenced targeted RHI and PPI scanning	2
Mt Stapylton radar	BoM	Meteor 1500-S	6 min volumetric cycle	Both
Marburg radar	BoM	WSR74-S	10 min volumetric cycle	Both
SODAR profiler	UQ	Scintec AG MFAS	Continuous	Both
RASS profiler	UQ	Scintec AG RAE1	Continuous	Both
Radiosonde System	BoM	Vaisala RS92	00Z and on request	Both
Mobile radiosonde System	UQ	Vaisala RS92	02Z and on request	2
Mobile weather station	UQ	Vaisala WTX520	Targeted Deployment	Both
Weather Stations	UQ	HOBOnet Systems	3 fixed deployments	Both
Weather Stations	BoM	Various	Continuous	Both

Figure 3.3: Photograph of the UQ-XPOL deployed with mobile weather station at Gatton, SEQ (see Fig. 2.5) on 26 November 2014.

Given that winds behind a gravity current boundary such as sea breezes or gust fronts are generally perpendicular to the boundary, radial winds observed at low elevation angles in scans aligned normal to the front would be expected to closely approximate the true wind velocity (Wakimoto 1982). This RHI scanning strategy was utilized extensively by CP-2, the mobile lidar and XPOL to capture the vertical wind structure for application to the aforementioned shear balance arguments. Complementary mobile thermodynamic observations were collected by a truck GPS sounding system and automatic weather station. The complex terrain, large areas of vegetation and limited road network of SEQ limit the availability of suitable deployment sites for mobile equipment. Given the time-critical observations required for convective storms, 109 sites were selected and manually verified across SEQ to improve deployment efficiency and minimise the potential for poor site selection (Fig. 3.4). Deployment sites ahead of convective storms which were expected to interact with the sea breeze circulation were selected on the fly as rioritised targets for CP-2 and UQ-XPOL during CCIE operations. Radar datasets were processed using the python Atmospheric Radiation Measurement (ARM) radar toolkit (py-ART) package (Helmus and Collis 2016).

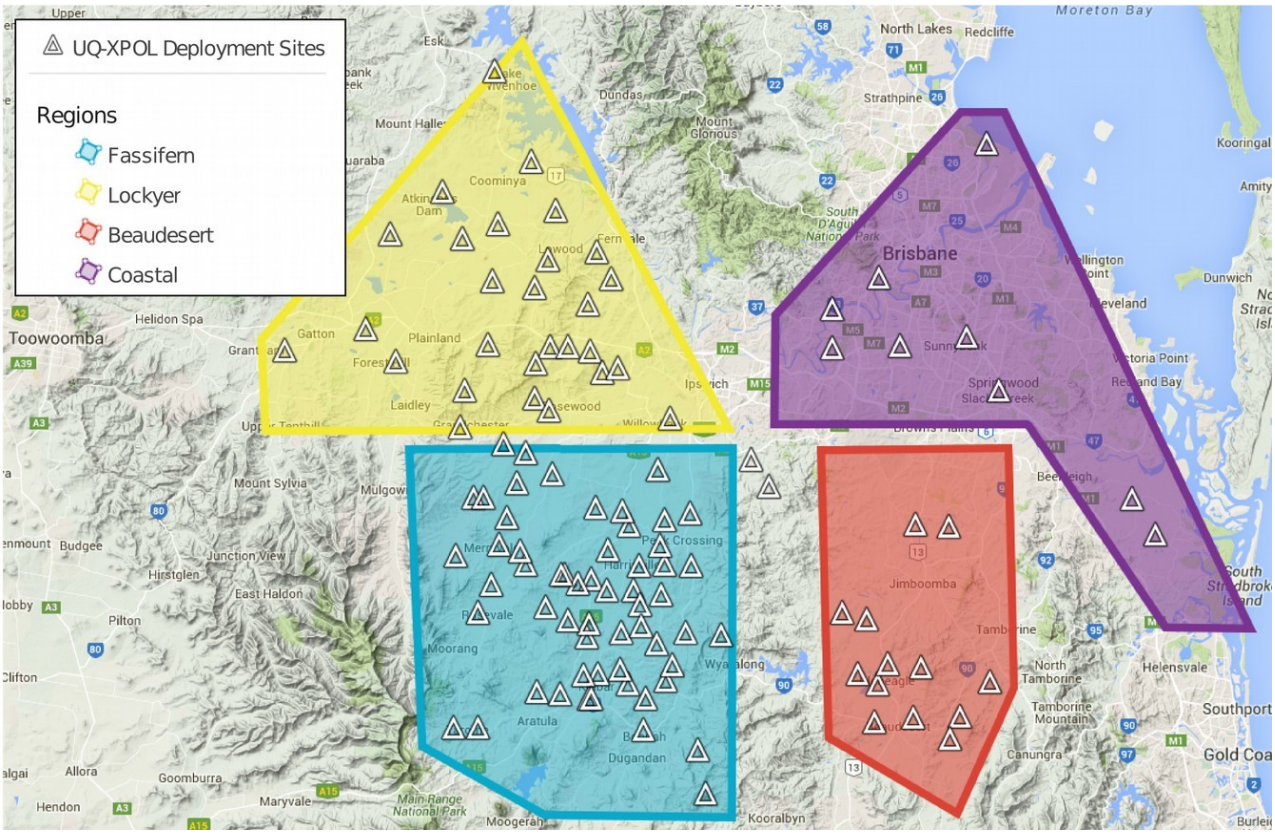

Figure 3.4: Operations map of UQ-XPOL deployment sites during the CCIE. Deployment sites grouped into four regions depending on location and topographical features.

3.4 Highlights of Preliminary Findings

The fine temporal and spatial resolution datasets collected during CCIE, particularly from the CP-2, UQ-XPOL radar and Doppler lidar instruments, highlight the complexity which inherently occurs at the meso-gamma scale of cold pool – sea breeze interactions. Here three examples are presented for different conditions: 1) the pulsed advance of a sea breeze front on 28 November 2013, 2) a multicell convective storm cold pool on 27 December 2013, and 3) a collision between a sea breeze and a squall-line cold pool on 11 December 2014.

3.4.1 Pulsed sea breeze of 28 November 2013.

On 28 November 2013, the sea breeze front was observed 31 km west of the coastline using the mobile pulsed Doppler lidar in the Brisbane suburb of Wacol, 8 km west of Archerfield (see Fig. 2.5). Lidar RHI scans through the sea breeze shows turbulent flow, particularly around 1300 m (Fig. 3.5a). Rather than propagating as a single front, a staggered passage of three temporally coherent sea breeze pulses was observed over a period of 28 minutes, each separated by a region of weak flow (not shown). Each pulse decreased in depth (1250 m to 750 m) and increased in inbound velocity (4 to 8 ms^{-1}) at a periodicity of approximately 10 minutes until the arrival of the stable maritime flow. In addition to these post-frontal oscillations, the scalloped boundary between the inbound gravity current and outbound return flow aloft in Fig. 3.5b suggests possible Kelvin Helmholtz wave activity (e.g., Chiba 1997; Plant and Keith 2006). Kelvin Helmholtz wave activity is also evident along the leading edge of the sea breeze front in the 03:04:49 UTC RHI (not shown). Puygrenier et al. (2005) noted that a complex physical setting (complex coastline, urbanised terrain, topography), similar to SEQ, is related to the pulsed behaviour of the sea breeze flow. The authors suggested that increased overland mixing depth of the sea breeze forces variability in the underlying land-sea pressure gradient, driving the observed pulses in maritime flow. This deviation from the standard gravity current description of a sea breeze front must be considered during an interaction with a convective storm cold pool.

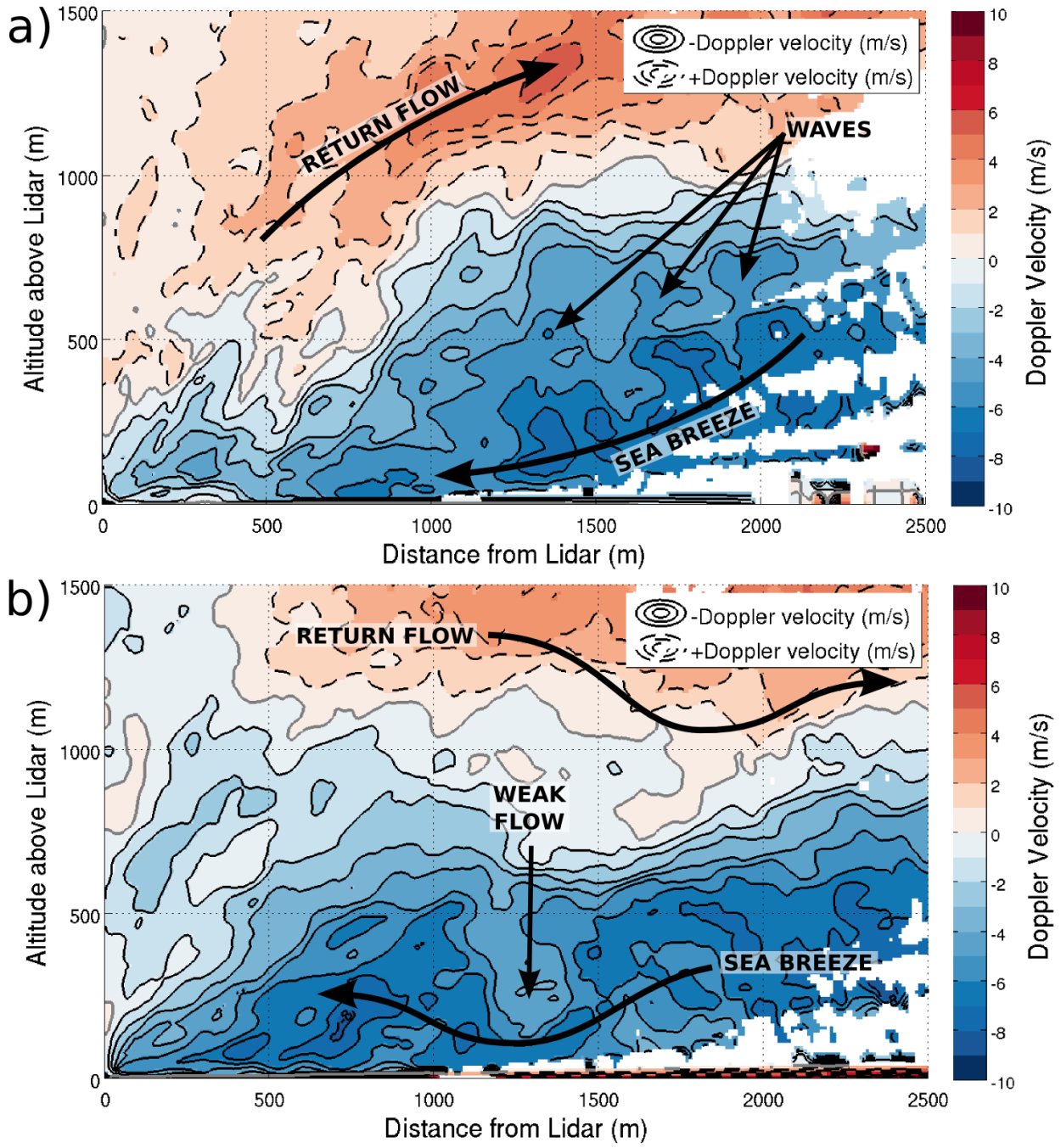

Figure 3.5: Vertical cross sections of Doppler lidar radial velocity for a sea breeze front advancing from the southwest (right to left) at (a) 03:10:07 UTC and (b) 03:25:50 on 28 November 2013 at -27.583°S 152.933°E (8 km west of Archerfield, Fig. 2.5) at an RHI azimuth of 42° TN. Inbound radial velocities are shaded in blue with solid contour lines, outbound radial velocities are shaded in red with dashed contour lines (contour intervals are 1 m s-1). The zero velocity isodop is shown in grey and arrows approximating the radial flow path shown in black.

3.4.2 Multicell Storm Cold Pool on 27 December 2013.

Convective storm cold pools are in a constant state of evolution from the initial downdraft to the dissipation of the convective cell, and the radially-outward-propagation of the gust front (e.g., Wakimoto 1982; Wilson and Megenhardt 1997). Doppler lidar observations of a multicell storm 8 km southwest of Marburg radar (see Fig. 2.5 for location) on the 27 December 2013 demonstrate this constant state of evolution. Marginal instability (SBCAPE of 1296 J kg^{-1}) and 0 – 6 km shear (8 ms^{-1}) observed by the Brisbane airport 00 UTC radiosonde release was indicative of a marginal multicell environment, suggesting cold pool evolution would be highly variable. In this case, two gust fronts were initially observed in the 03:20:22 UTC scan: a maturing gust front on the up-shear side of the cold pool exhibiting a tight velocity gradient at 1500 m from the lidar propagating into an older, less intense outflow region (Fig. 3.6a). Ninety seconds later, the maturing gust front collapsed from 500 m to approximately 250 m and the distinct boundary was lost as it merged with the existing gust front (Fig. 3.6b). Furthermore, an emerging convective downdraft evident in Fig. 3.6b leads to the deepening of the multicell cold pool from 250 m to 500 m at 03:25:08 UTC. This case highlights the rapid evolution of the cold pool depth and intensity on minute time scales. This variability again creates significant uncertainty that must be considered when analysing and predicting interactions with an advancing sea breeze front.

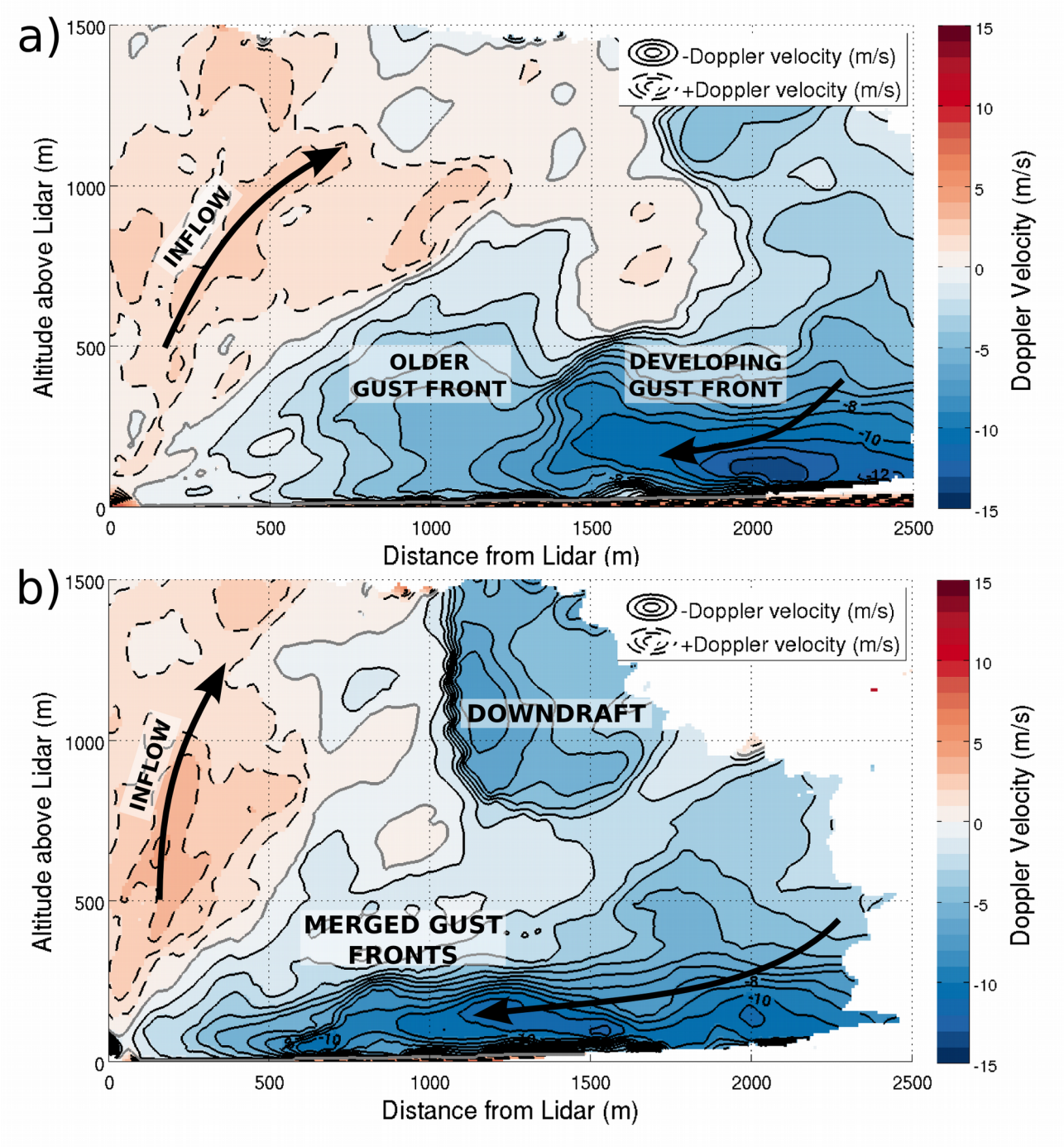

Figure 3.6: Velocity cross sections of Doppler lidar radial velocity for gust front at (a) 03:20:22UTC and (b) 03:21:58UTC on 27 December 2013 at -27.643°S 152.567°E (8 km southwest of Marburg radar; Fig. 2.5) at an RHI azimuth of 187.7° TN. Inbound radial velocities are shaded in blue with solid contour lines, outbound radial velocities are shaded in red with dashed contour lines (contour intervals are 1 m s-1). The zero velocity isodop is shown in grey and arrows approximating the radial flow path are shown in black.

3.4.3 Collision between a sea breeze and a convective storm cold pool on 11 December 2014

The sea breeze – convective storm cold pool interaction observed during CCIE on 11 December 2014 occurred approximately 50 km inland, a comparable distance to the majority of events observed throughout the two field campaigns. To explore the overland evolution of the sea breeze, three vertical wind profiles from various data sources were sampled along a northeast to southwest transect (Fig. 3.7a).

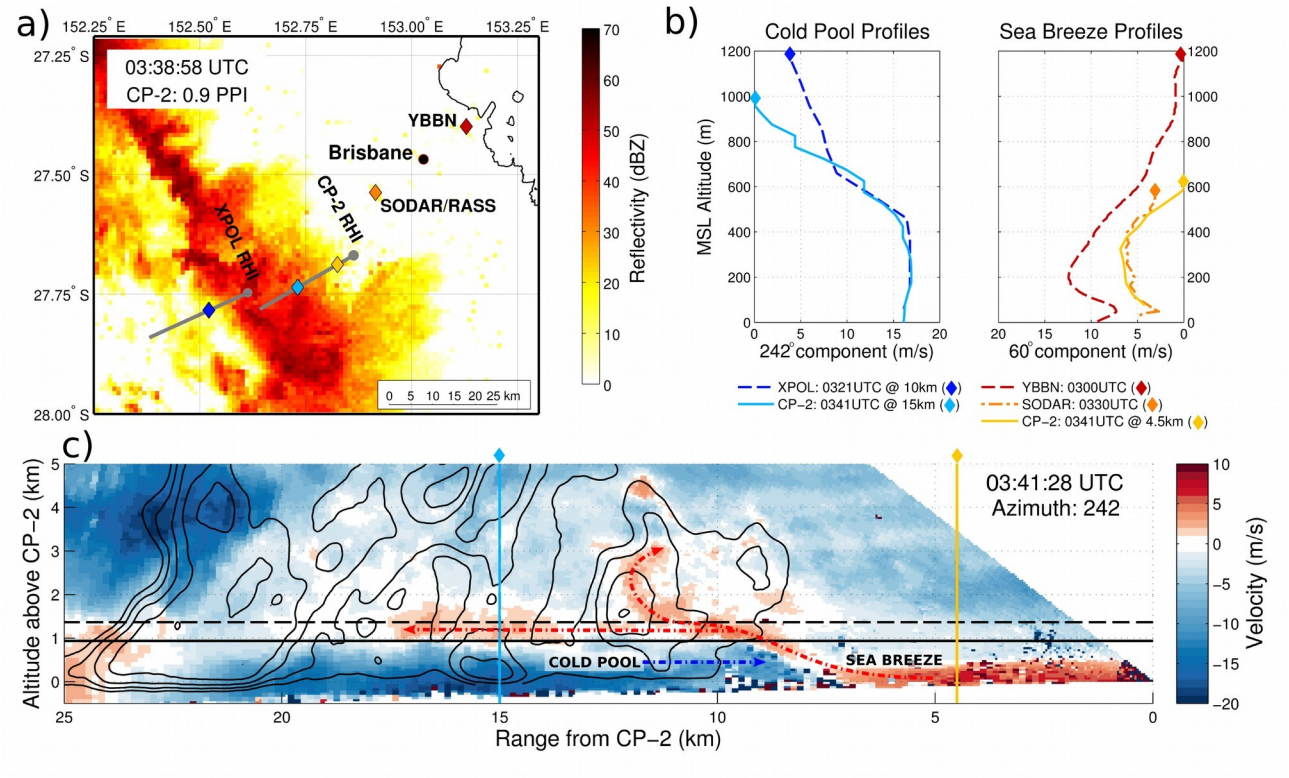

Figure 3.7: Analysis of a sea breeze and cold pool features on 11 December 2014. (a) 0.9° reflectivity PPI from CP-2 radar at 03:38 UTC with the locations of XPOL and CP-2 RHI scans (grey dots and lines) and associated vertical profiles (colored diamonds) shown. (b) Vertical profiles of the cold pool wind speed (242° component) based on CP-2 and XPOL; and the sea breeze wind speed (60° component) based on CP-2, airport radiosonde (YBBN) and SODAR observations. Colored diamonds associated with each vertical wind profile from (a) are shown in the legend and plot. (c) CP-2 RHI at 03:41 UTC with shaded radial velocity and contoured reflectivity from 35 dBZ in 5 dBZ steps. Level of free convection for the sea breeze (pre-sea breeze) air parcel is shown with a dashed (solid) line. Colored lines and diamonds indicate the location of profiles extracted from the CP-2 RHI for (a) and (b).

Starting from the northeast at Brisbane airport, an onshore wind profile derived from the 03:00 UTC (13:00 local time) radiosonde shows a distinct low level maximum of 12.5 ms^{-1} at 200 m within the 1200 m deep onshore component (60°) of the sea breeze circulation (red dashed profile in Fig. 6b). The next transect profile was observed 28 km to the south-west of Brisbane airport using a SODAR/RASS instrumentation at 03:30 UTC (orange dash-dot profile in Fig. 3.7b). Across this heavily urbanised segment of the transect, the sea breeze experienced a reduction in surface wind speed by approximately 50%, to 5 ms^{-1}. As previously noted in the pulsed sea breeze case study (28 November 2013), it is hypothesised that the increased surface roughness and urban heat island circulations across the city landscape contributed towards this modification of the sea breeze (Puygrenier et al. 2005). A final vertical wind profile was reconstructed using a CP-2 vertical cross section scan orientated 242°, opposite to the onshore component, at 03:41 UTC (yellow profile in Fig. 3.7b). This profile was extracted within the sea breeze air mass, immediately to the north-east of the cold pool gust front to provide a proximity wind profile representative of the interacting sea breeze. This profile shows limited change from the SODAR profile 11 minutes earlier, suggesting the sea breeze had reached a more steady kinematic state of inland propagation over the final 15 km segment (Fig. 3.7b).

Prior to the sea breeze interaction, the UQ-XPOL mobile radar was deployed 20 km south of Marburg Radar (Fig. 2.5) to observe the cold pool structure and dynamics. Analogous to CP-2, boundary-normal vertical cross section scans (Fig. 3.7a) were utilised to provide a pre-collision cross section of the cold pool structure. Between the 03:21 UTC UQ-XPOL scan and the 03:41 UTC CP-2 scan, the cold pool shear and depth appears unchanged (blue profiles in Fig. 3.7b). Such steady cold pool behaviour is dissimilar to the rapid evolution observed in the 27 December 2013 lidar case study (Fig. 3.6a,b). This continuity, in addition to the separation of the gust front from the convective cells (not shown for UQ-XPOL), suggests that the cold pool was in the later stages of its life-cycle (Wakimoto 1982). A mobile sounding launched 10 km north of Boonah at 02:30 UTC (not shown) indicates that the level of free convection (LFC) for an inland pre - sea breeze parcel was 986 m, approximately the same as the cold pool depth (Fig. 3.7c). Modifying this sounding using post sea breeze observations from Archerfield weather station at 03:00 UTC increased the LFC to 1251 m, above the depth of the cold pool induced lift (Fig. 3.7c). CP-2 radar observed the cooler (22° C) cold pool air collide and lift the warmer (28° C) sea breeze at 03:30:02 UTC (not shown). At 03:41:28 UTC a shallow 50 dBZ region is evident

behind (southwest of) the cold pool gust front head in the CP2 RHI (Fig. 3.7c) due to lifting in the region; however, the lofted sea breeze primarily manifested itself as horizontal flow above the cold pool. Kingsmill (1995) observed a similar lack of ascent above the cold pool following a sea breeze interaction and attributed this to a reduction in gust front depth. In contrast, no significant changes in gust front depth were observed immediately following the sea breeze collision for 11 December 2014 case study (Fig. 3.7b).

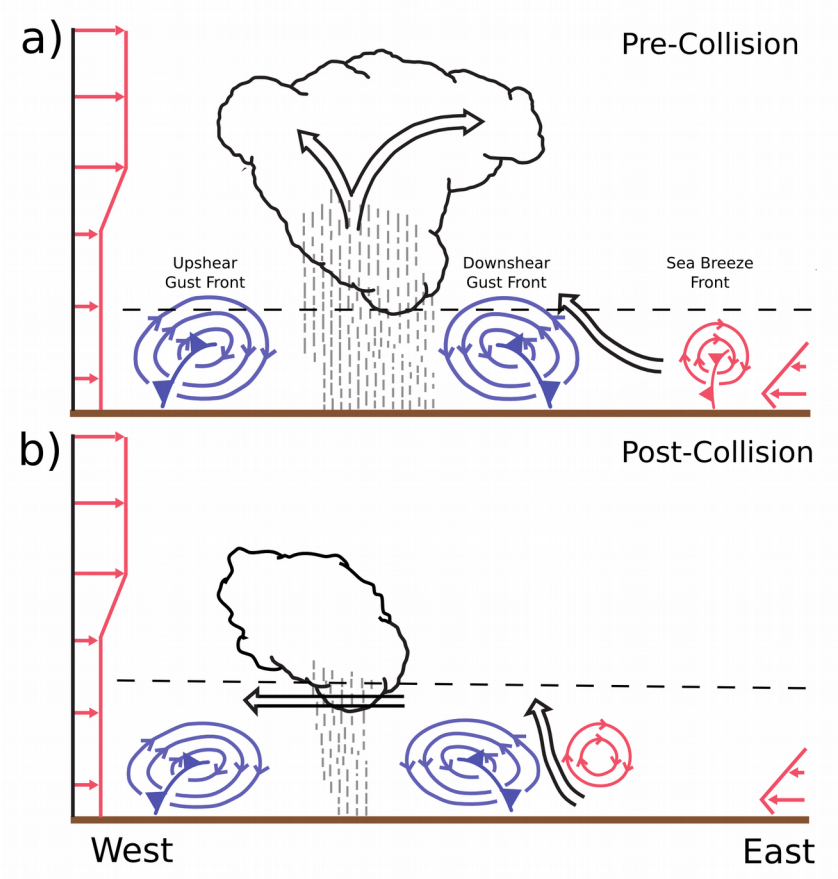

Figure 3.8: Conceptual analysis of 11 December 2014 convective storm – sea breeze interaction. (a) Prior to the collision, the cold pool circulation lifts surface air parcels above the ambient LFC (dashed line). (b) The introduction of the sea breeze circulation may reinforce the cold pool circulation and promote deeper lifting, however the higher LFC of the sea breeze air parcels (dashed horizontal line) remains above the deeper lifting depth, suppressing further updraft development. Adapted from Bryan et al. (2004), Fig. 3.

Following the sea breeze collision, the pre-storm surface to 1 km wind profile directed normal to the cold pool (Δu) transitioned from a weakly sheared environment (2.7 m s^{-1}) in the 02:10 UTC sounding profile at Boonah (not shown), to stronger shear (7.7 m s^{-1}) in the

03:41:28 UTC CP-2 RHI. Rotunno et al. (1988) showed that conditions for deep updrafts are optimised as the net vorticity generated in the low level shear balances the net buoyant vorticity from the cold pool. The convective storm cold pool boundary normal shear (Δu) at the time of collision (03:41:28 UTC) was 18.9 m s^{-1} through the surface to 1 km layer, suggesting that the sea breeze environment was more conducive for updrafts than the pre-storm environment. A conceptual schematic of the circulation tendencies associated with the sea breeze and cold pool shear is shown in Fig. 3.8 before and after the collision. Interaction between the cold pool gust front and sea breeze resulted in two counter-acting changes effecting updraft inflow: (1) deeper lifting from the opposing circulation tendencies and (2), a higher LFC. Despite this potential for deeper lifting, sea breeze air struggled to lift, possibly due to the elevated LFC, resulting in the rapid dissipation of deep convection as it crossed the sea breeze boundary (Fig. 3.8b).

3.5 Conclusion

The CCIE's integration of climatological analysis with an intensive field campaign has provided an opportunity for revealing complexities surrounding convective storm hotpots in complex physical settings like SEQ. An analysis indicates a relationship between the presence of the sea breeze activity at the Archerfield weather station site and an increase in hailstorms across the radar-derived climatology at Boonah. Field observations of the sea breeze – convective storm interaction events have begun to shed some light on the meteorology of convective storm hotspots in SEQ. In spite of the complex, fine-scale variability observed in sea breezes and cold pools, careful analysis of the 11 December 2014 event highlights the key thermodynamic and dynamical processes during an interaction for understanding the resultant storm activity. The future application of the concepts developed by the CCIE to sea breeze forecasts based on high resolution operational numerical weather prediction models is expected to improve operational nowcasting of events such as the 27 November 2014 hailstorm.

CHAPTER 4

SOUTHEAST QUEENSLAND HAILSTORM CLIMATOLOGY

Incoming storm at Rosewood on the 27 December 2013 (Christopher Chambers)

Chapter 4 is based upon the following submitted article

Soderholm JS, McGowan HA, Richter H, Walsh K, Weckwerth TM, Coleman M. 2016: Long-term trends and drivers of hailstorm variability in Southeast Queensland, Australia. ***Quarterly Journal of the Royal Meteorological Society.*** Accepted with minor revisions (8 June 2016)

Chapter 4. Southeast Queensland Hailstorm Climatology

4.1 Introduction

The following chapter builds upon the initial findings presented in chapter 3 (Soderholm et al. 2016) for the CCIE to develop an in-depth climatological understanding of climate, synoptic and local-scale drivers of hailstorms initiation, intensification and evolution in SEQ for the period extending from July 1997 to June 2015 (18 years). The datasets and methods applied in this study are presented in section 4.2, analysis and discussion of results are presented in section 4.3 followed by the conclusion in section 4.4.

4.2 Data and Methodology

4.2.1 Convective Storm Climatology

To generate a radar-derived climatology of SEQ convective storms, algorithms for identifying, tracking and analysing convective cells from the Weather Decision Support System – Integrated Information project were implemented (Lakshmanan et al. 2009, 2013; Lakshmanan and Smith 2010). Further information of the radar dataset and the climatology methods can be found in section 3.2.1. Reliability of hail detection using the MESH algorithm was tested using reports of hail (of any size) archived in the BoM Severe Storms Archive within 100 km radius of the Marburg radar site for dates overlapping the radar climatology dataset (305 reports). Verification was performed on a daily basis due to known issues with reporting times. Inconsistent recording of the hail report time throughout the archive limited the temporal resolution to the date of the event. Accordingly, report location and date was verified against the gridded MESH climatology using the minimum threshold of 21 mm to ensure the inclusion of all hail storms. Probability of detection (POD) by MESH (≥21 mm) within 10 km of a report was 79% across the 18 year archive, while the false alarm ratio (FAR), i.e. when a hailstorm is observed with MESH without a report, was 69%. For a smaller threshold for MESH, 10 mm, POD for reported hail increases to 92%, but at a cost of increased FAR (87%). The sparseness of public reports in the Severe Storms Archive is a significant factor in the high FAR of MESH, whereby a more consistent reporting source (i.e. insurance datasets) would be expected to improve the statistic. For the POD of the 21 mm MESH threshold, a similar value was calculated for municipal hail loss insurance data across 200 hailstorm days in Switzerland (average municipal area of

12.9 km^2) was calculated by Nisi et al. (2016), suggesting MESH is suitable for identifying hail in SEQ.

For the 1774 thunderstorms days identified in the Marburg radar climatology, 404 hailstorm days (with 3363 hailstorm cells) were identified as having at least one track containing a minimum of two associated cells from consecutive radar volumes, with at least one of these cells containing a MESH value ≥ 21 mm (see section 3.2.1). Additionally, the timing and location of hailstorm convective initiation (HCI) and hail development (HD) were computed. HCI is defined as the location of the first cell instance in a hailstorm track regardless of MESH value, comparable to the approach applied in previous studies (e.g., Lima and Wilson 2008; Weckwerth et al. 2011; Davini et al. 2012). Hail development is recorded when the maximum gridded MESH value of a cell transitions from < 21 mm in the previous time step to ≥ 21 mm in the current time step. This approach is similar to the convective enhancement detection technique developed by Weckwerth et al. (2011) to identify regions of storm intensification.

4.2.2 Sea Breeze Climatology

An automated, filter-based methodology developed by Azorin-Molina et al. (2011) was implemented for weather station data to diagnose sea breezes arrival times and inland penetration. Further information regarding the weather station dataset and sea breeze filter development is provided in section 3.2.2. The final algorithm consisted of a sequence of six filters designed to detect sea breeze through changes in wind direction and speed associated with the arrival, duration and cessation of the sea breeze, and an increase in relative humidity associated with the maritime air mass (Fig. 3.2).

4.2.3 Thunderstorm Synoptic Type Climatology

For the purpose of developing a robust synoptic-type climatology, the European Centre for Medium Range Weather Forecasting (ECMWF) ERA-Interim reanalysis was selected (Dee et al. 2011). Verification of ERA-Interim pseudo-soundings by Allen and Karoly (2014) for reported severe storm events within 200 km and 3 hours of an observed sounding indicated reasonable representation of deep layer shear (0 – 6 km) and convective available potential energy derived from lifting the lowest 50 mb layer. Allen and Karoly (2014) suggested that the 1.5º horizontal grid spacing of the reanalysis introduced bias in

some events when selecting the nearest grid point to an observed sounding. This has implications for complex physical settings such as SEQ, where circulations on much finer spatial scales are common (e.g., sea breeze). To provide a synoptic type analysis of the ERA-Interim dataset, the k-means clustering algorithm was implemented. This approach aims to partition the data into k clusters through a minimisation of the mean distance measure within each cluster (Hartigan and Wong 1979). K-means clustering has been previously applied for identifying the dominant convective regimes of SEQ through the quantisation of sounding derived parameters (Wilson et al. 2013; Peter et al. 2015). An inherent limitation when analysing point-based profile datasets is the representation of the broader synoptic environment, which becomes particularly critical during the passage of synoptic boundaries (Potvin et al. 2010). To resolve this issue, k-means clustering can be applied to develop a synoptic type analysis of reanalysis datasets to capture spatial features of the climatology (Hart et al. 2006). Theobald et al. (2015) demonstrated that this method provides a robust climatology of synoptic types for southeast Australia using the ERA-Interim reanalysis. Therefore, this method should be well suited for investigating the synoptic types of hailstorm for SEQ.

To identify the dominant synoptic types of SEQ, ERA-Interim reanalysis on a 0.75º grid were obtained for a domain bounded by latitudes 15º S – 40º S, and longitudes 135º E – 160º E for the 1774 convective storm days identified from the Marburg radar during the period July 1997 to June 2015. All storm days were used to develop an understanding of hailstorm variability in the context of the reoccurring thunderstorm synoptic types (TST) discussed by previous studies (e.g., Callaghan 1996; Peter et al. 2015) and recognised by regional forecasters. This domain is significantly larger than, but completely encompasses, the region shown in Fig. 2.5. The ERA-Interim variables extracted for hailstorm days consisted of mean sea level pressure (MSLP); zonal and meridional wind components (U and V) at 10 m, 850, 700, 500 and 250 hPa; and temperature at 2 m, 850, 700, 500 and 250 hPa. The 0600 UTC (1600 local time) reanalysis time step was selected to coincide with the mid-afternoon peak in storm frequency noted by Peter et al. (2015) across all regimes. In preparation for clustering, reanalysis fields were standardised on a monthly basis to remove the seasonal biases and to normalise inconsistent variable units for improved algorithm performance (Wilson et al. 2013; Gao et al. 2014).

Before the clustering of the reanalysis variables can begin, the number of clusters, k, must be specified. Peter et al. (2015) argued that three clusters corresponded with the qualitative understanding of TSTs developed by regional forecasters (Callaghan 1996), while further investigation of larger k values showed little benefit. Hierarchical average-linkage clustering provided Wilson et al. (2013) with a statistical first guess of 8 synoptic regimes to describe the meteorology of SEQ, three of which produced a majority of precipitation during the warm season. The consensus of three regimes between Peter et al. (2015) and Wilson et al. (2013) was selected as the initial k value for the current study. As a result, the mean TSTs for the three clusters returned by the k-means algorithm can be described as follows: (1) Weak surface trough with surface trade winds, (2) Coupled surface – upper level trough with prefrontal northeast flow preceding a southeasterly change, and (3) drylines with an upper level trough and northwest flow. These three TSTs respectively align with the trade wind, northeast and dry westerly regimes identified by Peter et al. (2015). A spatial distinction can now be made regarding the synoptic air mass boundaries. Clusters with higher k values of 4 and 5 resulted in the division of the weak surface trough and dryline types, respectively. Given the weak surface trough and dryline TSTs account for less hailstorm cells (21% and 32%, respectively) than the southeasterly change (48%), higher k values provide limited benefit towards discriminating the dominant drivers of hailstorm variability in SEQ.

4.3 Climatological Analyses

4.3.1 Seasonal and inter-Annual Climate Variability

The 18-year radar climatology for the SEQ region shows that hailstorms occurred on 6% of all days, with an annual mean of 22.5 days. Sea breeze days are significantly more frequent in SEQ, with an annual mean of 108 days (29.6%) recording the passage of a sea breeze front at the Archerfield weather station. Fig. 4.1 presents the annual (a) and monthly (b) variability of these two statistics across the 18-year record. A potential positive linear correlation is apparent between the sea breeze and hailstorm time series, with local maxima at 1997, 2004-2005 and 2014, and local minima at 1999 and 2010-2012 approximately in phase. Given the small sample size (18 years) and significant lag-1 autocorrelation within the sea breeze ($\rho_1 = 0.37$) and hailstorm ($\rho_1 = 0.31$) time series, consideration for a limited sample independence is required when testing the confidence of a linear correlation. Dawdy and Matalas (1964) showed that the ρ_1 parameter can be

applied to calculate an effective sample size to compensate for the inflated sampling variance of the mean due to first-order serial dependence. Taking into consideration the smaller effective sample size (14.78 years), statistical analysis of this relationship still shows a strong linear correlation coefficient of 0.76 and a null hypothesis (no correlation) p-value of 0.01 (two-tailed), indicating a valid relationship at the 99% threshold. This is consistent with the ability of the sea breeze to trigger convection along its boundary (Fovell 2005). The annual persistence of the hailstorm and sea breeze time series is unexpected, given these phenomena have negligible dependence upon the following day's weather, much less the subsequent month or year. It therefore seems reasonable to conclude that larger scale processes are dominating the year to year variability. Comparable results are absent from the literature possibly due to limited long-term observational records.

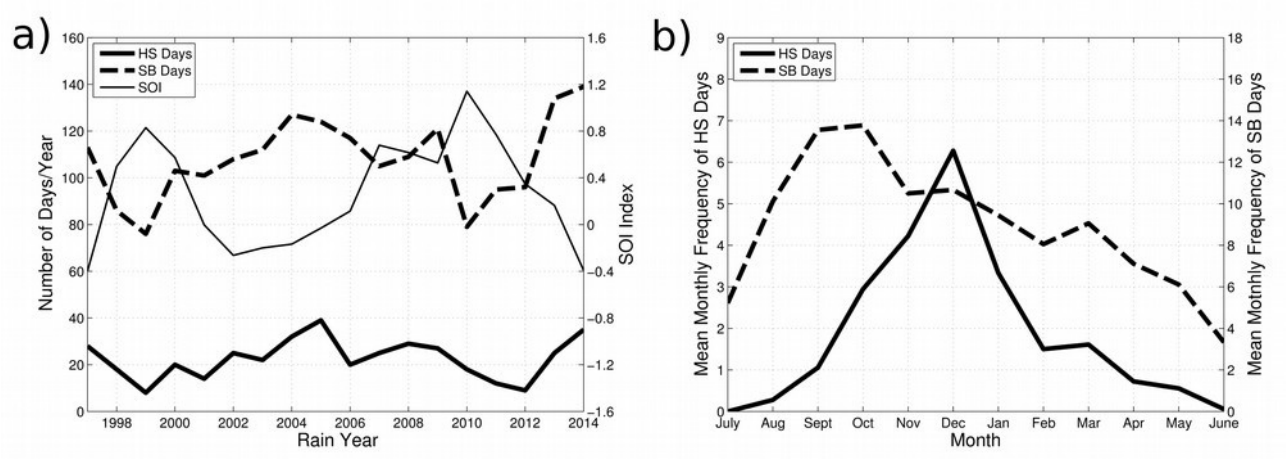

Figure 4.1: Time series plots of (a) rain year (1 July - 30 June) frequency of hailstorm (HS) days using a minimum MESH threshold of 21 mm (thick solid line), sea breeze (SB) days (dashed line) and the mean monthly Southern Oscillation Index (SOI) (thin solid line) value for the rain year; and (b) mean monthly frequency of HS (solid line) and SB (dashed line). The SOI represents the standardised anomaly of the Mean Sea Level Pressure difference between Tahiti and Darwin provided by the Australian Bureau of Meteorology.

The influence of large-scale climate oscillations upon the Australian weather are recognised by numerous studies through a rainfall and temperature response (e.g., Nicholls et al. 1997; Power et al. 1999; Cai and van Rensch 2012; King et al. 2014). Situated on the subtropical western Pacific coast, the climate of SEQ is modulated by ENSO on multi-year timescales and the Inter-decadal Pacific Oscillation (IPO) (Cai and van Rensch 2012). The potential teleconnection between the Pacific Ocean climate and

deep convection in SEQ was first examined by Yeo (2005) through an investigation of the BoM Severe Storm Archive from 1956 to 2000. Yeo noted that severe storm reports for the inner Brisbane city region were most frequent during neutral phases (-3.0 < Southern Oscillation Index (SOI) < 3.0) followed by El Niño (SOI ≥ 3.0) phases of ENSO, particularly during the pre-1977 negative IPO phase. More recently, Allen and Karoly (2014) applied an Australian-wide analysis of environmental shear and buoyancy as a proxy for severe storm trends using the ERA-Interim dataset for the period 1979 to 2011. Severe storm environment frequency for SEQ was found to hold no significant inter-annual correlation with the SOI; however, an increase in the number of severe environments for SEQ was noted during El Niño years in comparison to other years.

While the conclusions presented by Yeo (2005), and Allen and Karoly (2014) are limited by the uncertainty of public reporting and parameterised convective environments, such uncertainty is less of an issue for a long-term observational analysis on the scale of deep convection (1 km). The linear correlation coefficient between the SOI (Fig. 4.1a) for the sea breeze and hailstorm frequency time series was calculated to be -0.69 and -0.52 respectively, with effective sample size adjusted p-value for correlation rejection at 0.01 and 0.06 respectively. The negative correlation with SOI is consistent with earlier comments made by Allen and Karoly (2014) regarding a notable increase in SEQ hailstorm frequency during El Niño events and possible suppression during La Niña (Allen and Allen 2016). To understand the mechanisms by which ENSO modulates sea breeze and hailstorm frequency in SEQ, the larger scale effects upon synoptic patterns must be considered.

A possible explanation for this correlation may relate to changes in boundary layer characteristics under different ENSO phases. For La Niña events (negative SOI), the zonal Walker Circulation shifts westward, strengthening trade winds in the southwest Pacific (Oort and Yienger 1996; Garcia and Kayano 2007). This increases the prevalence of maritime flow across SEQ with associated cloudy conditions, suppressing the land-sea temperature gradient required for sea breeze circulations (Simpson et al. 1977). Furthermore, the prevalence of synoptic ridges during strengthening trade flow caps the convective environment while stabilising the boundary layer (Yeo 2005). During El Niño conditions (positive SOI), the Walker Circulation is shifted eastwards, thereby potentially

reducing both the prevalence of trades and the associated suppression of storms and sea breezes in SEQ.

Seasonal drivers of convective storm and sea breeze frequency are relatively well understood in comparison to climate teleconnections. For SEQ, the month of October is most active for sea breezes, most likely due to the strong land-sea diurnal pressure gradient between residual cold ocean temperatures following winter and the hot adjacent land mass during the start of the warm season (Fig. 4.1b). Increasing cloud cover during summer associated with the peak rainfall period and a weakening land-sea temperature gradient due to the warming of the Coral Sea suppresses sea breezes during this period. For hailstorm frequency, a distinct maximum occurs in December, with an average of 6.2 hailstorm days for the month. The later peak of hailstorm activity reflects the dependence of deep convection upon both the boundary layer and free atmosphere aloft. The late spring – early summer period marks the transition from mid-latitude driven weather to more ambient, humid tropical conditions in SEQ, thus providing the optimal combination of strong tropospheric instability and low-level moisture for hail development (Knight and Knight 2001).

4.3.2 Hailstorm Convective Initiation and Hail Development

To quantify the distribution of HCI in the Marburg radar climatology, the centroids of the first cells associated with a hailstorm track (which contains at least one cell with MESH ≥ 21 mm) were tallied on an 8 km^2 grid. A grid spacing of this size was found to provide sufficient accumulations while maintaining a fine spatial resolution. The accumulated grid was then averaged to provide mean annual frequency and contoured for Fig. 4.2a. An average of 70.6 hailstorm tracks initiated annually within SEQ, with clustering around the western and southern ranges, similar to observations by previous studies (Callaghan 1996; Peter et al. 2015). However, closer inspection of HCI indicates a preference for the eastern slopes of the Great Dividing Range, as opposed to the highest peaks or western plateau. This behaviour is particularly evident within the Boonah region (BNH) of southwest SEQ, where a broad area of high HCI frequency extends over approximately 500 km^2. Peter et al. (2015) showed a similar HCI focus in the greater Boonah region; however the exact placement was less certain due to the coarse grid resolution of 17 km^2 of their study. The HCI along the eastern slopes may be explained by the potential

formation of a lee trough along the Great Dividing Range (Fig. 2.5) in westerly to north-westerly surface flow regimes. Lee troughs have been attributed to enhanced convective initiation along the eastern slopes of the Appalachian Mountains of North America (Weisman 1990b) and the Madeleine Heights of central France (Vinet 2000), which both have a comparable elevation to the Great Dividing Range in SEQ (1000 - 1200 m). Peter et al. (2015) noted that boundary layer flow with a westerly or northerly component occurred for 59% of storm days, suggesting favourable conditions for ridge top convergence along the eastern Great Dividing Range.

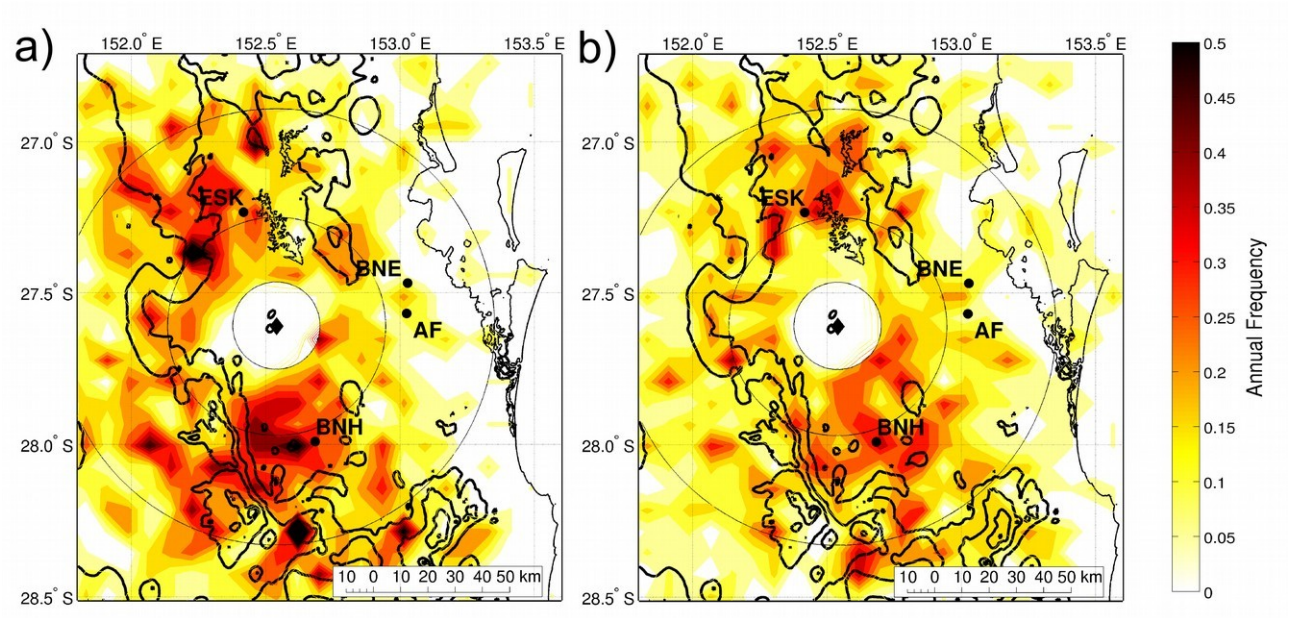

Figure 4.2: Colour contoured maps of (a) mean annual hailstorm convective initiation (HCI) frequency (days/year) and (b) mean annual hail development (HD) frequency on an 8 km2 grid for hailstorms using the 21 mm minimum threshold of MESH across the same analysis period as Fig. 4.1. Towns marked include Brisbane (BNE), Esk (ESK), Boonah (BNH) and Archerfield (AF). The location of the Marburg radar is marked with a black diamond and range rings are shown at 16 km, 40 km and 80 km. Topographical contours shown with solid black lines from 300 m at an interval of 200 m. Lake Wivenhoe and Lake Somerset are outlined with solid black lines.

Once a storm cell produces a significant reflectivity column (≥ 40dBZ) above the freezing level, a valid estimate of maximum hailstone size can be calculated using the empirical MESH technique (Witt et al. 1998). For visualising the spatial distribution of HD, an approach similar to HCI is taken: the centroid of cells which satisfied the HD criteria are collated on an 8 km^2 grid and contoured. Fig. 4.2b shows HD is clustered around the

Boonah and Esk regions of SEQ. These local maxima are offset to the east of HCI maxima, presumably in response to the dominant westerly wind component above the boundary layer. HD local maxima can also be found to the east of Esk, over the Lake Wivenhoe and Lake Somerset (see Fig. 2.5 for locations). The largest lake, Wivenhoe, with a 110 km^2 surface area, a shallow average depth of 11 m and a summer surface water temperature of approximately 29 °C (McJannet et al. 2008), suggests potential exists for sizable latent heat fluxes to the boundary layer during the warm season. For the Boonah region, a large maximum of HD bifurcates into a northern and southern limb, both extending northeast onto the coastal plains of Brisbane. Within 25 km of the coast, HCI and HD frequency are minimal, possibly due to the increasing influence of the maritime boundary layer (Darby et al. 2002; Miller 2003). Simulations of the SEQ sea breeze show it can extend into western SEQ by the mid-afternoon (0500 UTC) (Physick 1993), possibly contributing towards the HD across the southwest plains about the Boonah region (Fig. 2.5).

Explicitly resolving convective storm evolution in response to the sea breeze requires comprehensive observations that are typically only collected during field experiments (Wakimoto and Atkins 1994). Nevertheless, standard observations can provide a useful statistical analysis of sea breeze propagation and arrival times. In the absence of suitable satellite data for observing the cloud field associated with a sea breeze, Simpson et al. (1977) demonstrated that a transect of three or more weather stations arranged in a line normal to the coastline can be utilised for studying the inland progression of the sea breeze front. A lack of long-term weather station sites within the Boonah and Esk regions necessitated that the transect for this study utilised three available sites through central SEQ. This transect starts at Archerfield weather station, extends 30 km west to the Amberley site and again a further 35 km west to the Gatton site (see Fig. 2.5 for locations). This transect does not directly encompass the regions of HCI and HD maxima (Boonah and Esk) identified in the climatology, but rather provides a useful indicator of the inland progression of the sea breeze. The most frequent arrival time at each of these stations for the 18-year analysis period is marked on Fig. 4.3a. In addition, the hourly frequency of HCI and HD for sea breeze days and other days is shown in Fig. 4.3a and 4.3b, respectively. Fig. 4.4 provides a spatial perspective of the sea breeze arrival times across SEQ in relation to the HCI and HD hotspots.

The sea breeze most frequently arrived at the eastern transect site, Archerfield, by 0300-0330 UTC (1300 local time), and the central transect site, Amberley, by 0330-0400 (Fig. 4.3a). Unobstructed low-level coverage by the clear-air sensitive Mt Stapylton radar (see Fig. 2.5 for location; Meteor 1500 S-band Doppler) provided the opportunity for tracking low-level reflectivity fine lines created by the sea breeze boundary across the transect (e.g., Wakimoto and Atkins 1994; Richter et al. 2014). This analysis showed that the sea breeze is channelled between the D'Aguilar Ranges and Teviot Ranges (both with maximum elevation of 400 – 600 m; see Fig. 2.5 for locations) on its passage to Amberley, forcing the boundary into a distinct bow shape (Fig. 4.4).

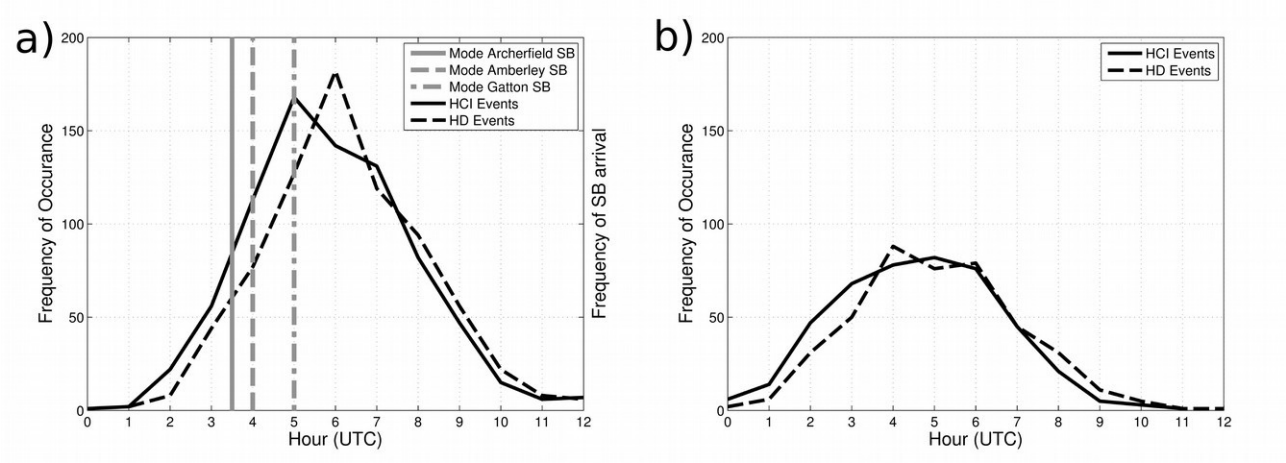

Figure 4.3: Hourly frequency of hailstorm convective intiation (HCI) (solid) and hail development (HD) (dashed) occurrence for (a) sea breeze days; and (b) non-sea breeze days across the 18 year climatology. Mode arrival times for the sea breeze at Archerfield (solid), Amberley (dashed) and Gatton (dash-dot) weather stations shown in (a) with vertical grey lines.

Inland of these topographical barriers, the bow shape expands into the northern Esk region and southern Boonah region. For the western transect site of Gatton, sea breeze arrival was most frequent between 0430 – 0500 UTC, coinciding with the peak period of HCI frequency across SEQ (Fig. 4.3a). Continuity of the sea breeze boundary south of Gatton positions it in the vicinity of the Boonah HCI hotspot (Fig. 4.4). In addition to HCI from the adjacent ranges, it is possible that additional HCI triggered by convergence along the sea breeze boundary may occur in this region. During the subsequent hour, 0600-0700 UTC, HD peaks across the plains of SEQ. By this time, 79% of sea breezes were detected at Gatton (87% for Amberley), indicating the HD events during the peak were most likely situated within the sea breeze air mass (Fig. 4.4). Rather than solely acting to increase

boundary layer stability over central and western SEQ, the sea breeze air mass appears to be potentially favourable for HD (compare Fig. 4.3a with Fig. 4.3b). On non-sea breeze days, the peak in both HD and HCI is considerably broader (Fig. 4.3b). This trend is possibly attributed to a lack of additional HCI from the sea breeze boundary; however, consideration for the TSTs must also be made (see next section).

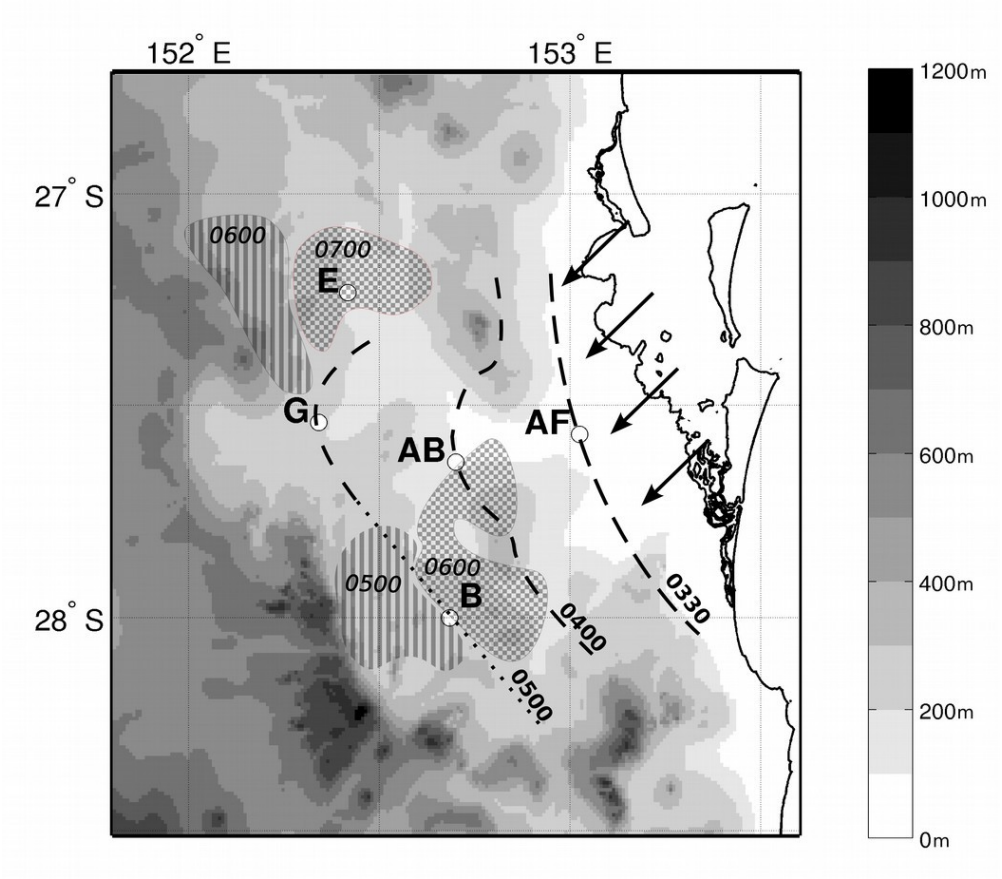

Figure 4.4: Schematic of sea breeze propagation across the weather station transect. These stations include Gatton (G), Amberley (AB) and Archerfield (AF). Representative sea breeze isochrones constructed from manual radar fine-line analysis across multiple sea breeze cases are shown with black dashed lines for each station along with the mode arrival times (UTC). Estimated sea breeze isochrone in Boonah region is shown with a black dotted line due to insufficient radar coverage. The primary regions of frequent hailstorm convective initiation (HCI) for hailstorms are annotated with vertical lines and regions of frequent hail development (HD) are annotated with gridded shading, along with the times of maximum occurrence. Topography elevation is shown in 100 m intervals above mean sea level. The towns of Boonah (B) and Esk (E) are also marked. Arrows indicate onshore flow of sea breeze at the surface.

4.3.3 Synoptic and Sea Breeze Forcing

To explore the combined impact of sea breezes and TSTs upon the distribution of hailstorms in SEQ, the radar climatology database was divided according to the ERA-Interim k-mean clusters of TSTs and sea breeze incidence. For each environmental combination, the annual mean spatial frequency of hailstorms tracks is visualised as a mosaic in Fig. 4.5. Sea breeze presence (Fig. 4.5e, f, g, h), absence (I, j, k, l) and all (m, n, o, p) components are arranged in rows, while the TST combinations weak trough (Fig. 4.5e, I, m), southeasterly change (f, j, n), dryline (g, k, o) and all TSTs (h, I, p) are arranged in columns. To provide an overview of the large-scale meteorology for each TST, the mean 500 hPa temperature and MSLP fields are shown (Fig. 4.5a, b, c). An accompanying statistical analysis of environmental combinations is provided in Fig. 4.6 of hailstorm cell and day frequency.

The most frequent TST across the climatology (39% of 1774 radar detected days, not shown) were weak troughs; however this group produced the least number of hailstorm days (29% of 404 radar detected days). Synoptic conditions for this type consisted of strong easterly surface flow over SEQ into a weak surface trough (Fig. 4.5a), a marginal environment for hail development. Southeasterly changes (Fig. 4.5b) were the second most common TST (34% of 1774 radar detected days, not shown) and the most favourable environment for hailstorms (40% of 404 radar detected days). Steep lapse rates in the presence of an upper level trough and a warm, maritime surface flow ahead of a zonally oriented cold front moving north provide ideal preconditioning and trigger ingredients. Behind the change resides cooler southeasterly flow moving northwards along the east coast of Australia. Drylines were least common TST (27% of 1774 radar detected days, not shown), yet the second most common hailstorm environment (31% of 404 radar detected days). These conditions were characterised by a broad dryline trough extending across central Queensland, advecting a more continental surface air mass over SEQ and a mean upper-level trough position displaced to the west (Fig. 4.5c). Mean synoptic conditions (Fig. 4.5d) for all hailstorm days highlight the prominence of the low pressure trough over eastern Australia and maritime northeasterly flow across SEQ.

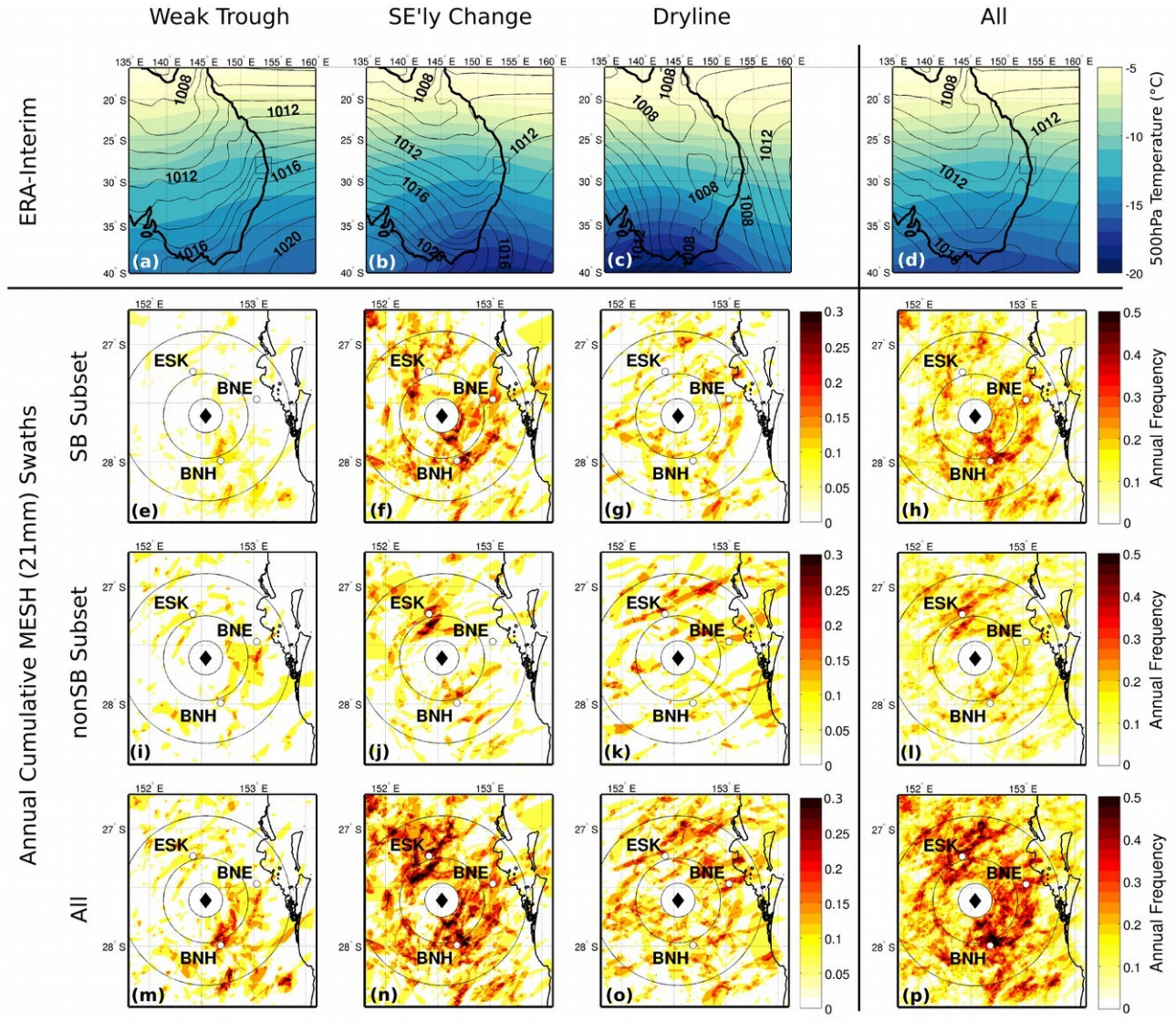

Figure 4.5: Analysis of hailstorm spatial distribution under different combinations of thunderstorm synoptic type (TST) (columns) and sea breeze presence (rows). Averaged mean sea level pressure and 500hPa temperature for each TST are shown in (a,b,c) and across all hailstorm cases in (d). Sea breeze day subsets for each TST are shown in (e-g), with all hailstorms on sea breeze days shown in (h). The spatial distributions of non-sea breeze day subsets for each TST are presented in (i-k), with all hailstorms on non – sea breeze shown in (l). The spatial distributions of hailstorms for each TST on days with and without a sea breeze are shown in (m-o) and the distribution of all hailstorms shown in (p). Locations Brisbane (BNE), Esk (ESK) and Boonah (BNH) are marked. Location of Marburg radar shown with black diamond and range rings given at 16 km, 40 km and 80 km for (e-p) and study region outlined in (a-d)

The largest portion (47% of 3633 instances) of hailstorms cells and the most frequent number of hailstorm days occurred during southeasterly change conditions (Fig. 4.6), supporting the preliminary analysis of Callaghan (1996). Peaks in hailstorm frequency for this TST are present across the Boonah and Esk regions, while the western and southern suburbs of Brisbane experience more frequent hailstorm activity than any other TST (Fig. 4.5n). When southeasterly change hailstorms are separated according to the sea breeze climatology, clustering around the Boonah region appears more frequent on sea breeze days (cf. Fig. 4.5f, j). Furthermore, 30% of all hailstorm cells occur with a southeasterly change on sea breeze days, significantly more than any other combination (Fig. 4.6). Dryline conditions accounted the second highest number of hailstorm cells (32%), with 18% of cells occurring on sea breeze days and 14% on non-sea breeze days within this type (Fig. 4.6).

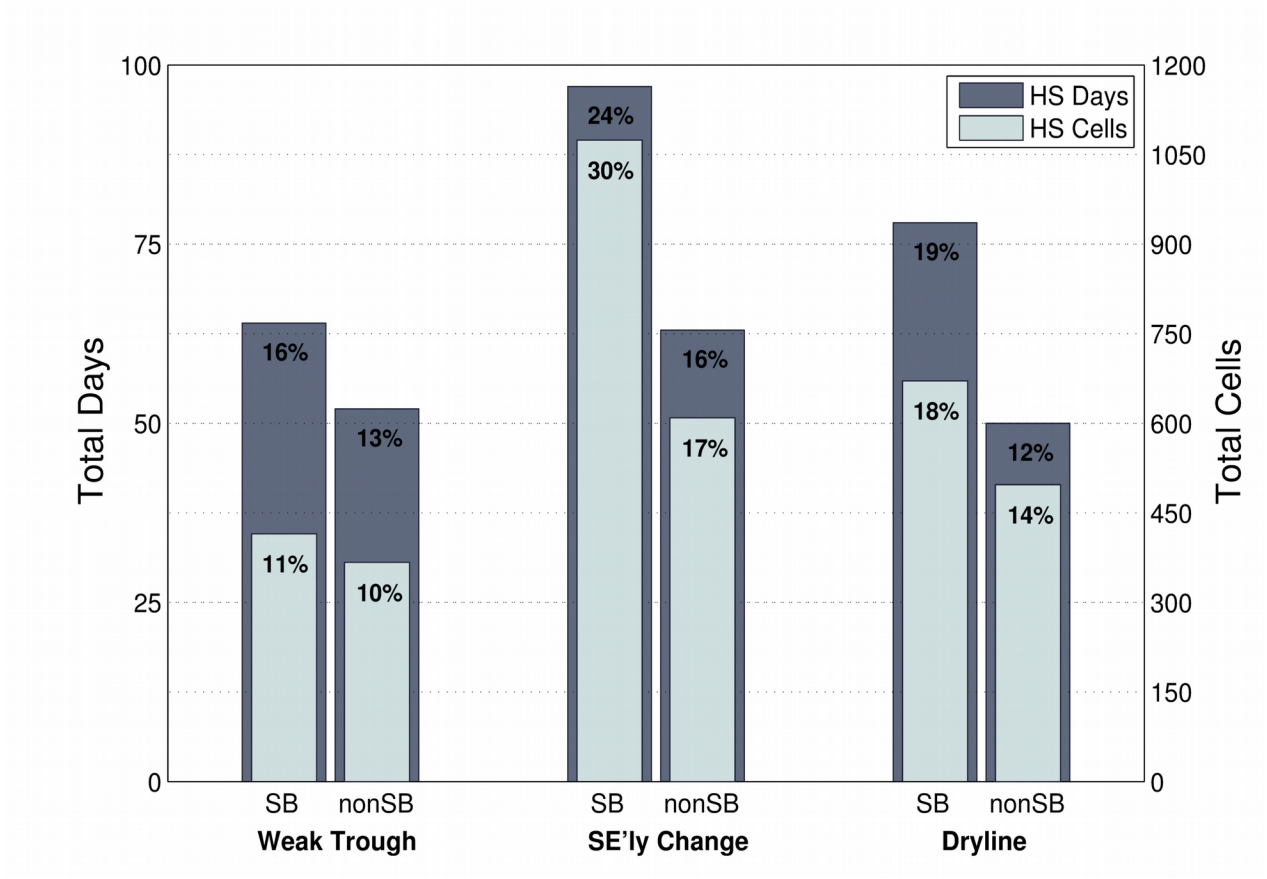

Figure 4.6: Total frequency of hailstorm (HS) days and cells for each combination of thunderstorm synoptic type (Weak Trough, SE'ly Change and Dryline) and sea breeze activity (presence and absence).

In a spatial context, dryline hailstorms are less clustered across SEQ than the southeasterly change type (Fig. 4.5o), with sea breeze combinations showing limited variability (Fig. 4.5g, k). The northern regions of SEQ appear slightly more favoured for hailstorms during dryline conditions, particularly throughout the northeast Esk region. The fewest number of hailstorms occur under weak trough pattern (21% of cells), despite this TST occurring most frequently across all hailstorm days. The Scenic Rim region (see Fig. 2.5 for location) is particularly favoured in this regime, possibly due to increasing buoyancy of the easterly flow as it advects inland and is lifted by the Scenic Rim ranges. Consideration must be given that limited hailstorm sample size in some environmental combinations (e.g., Fig. 4.5e, I, g, k) is likely representative of multi-annual variability rather than the true long-term mean. Aggregated hailstorm frequency (Fig. 4.5p) highlights the hailstorms prevalence across the urbanised south and southwest regions of Brisbane (see Fig. 2.5 for location), particularly during sea breeze conditions.

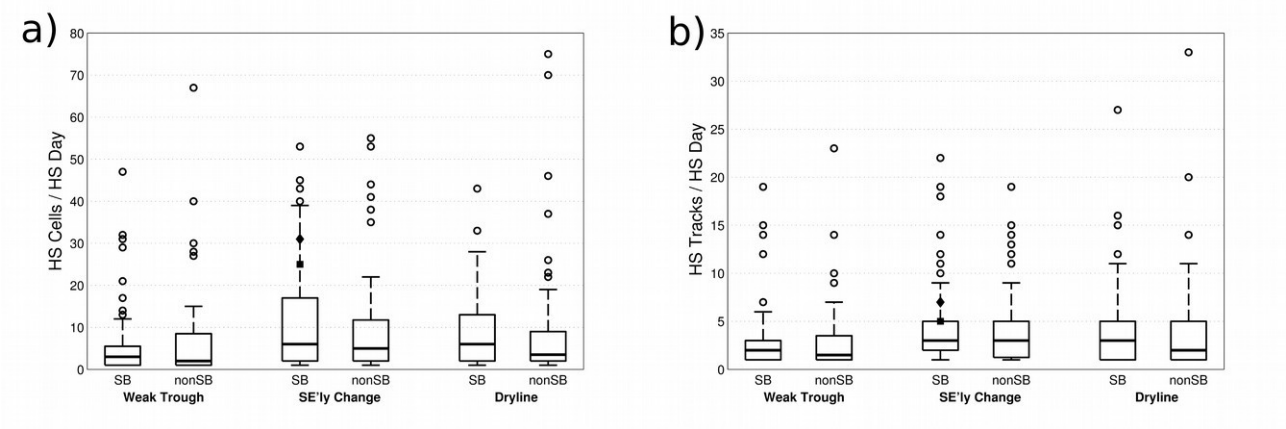

Figure 4.7: Boxplot analysis of hailstorm cells per hailstorm (HS) day (a) and hailstorm tracks per hailstorm day (b). Distributions are shown for each combination of thunderstorm synoptic type (Weak Trough, SE'ly Change and Dryline) and sea breeze presence (presence and absence). Box plots show first and third quartiles with whiskers representing ±1.5 times the interquartile range and outliers shown with circles. Recent events which resulted in significant losses shown with filled markers for the 27 November 2014 (diamond) and 16 November 2008 (square).

Given the evidence of hailstorm cell frequency varying under different environmental conditions, the question remains whether this variability is partitioned into longer duration tracks or more individual tracks. Changes in track length are particularly important for understanding whether hailstorm cells from the western HCI hotspots (Fig. 4.5) have an

increased likelihood of impacting the coastal urban areas of SEQ. To explore this further, Fig. 4.7 illustrates the distribution of hailstorm cells (a) and tracks (b) per hailstorm day under different combinations of environmental conditions. Comparison between (a) and (b) indicates that the greatest difference of the upper inter-quartile and tail occurs for the cells per day frequency distributions (a), with the southeasterly change – sea breeze group substantially larger than all other categories, while the track distributions show less difference across the TSTs. This observation suggests that the increase in cells noted in Fig. 4.6 is possibly attributed to an increase in track duration, rather than an increase in the number of tracks.

Two-sample t-tests probability values shown in Table 4.1 and Table 4.2 were calculated to test for significant difference between TST and TST with sea breeze presence distributions, respectively, using the mean. The weak trough TST produced the smallest track and cell distributions (Fig. 4.7); however these were significantly different from other TSTs as a result (Table 4.1). The southeasterly change and dryline conditions showed the least difference, particularly for the number of hailstorm tracks per day. Sea breeze presence (Table 4.2) for each TST failed the 95% confidence limit (probability value ≤ 5%), signifying that the sea breeze presence does not significantly alter hailstorm cell or track frequency within TSTs. Table 4.2 also tests whether the sea breeze presence amplified the difference between TST (e.g., TST 1 SB vs. TST 2 nonSB). Results indicate that the sea breeze presence reduces the significance between TSTs, confirming that synoptic conditions are the primary drivers of hailstorm cell and track variability. Exceptional cases can be seen in the box plot outliers of Fig. 4.7a,b, particularly for the dryline – non sea breeze environment. Investigation of these cases reveals that hailstorm cells were small and of marginal severity in comparison to the few but severe cells which are often documented for high impact southeasterly change - sea breeze cases (e.g., Holcombe and Moynihan 1978; Callaghan 1996; Richter et al. 2014; Parackal et al. 2015). For the two most recent high impact cases, 16 November 2008 and 27 November 2014, the cell instance and track frequency are shown in Fig. 4.7a,b using square and diamond markers respectively. Both of these events occur within the upper tails of the southeasterly change – sea breeze distributions, opposed to significant outliners.

Table 4.1: Two-sample t-tests for the null hypothesis (same means) of thunderstorm synoptic types (TSTs) for hailstorm (HS) cells and track distributions shown in Fig. 4.7. TST classes 1, 2, 3 represent weak trough, southeasterly change and dryline groups respectively.

Two-sample *t*-test probability values			
	TST 1,2	TST 1,3	TST 2,3
HS Cells	0.7%	9.0%	32%
HS Tracks	1.1%	3.6%	95%

Table 4.2: Two-sample t-tests for the null hypothesis (same means) of combinations of thunderstorm synoptic types (TSTs) and sea breeze (SB) presence for hailstorm (HS) cells and track (in brackets) distributions shown in Fig. 4.7. TST classes 1, 2, 3 represent weak trough, southeasterly change and dryline groups respectively.

Two-sample *t*-test probability values			
	TST 1 nonSB	TST 2 nonSB	TST 3 nonSB
TST 1 SB	77% (93%)	11% (9.8%)	15% (12%)
TST 2 SB	5.1% (7.2%)	47% (77%)	63% (92%)
TST 3 SB	38% (16%)	55% (96%)	53% (73%)

4.3.4 Cell-based Analysis

The previous analysis confirms the importance of meteorological conditions for hailstorm frequency and spatial distribution in SEQ. Previous studies (e.g., Kumar et al. 2013; Peter et al. 2015) have shown that convective cloud properties (e.g., convective intensity and hail size) can also be influenced by the environmental conditions. To explore this relationship further, Fig. 4.8 provides an analysis of convective intensity and hail size for cells that occur during sea breeze and non-sea breeze days (a,b), and for cells from each of the three TSTs (c, d). Convective intensity is represented by taking the vertical profile of maximum radar reflectivity within individual hailstorms (single value at every level) within every 10 minute volume scan and collated across all time steps that occurred for each of the six environmental scenarios from Fig. 4.5 to provide a mean profile of vertical reflectivity. Within the convective intensity plots, probability distribution function (PDF)

curves of the 0 °C and -20 °C altitudes derived from 00 UTC Brisbane Airport (see Fig. 2.5 for location) sounding are shown to investigate changes in the hail growth layer (Witt et al. 1998). The combination of these two statistics is important for developing an understanding of the MESH PDFs.

Contrasting sea breeze and non-sea breeze days, the reflectivity profiles show little variability (Fig. 4.8a, b). The PDF curves of 0 °C and -20 °C altitudes shows a broader temperature distributions for non-sea breeze days, suggesting more variability in upper level trough activity, however mean temperature showed only slight variability. As a result of similar upper temperature distributions and reflectivity profiles, limited variation is present between the two MESH PDFs. These statistics are also influenced by the indiscriminate sampling of hailstorms on sea breeze days. No distinction is made between cells on either side of the sea breeze boundary, thereby reducing the representativeness of the derived statistical distributions for MESH and reflectivity. The sea breeze circulation would be expected to have negligible impact on the atmosphere above the boundary layer (Miller 2003), except through the provision of sea breeze derived air parcels during surface based convection. Conversely, it appears that the upper level temperature has no discernible relationship with the presence of the sea breeze on hailstorm days.

Unlike sea breezes, TSTs influence both the boundary layer and overlying free atmosphere through various preconditioning and trigger mechanisms (Doswell 2001). The difference between the maximum reflectivity profiles shown in Fig. 4.8c can be understood through an examination of the synoptic conditions for each type. Within the first 4 km above the ground, hailstorms on dryline days exhibit the lowest average maximum reflectivity (Fig. 4.8c). An examination of the MSLP chart shown in Fig. 4.5c indicates that mean surface flow in SEQ on dryline days originates from mixed northwesterly continental/coastal origin. This suggests that available boundary layer moisture may be limited for some hailstorm days, thereby increasing the incidence of higher lifting condensation levels and reducing the reflectivity profile in this layer (Corfidi et al. 2008). Above 4 km, maximum reflectivity for the dryline TST converges with the southeasterly change profile, indicating more favourable conditions aloft for deep convection. This is supported by the 500 hPa temperature plot, where the mean upper level trough axis is positioned over western Queensland. A deepening upper level trough was noted by Shin et al. (2005) as an important factor for the development of unusually severe storms along the

dryline inland in central Queensland, and is often an important preconditioning process for convective storm environments globally (Johnson and Mapes 2001).

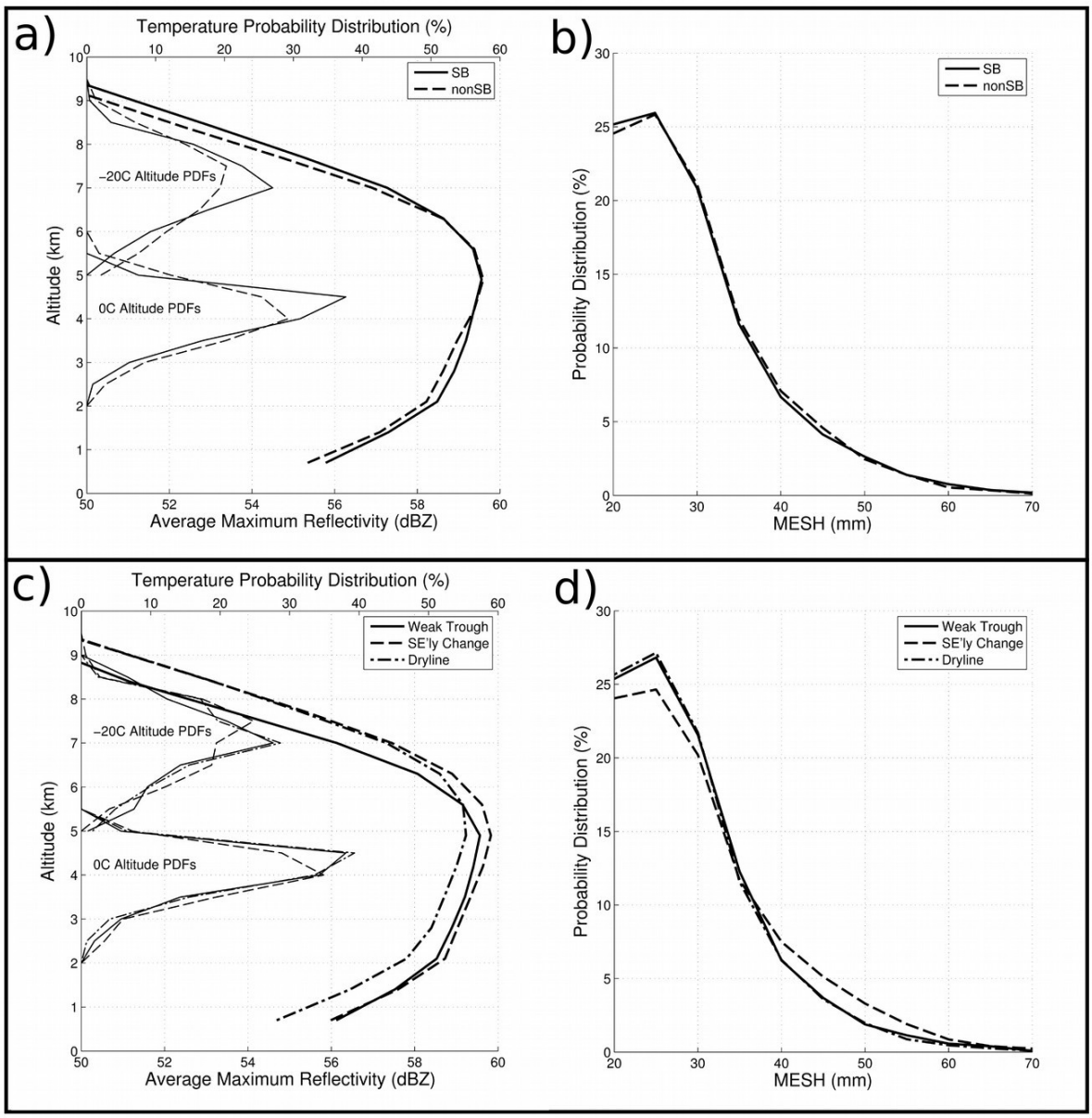

Figure 4.8: Analysis of hailstorm (HS) cell statistics for sea breeze occurrence (a,b) and thunderstorm synoptic type (c,d) conditions. The average maximum reflectivity profile for hailstorm cells is shown with bolder lines (a,c) in conjunction with the probability distribution functions for the 0° C and -20° C altitudes derived from the 00 UTC Brisbane airport radiosonde data shown with finer lines and using the upper x axis. The probability distribution functions for MESH between 20 mm and 70 mm with 5 mm bin width is shown in (b and d).

During weak trough and southeasterly change types, the MSLP analysis indicates maritime flow prevails across SEQ (Fig. 4.5a, b), increasing low-level moisture and thus the potential for enhanced low-level reflectivity shown in Fig. 4.5c. Above 4 km in altitude, the reflectivity profile of the weak trough TST is shallower than the other types. The 500 hPa temperature chart for the weak trough TST (Fig. 4.5a) lacks a distinct position of the upper level wave (possibility due to increased variability), lowering the average hail growth potential through this critical layer in comparison to southeasterly changes and drylines. For southeasterly types, the mean 500 hPa trough axis is ideally located just west of SEQ, increasing upper level divergence and mid-troposphere temperature lapse rates. This proximity of the upper level trough is reflected in marginally lower 0 °C heights (Fig. 4.5c) than other TSTs; however no substantial influence can be seen at the -20 °C level. The combination of a convectively supportive upper level and boundary layer during southeasterly changes provides a broad-scale understanding of the high spatial (Fig. 4.5n) and temporal (Fig. 4.6) frequency of hailstorms observed during this TST. Furthermore, the passage of a change during this type provides an additional boundary for the development of convection. This favourability is reflected in the larger upper tail of the MESH PDF curve shown in Fig. 4.8d. Southeasterly changes are clearly significant high-end hail producers, confirming the long-standing proposition drawn from earlier case studies and reports (e.g., Callaghan 1996; Richter et al. 2014; Insurance Council of Australia 2015)

4.4 Discussion and Conclusions

Owing to the rapidly increasing population in a region of frequent hail impacts, the forecasters, industry, and public of Southeast Queensland (SEQ) benefit from an enhanced understanding of regional hailstorms. Integration of volumetric radar, sounding, surface weather station, archived storm reports, and model reanalysis data as part of the Coastal Convective Interactions Experiments (CCIE) provide the first mesoscale climatological analysis of a convective environment across an 18 year period for SEQ. This extensive dataset was sufficient to explore the multi-year effects of ENSO upon sea breeze and hailstorm frequency. A statistically significant relationship was found across the climatologically short record, whereby the El Niño (La Niña) phases of ENSO increase (supress) the frequency of hailstorm and sea breeze days in SEQ. Recent long term climatology studies from Switzerland (Nisi et al. 2016) and Atlanta, US (Haberlie et al. 2014) have not explored this link. Such a lengthy analysis was also necessary for

developing a spatial climatology of hailstorms on a scale sufficient for resolving preferred track location on a local-scale (< 10 km). This analysis supported previous findings of hailstorm convective initiation (HCI) near the ranges which encompass western and southern SEQ (Callaghan 1996), with possible lee trough forcing similar to that proposed by Weisman (1990b) and Vinet (2000) for the Appalachian mountains and central France, respectively. Hail development (HD) was most common over the southwest and northwest valleys of SEQ, offset to the northeast of the HCI.

The role of the sea breeze propagation was considered as a possible mechanism for HD following previous case study reports of high impact events (Callaghan 1996). Building upon the preliminary results presented in chapter 3, the spatial and temporal HCI maximum was found to occur concurrently with the passage of the sea breeze front while HD peaked within the post sea breeze maritime air mass. While the sea breeze is most likely initially stable as surface parcels flow onshore, the spatial climatology results suggest that at a sufficient distance inland the sea breeze may become favourable for deep convection due to modification of sea breeze parcels travelling over a warming land surface. A similar change in sea breeze thermodynamics with inland distance has been shown along the Mediterranean coast (Puygrenier et al. 2005) and the south English coast (Simpson et al. 1977). Consideration must be given for hailstorms which source convective parcels from above the surface bound sea breeze; further investigation of sea breeze depth and interactions with convection required to quantify this process.

Callaghan (1996) observed that southeasterly change environments were particularly favourable for severe storms in SEQ. To explore this further and to develop an understanding of potential large-scale support of hailstorms on sea breeze days, a thunderstorm synoptic type (TST) analysis was developed using k-means clustering. The southeasterly change on sea breeze days was identified as the most favourable environment for hailstorms (24% of hailstorm days, 31% of hailstorm cells), particularly for the repeatedly impacted Boonah region. Investigation indicated an increased number of hailstorm cells per hailstorm day compared with other TSTs. While the remaining dryline and weak trough types also produced more hailstorms on sea breeze days, this difference was not statistically significant. It was also shown the frequency of hailstorm cells and tracks during weak trough types was significantly different to the other types, reflecting the lower frequency of hailstorm development under this synoptic condition. An analysis of the

maximum reflectivity profile technique, hail growth layer (0 °C to -20 °C) and MESH across individual cells further supported the favourability of the southeasterly change type, however, struggled to find any meaningful distinction between the cell and track frequency statistics on remaining types (weak trough, dryline) and for sea breezes.

CHAPTER 5

DIURNAL PRECONDITIONING OF SUBTROPICAL COASTAL STORM ENVIRONMENTS

UQ-XPOL deployment at Beaudesert on the 10 December 2015 (Joshua Soderholm)

Chapter 5. Diurnal Preconditioning of Subtropical Coastal Storm Environments

5.1 Introduction

In this chapter an investigation of the effects of diurnally forced near-surface and PBL variability upon convective storms in SEQ is presented. Observational datasets collected during the CCIE field campaign (introduced in chapter 3) are analysed to determine the critical processes which favour convective storms. This analysis builds upon the climatological evidence of sea breeze forcing of convective initiation and intensification in chapter 4 through an understanding of the underlying meteorological processes. Observational platforms and datasets from CCIE are discussed in section 5.2. A conceptual model of near-surface and PBL processes is developed through the investigation of multi-season datasets in sections 5.3 and 5.4, respectively. These concepts are applied to explore the storm evolution for the 27 November 2014 case study in section 5.5. A summary and concluding remarks are presented in section 5.6. Chapter 5 has also been submitted to the Monthly Weather Review journal for publication.

5.2 Methodology

In addition to data from the observational platforms of the Australian BoM across SEQ already discussed throughout this thesis (sections 3.2.1, 3.2.2), near-surface observations are obtained from a network of twenty AWSs (see Fig. 2.5 for locations) situated to minimise local influences (e.g., urban effects, tall vegetation). Out of the twenty AWSs, only three are located in proximity to the southwest region of frequent convective initiation and hailstorm development (Soderholm et al. 2016). To fill this observational gap, two additional AWSs were deployed by The University of Queensland for the duration of CCIE (November 2013 to January 2015). The Kalbar (KBR) and Grandchester (GCH) sites (see Fig. 2.5 for locations) were located adjacent to irrigated and dry pastoral land, respectively, potentially measuring associated local agricultural effects. Furthermore, the CCIE wind sensors were positioned at a non-standard height of 2.5 m, and their measurements are more strongly influenced by surface friction in contrast to BoM wind sensors at 10 m. A further fourteen AWSs maintained by the Queensland Government Department of Environmental and Heritage Protection (EHP) were also incorporated into this study to increase spatial resolution. EHP AWSs are operated to monitor local pollution levels within

urban, industrial and mining environments and therefore are more subject to anthropogenic local effects (e.g., paved surfaces and buildings) in contrast to the BoM sites. Observations from EHP sites are collected at standard heights (10 m for wind observations and 2.5 m for thermodynamic and pressure observations) Santamouris (2015) proposes that the non-standard EHP configuration is more suitable for observing the urban heat island due to the dominant thermal contribution of the localized environment. Median distance between the CCIE, BOM and EHP stations is 0.56° (62.5 km), comparable to the ERA-Interim reanalysis grid resolution of 0.7°.

To assist the spatial interpretation of thermodynamic observations from the BoM, EHP, and CCIE networks (36 sites in total), these datasets were interpolated onto a 0.1° grid at a 6-minute interval to provide an automated mesoanalysis using smoothing plate splines . This type of analysis is an important tool for both forecasters and researchers, particularly when identifying the spatial positioning of air mass boundaries (Atkins and Wakimoto 1997; Koch and Ray 1997). Given the sparseness of observations across large areas of SEQ, the bivariate thin-plate spline interpolation technique was implemented to ensure a physically realistic near-surface fields (Boer et al. 2001; Tait and Woods 2007). Grid points above 300 m in elevation and those located offshore of SEQ were removed from the interpolated fields due to insufficient observations across these differing surfaces.

Aerological sounding datasets were obtained using fixed and mobile instrumentation during CCIE. Daily operational soundings from Brisbane Airport (YBBN) at 09:00 Australian Eastern Standard Time (AEST = UTC + 10 hours) were provided by the BoM in addition to adaptive afternoon releases on storms days as part of the CCIE. Adaptive soundings were released between 12:00 AEST to 16:00 AEST depending on the expected time of storm development. Mobile soundings were conducted during CCIE field days by The University of Queensland at 12:00 AEST from Kalbar (KBR in Fig. 2.5) in southwest SEQ. In contrast to the coastal location of the Brisbane Airport profiles, soundings at Kalbar provide the opportunity to sample the developing continental CBL in the absence of a sea breeze. Sounding datasets were processed using the Sounding/Hodograph Analysis and Research Program in Python (SHARPpy) package (Halbert et al. 2015).

5.3 Near-Surface Environment

5.3.1 Transect Analysis

To compare the cross-coastline environment of sea breeze and non-sea breeze conditions, transects of warm season mean temperature, dewpoint and wind speed were constructed. Both CCIE and BoM AWSs are utilised to cover a geodesic distance of 133 km (dash-dot line in Fig. 2.5). This transect extends from the southwest region of frequent hailstorm initiation (Kalbar (KBR) and Grandchester (GCH) sites), through to the densely populated coastal plains (Amberley (AMB), Archerfield (ACH) and Brisbane City (BNE) sites) and across the coastline (Brisbane Airport (YBBN)) to the maritime climate of an offshore sand island (Cape Moreton Lighthouse (CML)), providing a comparison of the diverse near-surface environments of SEQ.

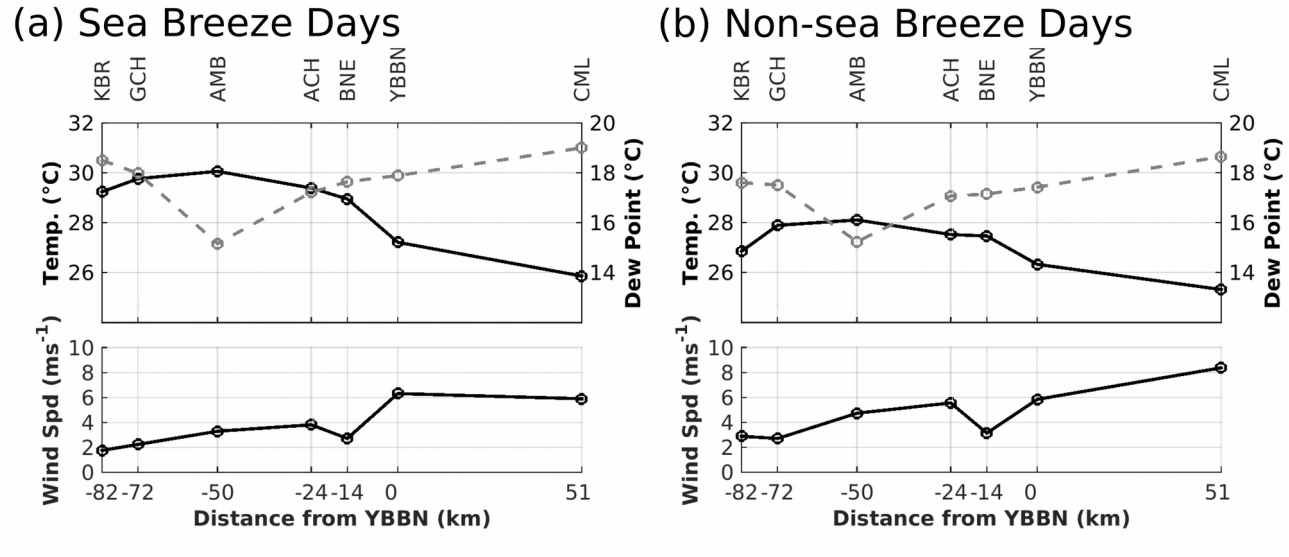

Figure 5.1: Composite surface transects at 12:00 AEST for (a) 91 sea breeze days and (b) 157 non-sea breeze days during the warm season months (Oct - Mar) between Nov 2013 and Jan 2015. The weather stations used in the transect are Kalbar (KBR), Grandchester (GCH), Amberley (AMB), Archerfield (ACH), Brisbane (BNE), Brisbane Airport (YBBN) and Cape Moreton Lighthouse (CML). Mean surface temperature (black lines) and surface dewpoint (grey dashed lines) along the transect are shown in the top panels, and mean 10 m wind speed (black lines) are shown in the bottom panels. Geodesic distance from YBBN shown on the horizontal axis. Note: dew point temperature and temperature axis have different limits.

Temperature, dewpoint and wind speed values at 12:00 AEST were obtained for sites along the transect during warm season months (October to March) between November 2013 and January 2015. Mean values for days when the sea breeze was present and absent are shown in Fig. 5.1a and 5.1b, respectively. Lower wind speeds and higher mean 2 m temperature across the inland portion of the transect are more apparent for sea breeze days, indicative of a stronger land-sea thermal contrast. This thermal contrast is strongest between Brisbane Airport (YBBN) and Brisbane (BNE), particularly for sea breeze days where weaker synoptic flow permits earlier warming of the lower boundary layer air. Dewpoints between Brisbane Airport and Brisbane were comparable regardless of sea breeze presence.

The most common arrival time for the sea breeze at Archerfield was 13:30 AEST (Soderholm et al. 2016), indicating that most of the inland section of the 12:00 AEST transect represents a warming continental air mass. For this inland segment, the Amberley site recorded both the warmest mean temperature and a remarkably low mean dewpoint (< 16 ºC) regardless of sea breeze presence. Comparison with the nearest rural BoM site (Gatton; GAT) shows that near-surface moisture at Amberley mixes out earlier (Fig. 5.2), contributing to the lower dewpoint observations at 12:00 AEST. This earlier mixing of near-surface moisture may be a result of enhanced local heating from dry pastoral land and a large Air Force base in proximity to the Amberley AWS.

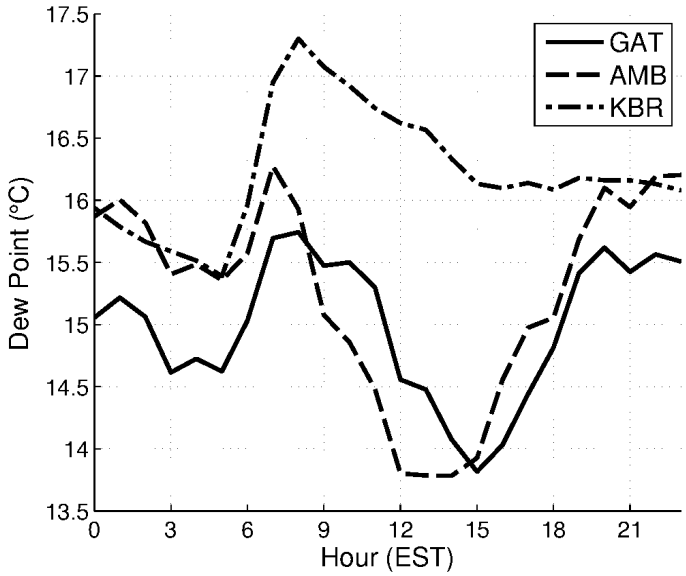

Figure 5.2: Observed mean hourly surface dewpoint for warm season months (Oct - Mar) between Nov 2013 and Jan 2015 from Gatton (GAT), Amberley (AMB) and Kalbar (KBR).

Further inland, mean near-surface moisture increases to levels comparable with Brisbane Airport (~18 ºC), particularly for Kalbar on sea breeze days, while the mean temperature decreases. Extensive irrigated agriculture surrounding the Kalbar site (Fig. 2.5) likely favours latent over sensible heat fluxes in comparison to non-irrigated sites (Clark and Arritt 1995), leading to higher dewpoints throughout the diurnal cycle (Fig. 5.2). Kalbar also experiences the lowest 12:00 AEST wind speeds for the transect, possibly due to elevated topography surrounding the region to the west (800 - 1200 m), south (600 - 1200 m) and east (300 - 500 m). This topographical "block" may contribute to the enhanced dewpoints through reduced advection of near-surface moisture away from the area. Low wind speeds are also observed at Brisbane despite its exposure to onshore flow, presumably due to the higher surface friction of the city landscape (Dandou et al. 2009).

5.3.2 Urban Heat Island Intensity

City landscapes also modify the local atmosphere through the UHI effect, where the intensity of the temperature anomaly varies as a function of the urban landscape, physical setting and meteorological environment (Santamouris 2015). To quantify the UHI intensity for Brisbane, the temperature distributions from four AWSs situated in the city are compared with three AWSs in a comparable and nearby rural coastal setting using 09:00 AEST observations, prior to sea breeze onset (Fig. 5.3). City AWSs consisted of one BoM site (Brisbane) located in a lower density suburban environment and three EHP sites: South Brisbane (SBNE), Woolloongabba (WLG) and Central Brisbane (CBNE) located in higher density urban settings (e.g., major highways and inner-city). The proximity of the EHP sites to local urban effects leads to significantly (2 sample t-test at 99% level) warmer mean temperatures (1.6 – 1.8 °C) than the BoM city site. The three baseline rural sites of Nambour (NMB), Beerburrum (BER) and Logan (LGN) were selected to be approximately the same distance from the coastline as Brisbane city (15-20 km), thus minimizing differences due to the land-sea boundary. Temperature distributions among the three rural sites are consistent, with no significant difference between their mean 09:00 AEST values (~25 °C), thus providing a robust measure of the ambient environment. Rural sites were found to be on average 1 °C cooler than the BoM city site and 2.6 – 2.8 °C cooler than the EHP city sites, which we take to signify the intensity of the Brisbane UHI prior to sea breeze modification.

The intensity of the 09:00 AEST warm season Brisbane UHI is comparable to the average maximum daily UHI intensity (difference between city and nearby rural temperature) for the Australian coastal cities (Melbourne ~2.7 °C, Sydney ~3.5 °C) and internationally (e.g., Osaka, Japan ~3.1 °C and Incheon, South Korea ~2.5 °C; Santamouris 2015). Simulations of the Brisbane UHI by Khan and Simpson (2001) showed that anthropogenic heat flux contributed 3.5 °C during mid-afternoon (14:00 AEST) and up to 6 °C at night. The authors also noted that the simulated Brisbane UHI can substantially modify the local wind field in mesoscale model simulations. In addition to increased surface friction and enhanced aerosol release, the effect of the Brisbane city UHI must be considered a potential influence upon convective preconditioning of the city PBL through increased near-surface parcel buoyancy.

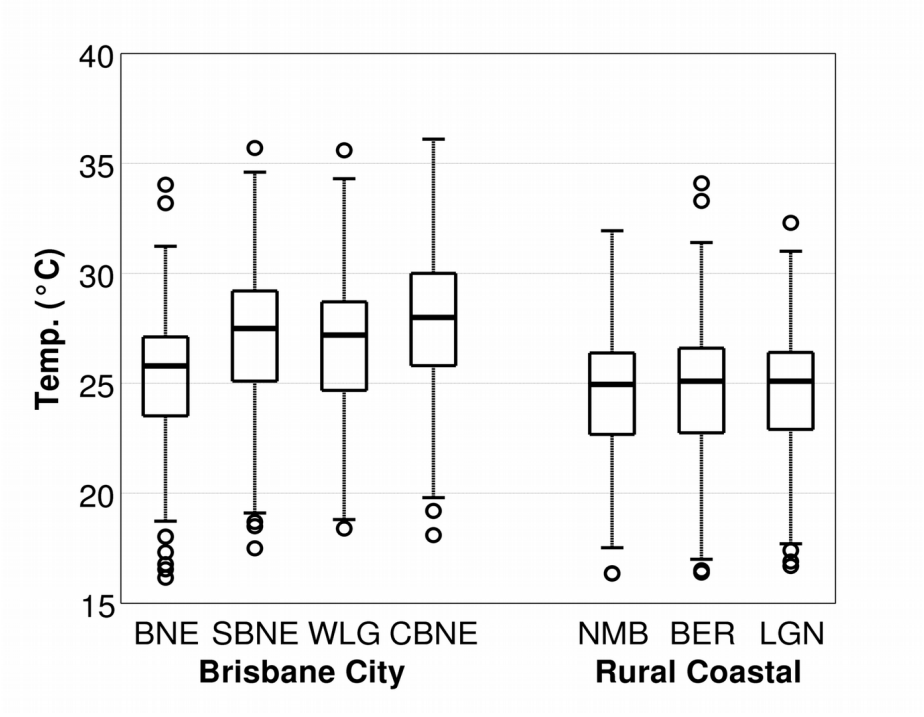

Figure 5.3: Boxplots of 09:00 AEST temperature distributions for Brisbane City weather stations and coastal rural sites for warm season months (Oct - Mar) between Nov 2012 and Jan 2015. Box plots show first and third quartiles with whiskers representing ±1.5 times the interquartile range and outliers shown with circles. Weather stations used in this transect include Brisbane† (BNE), South Brisbane (SBNE), Woolloongabba* (WLG), Central Brisbane* (CBNE), Nambour† (NMB), Beerburrum† (BER) and Logan† (LGN). * Stations operated by the Queensland Government Department of Environment and Heritage Protection. † Stations operated by the Australian Bureau of Meteorology.*

5.3.3 Spatial mesoanalysis

To explore the spatial extent of characteristics identified from the transect and UHI analyses, mesoanalysis of mean warm season (October - March) conditions during the CCIE (November 2012 – January 2015) at 12:00 and 15:00 AEST on sea breeze (a,c) and non-sea breeze days (b,d) are shown in Fig. 5.4. Additionally, derived equivalent potential temperature (θ_e) is included for comparison of near-surface parcel stability. In agreement with the transect analysis, sea breeze days are clearly the highest energy environments, with a southwest SEQ θ_e maximum exceeding 336 K at 12:00 AEST (Fig. 5.4a). A secondary θ_e maximum centred over Brisbane is a result of maritime moisture (16 °C dewpoint contour) displaced an additional 15 - 25 km inland compared to other coastal locations, and particularly warm near-surface temperatures (29 °C) over the city. Previous modelling studies have shown that this increased maritime flow is attributed to UHI modification of sea breeze forcing in locations including Brisbane (Australia; Khan and Simpson 2001) and São Paulo (Brazil; Freitas et al. 2007). The UHI enhanced land-sea temperature gradient leads to a faster propagation speed and therefore earlier arrival of the sea breeze, increasing moisture levels across the city environment.

Between 12:00 and 15:00 AEST (Fig. 5.4c), sea breeze moisture (16 °C dewpoint contour) builds more rapidly over rural coastal areas in contrast to areas west of Brisbane. Modelling studies suggest this may be related to increased friction from the urban canopy (Gedzelman et al. 2003; Dandou et al. 2009) or interactions with the UHI circulation (Freitas et al. 2007), stagnating the flow of the sea breeze inland of the city and possibly displacing the UHI downwind. Evidence of these processes in the mesoanalysis is less apparent due to sparse observations west of the city. The early arrival of the sea breeze also appears to suppress further warming (and θ_e increase) over Brisbane between 12:00 and 15:00 AEST in contrast to rural areas, where θ_e increased notably in response to the afternoon arrival of the sea breeze. On non-sea breeze days the cross-coastal surface temperature gradient is weaker, leading to comparatively low θ_e values across the coastal environment. Inland of the coast, an axis of warm, comparatively dry air resides to the west of the D'Aguilar and Teviot ranges on both sea breeze and non-sea breeze days (see Fig. 2.5 for locations). Dry pastoral agriculture through this region may promote early and deep CBL development through increased sensible heating in contrast to irrigated areas (cf. Amberley observations discussed in section 5.3.1). In southwest SEQ, a region of

enhanced θ_e is evident on sea breeze days in response to near-surface moisture, most likely due to stronger latent heat fluxes from the irrigated land surrounding the Kalbar site (Fig. 5.4a,c). Cooler temperatures on non-sea breeze days account for a reduced θ_e maximum in this area (Fig. 5.4b,d). For northwest SEQ, analysis is limited by a lack of AWS observations across the region.

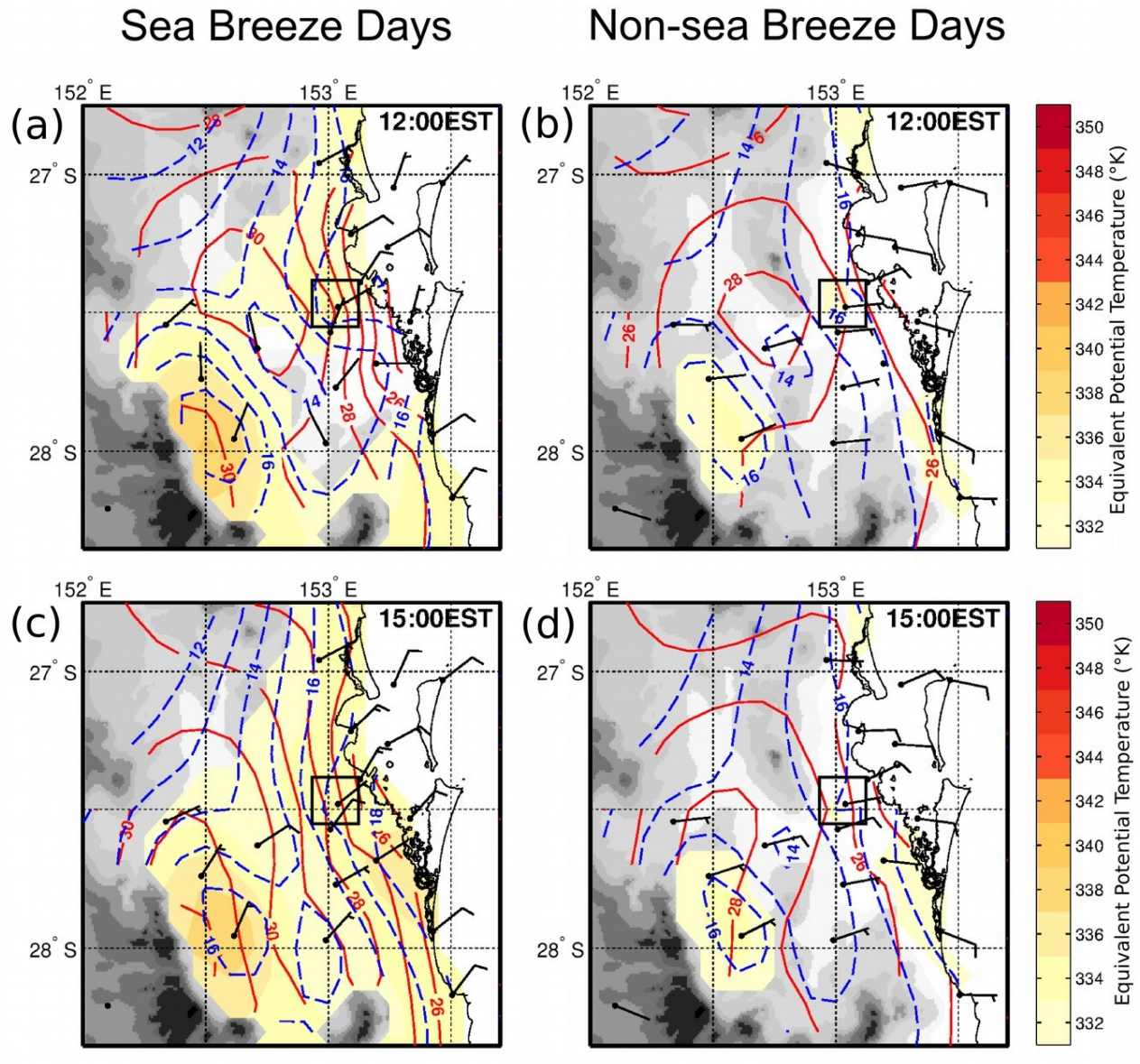

Figure 5.4: Contour plots of interpolated surface temperature (red solid lines), dewpoint (blue dashed lines) and equivalent potential temperature (shaded contours) for sea breeze days (a,c) and non-sea breeze days (b,d) at 12:00 AEST (top row) and 15:00 AEST (bottom row) for warm season months (Oct, Nov, Dec, Jan, Feb, Mar) between Nov 2012 and Jan 2015. Winds are shown with half barbs for 2.5 ms^{-1} and full barbs for 5 ms^{-1}. Topography shaded in 250 m intervals and the box indicates the Brisbane urban region.

5.4 Planetary Boundary Layer

Small-scale changes in near-surface and CBL conditions have been shown to significantly influence both the initiation (e.g., Weckwerth 2000; Wakimoto and Murphey 2009) and development of existing convective storms (Smith et al. 2000). However, the representativeness of near-surface observations are limited in the absence of a well-mixed boundary layer (Mueller et al. 1993; Weckwerth et al. 1996). Furthermore, even for storms which are considered surface based, the inflow layer may extend well above the surface (Thompson et al. 2007). Therefore, the careful consideration of the entire PBL depth is required for understanding the influence of near-surface conditions on deep moist convection, particularly in the presence of a sea breeze.

5.4.1 Sea Breeze Structure

Six sea breeze days were observed by CP-2 radar during the 2014/2015 campaign of the CCIE, providing an opportunity to explore the clear air structure (Fig. 5.5). A fixed azimuth of 70 degrees was used for all RHI scans (dashed line segment in Fig. 2.5), with onshore east-northeast flow shown as negative radial velocities (blue shading) and the return west-southwest flow aloft as positive radial velocities (red shading). Vertical cross sections were selected at times after the passage of the sea breeze boundary at the radar site to sample an approximately steady state of the circulation. Despite these efforts, Kelvin-Helmholtz waves between the onshore and return flow can be seen in half of the cases (Fig. 5.5a,c,e), likely resulting from shear at this interface and insolation forced thermodynamic instability (Simpson et al. 1977; Atkins et al. 1995; Chiba et al. 1999; Plant and Keith 2006).

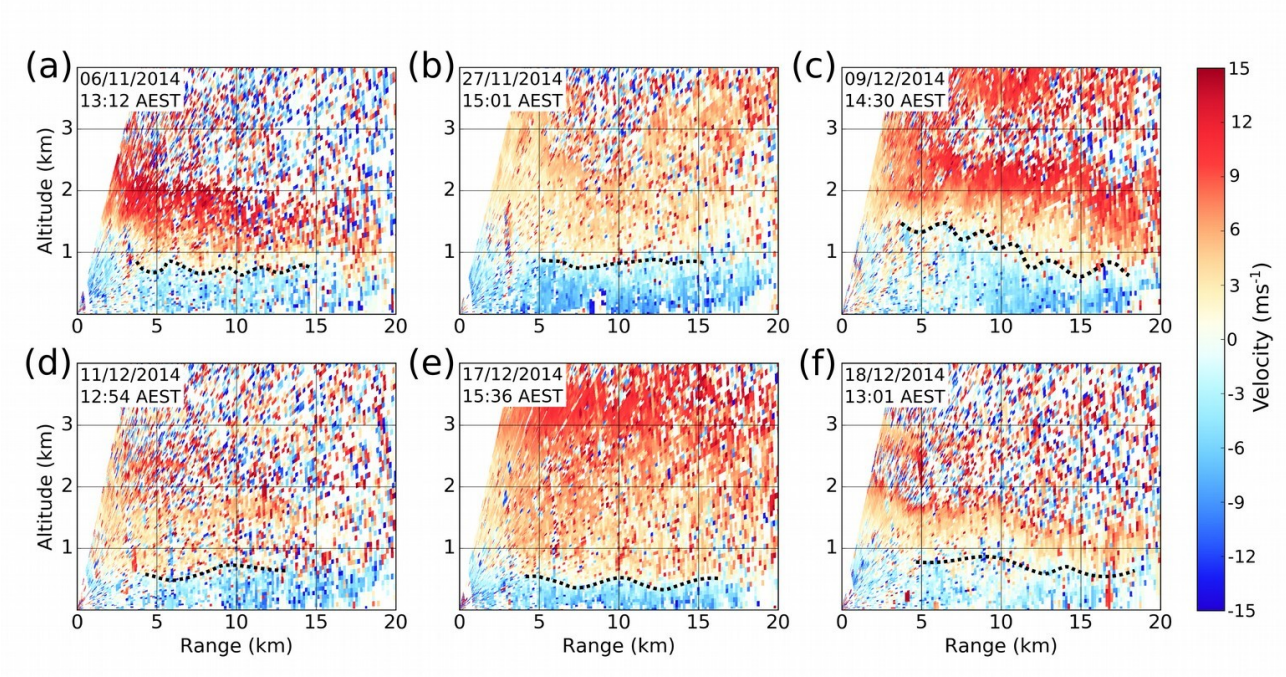

Figure 5.5: Vertical cross sections of Doppler velocity from six sea breeze events captured by CP-2 radar. All cross sections were captured at fixed RHI azimuth of 70°. The approximate location of the 0 ms^{-1} isodop between the onshore surface limb of the sea breeze and the return flow aloft is shown with a dotted line. Range from CP-2 shown on the horizontal axis and height above the radar shown on the vertical axis.

The depth of the onshore flow varied between ~ 500 m in case (e) to ~ 1.5 km AGL in case (c), while maximum onshore wind speeds were often located close to the surface and ranged from 9 ms^{-1} (b) to less than 2.5 ms^{-1} (a,f). Westerly return flow aloft was typically of greater depth (500 m – 2.5 km AGL) and intensity (5 ms^{-1} - 10 ms^{-1}) than the sea breeze, suggesting a disproportionate mass flux within this limb of the circulation. Reflectivity of this layer ranges from 0 to 25 dBZ (not shown) across the six cases, supportive of particulate scattering (e.g., insects) being responsible for the clear-air returns (Wilson et al. 1994). Particulates are generally an indicator of a well-mixed air mass, therefore it is hypothesised that the return flow is coupled with an eastward advected inland CBL above the sea breeze. Synoptic winds with a westerly component are typical of SEQ storm environments above the PBL (Callaghan 1996; Peter et al. 2015; Soderholm et al. 2016), thus an advected CBL is likely to be of continental origin.

5.4.2 Boundary Layer Variability

Although the sea breeze is relatively shallow, the hypothesised advection of an inland CBL aloft could provide a significantly deeper layer of conditionally unstable air for convective storm development. To further investigate the thermodynamic evolution of the coastal PBL, morning (09:00 AEST) and afternoon (adaptive time for operations) Brisbane Airport soundings are shown in Fig. 5.6 for 15 separate warm season days on which sea breezes occurred, and storms were anticipated. A majority of cases except for Fig. 5.6f,g,k, morning profiles exhibit a well-mixed CBL to a depth of approximately 1 to 1.5 km AGL. Mean winds through the morning CBL were light on sea breeze days (2.5 – 5 ms^{-1}), backing from the north to northwest (thin barbs of Fig. 5.7c). Above the CBL, conditions during the morning were considerably more varied, ranging from dry, continental air masses (Fig. 5.6l,n) to moist, well-mixed flow (b, c) from the southwest (l) to northwest (d).

By afternoon, the distinctive shallow, surface bound intrusion of maritime sea breeze air from the northeast can be seen for a majority of profiles (Fig. 5.6). The depth of onshore flow varied between 300 - 600 m, comparable with afternoon CP-2 observations (cf. Fig. 5.5). Thermodynamic changes associated with the sea breeze were diverse, with some cases showing low-level warming (Fig. 5.6c,e,j,l,m,o) and moistening (a,d,h,i,j,k,l) relative to morning conditions, while others (b,f,g,n) showed marginal temperature change and moistening. Conceptually, sea breeze air which originates from more northerly directions may have a trajectory closer to the coastline and possibly entrain air which has been warmed over land; however in this sample no relationship can be seen between the wind direction and thermodynamic trends.

Above the sea breeze current (approx. 750 m; cf. Fig. 5.5), the transition from the return flow to the free atmosphere is indistinct, except for an increasing westerly wind component. Warming ranging from 2 °C for (Fig. 5.6g) to 9 °C (Fig. 5.6l) is also observed above the sea breeze current for a majority of cases. As a result, the mean temperature difference between afternoon and morning profiles reaches a maximum of 2.8 °C at 800 m (Fig. 5.7a), while at the surface and above 1.5 km AGL, 0.5 °C (or less) of warming occurs. Mean dewpoints also show a consistent region of moistening above this warming layer, with a dewpoint increase of more than 4 °C at 1.5 km AGL (Fig. 5.7b). Figure 5.6d most clearly represents the mean changes observed in Fig. 5.7. Examination of the afternoon

profile for this case shows two well-mixed layers are present, the lowest within the north-northeast sea breeze in the lowest ~500 m AGL, and a second elevated mixed layer within 7.5 - 10 ms^{-1} northwest flow to a depth of 1.8 km AGL (~810 hPa). Elevated westerly flow implies the advection of the inland continental boundary layer towards the coast, which would continue to deepen and warm throughout the afternoon separate to the sea breeze.

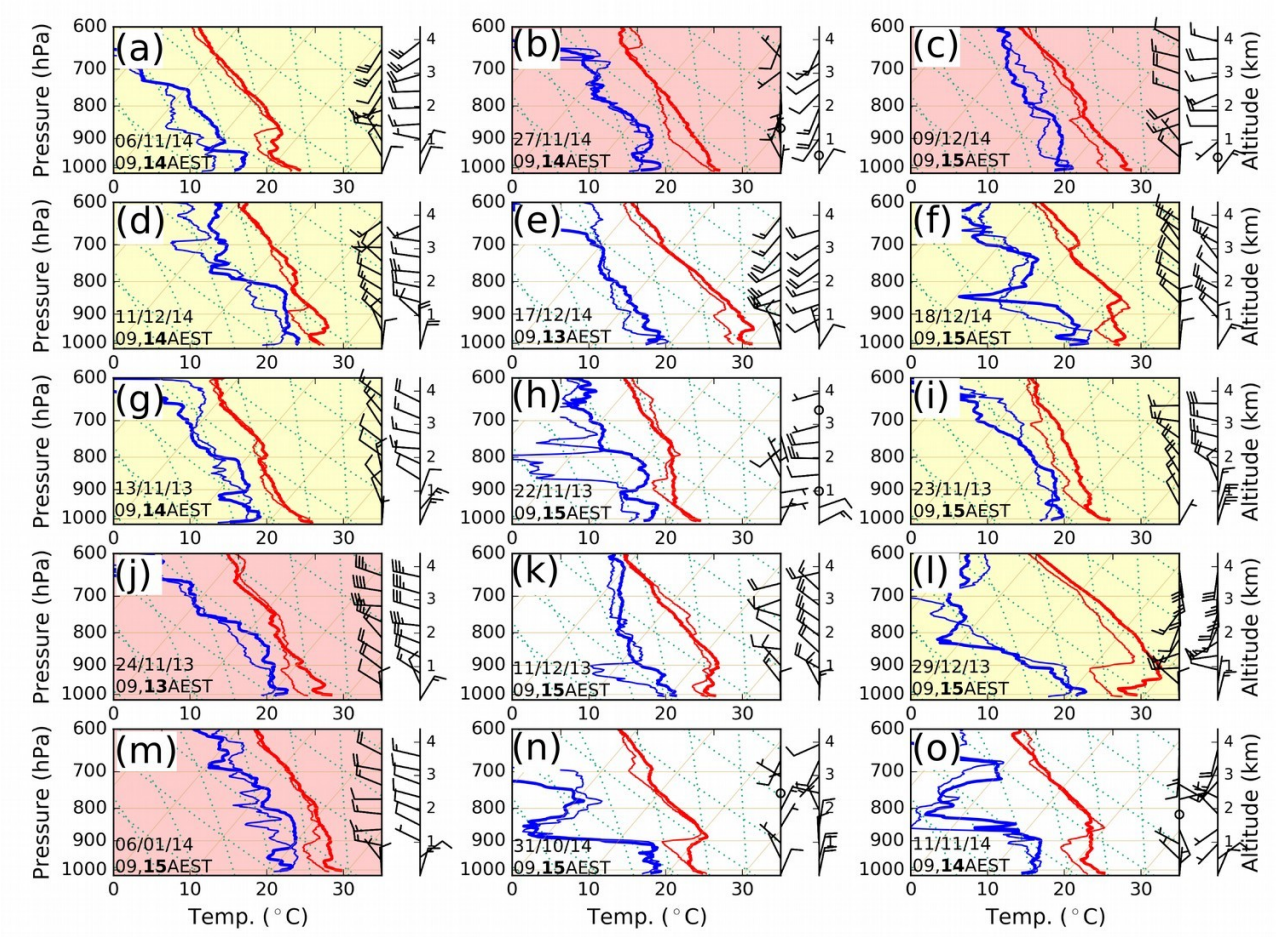

Figure 5.6: Morning (thin lines) and afternoon (bold lines) radiosonde profiles of temperature (red lines) and dewpoint (blue lines) from Brisbane Airport for sea breeze days. Dates (day/month/year, AEST) for each pair of profiles are shown in the bottom left corner of each panel, in addition to the time (hour, AEST) of the morning and afternoon profiles. Wind barbs for the morning and afternoon profiles are shown in the left and right columns, respectively, with half barbs for 2.5 ms^{-1} and full barbs for 5 ms^{-1}. Panel shading indicates thunderstorm mode within the Brisbane urban region, whereby white, yellow and red denotes null (no storms in SEQ), weakening (storms weaken near the coast) and convective (storms sustained/intensify near coast) modes, respectively. The first six plots (a-f) correspond to the dates of the six CP-2 cross sections of the sea breeze in Fig. 5.5.

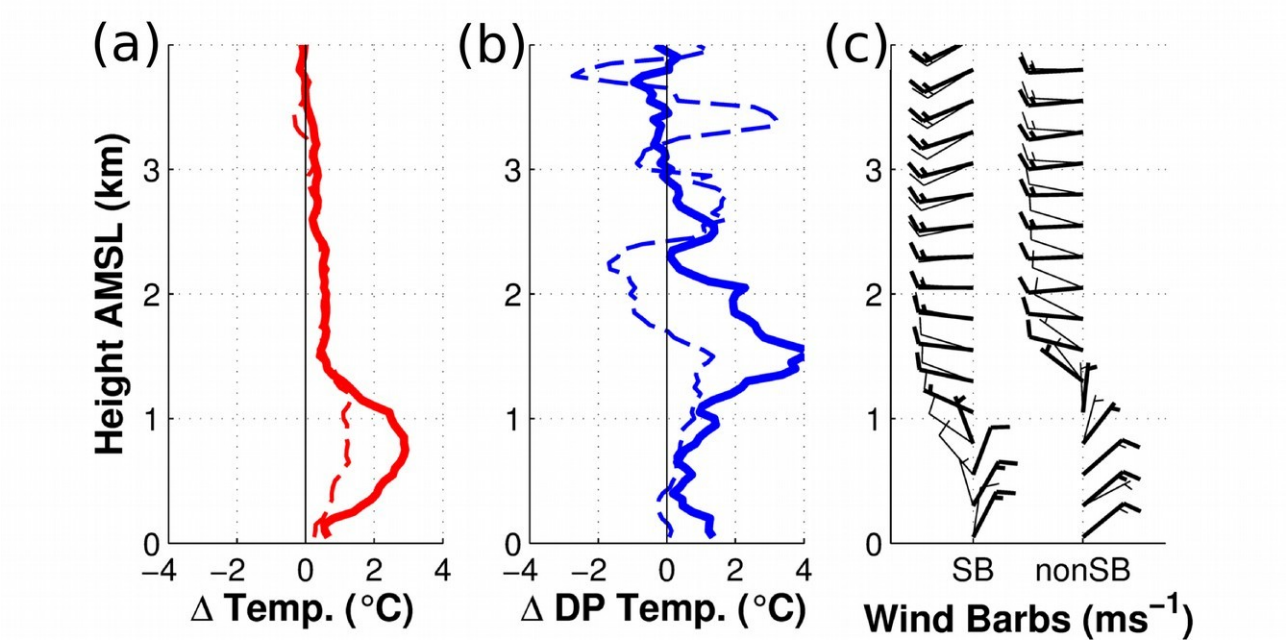

Figure 5.7: Composite of Brisbane Airport radiosonde profiles for 15 sea breeze days (solid lines in a,b; left column in c) and 11 other days when no sea breeze was detected (dashed lines in a,b; right column in c) between November 2013 and January 2015. Mean difference between afternoon (adaptive time) and morning (23Z) temperature and dewpoint profiles shown in panels (a) and (b), respectively. Panel (c) shows mean wind profiles from morning (23Z; thin barbs) and afternoon (adaptive; thick barbs) flights with half barbs for 2.5 ms^{-1} and full barbs for 5 ms^{-1}.

A conceptual model summarising the diurnal evolution of the coastal PBL developed from Fig. 5.6d is shown in Fig. 5.8. The advection of the continental CBL above the sea breeze results in warming, particularly for the layer which contained the cooler, morning CBL. Notable moistening occurs above the morning CBL, where the drier free atmosphere of the morning is replaced by the deeper afternoon continental boundary layer. This moisture most likely results from thermals within the deep continental CBL vertically transporting near-surface moisture while adiabatically cooling, increasing relative humidity with height. Cases of deep return flow (> 2.5 km AGL) in CP-2 RHI scans (Fig. 5.5b,e) corresponds with exceptionally well mixed profiles (Fig. 5.6b,e) above the sea breeze inversion. Anticipated warming of the sea breeze (e.g., Abbs 1986; Finkele et al. 1995; Chiba et al. 1999) as it propagates inland from the coastal Brisbane Airport site is also shown, leading to the part-erosion of the maritime inversion and, in some cases, deepening of the elevated mixed layer downward to the surface (cf. Fig. 5.6b,c,g).

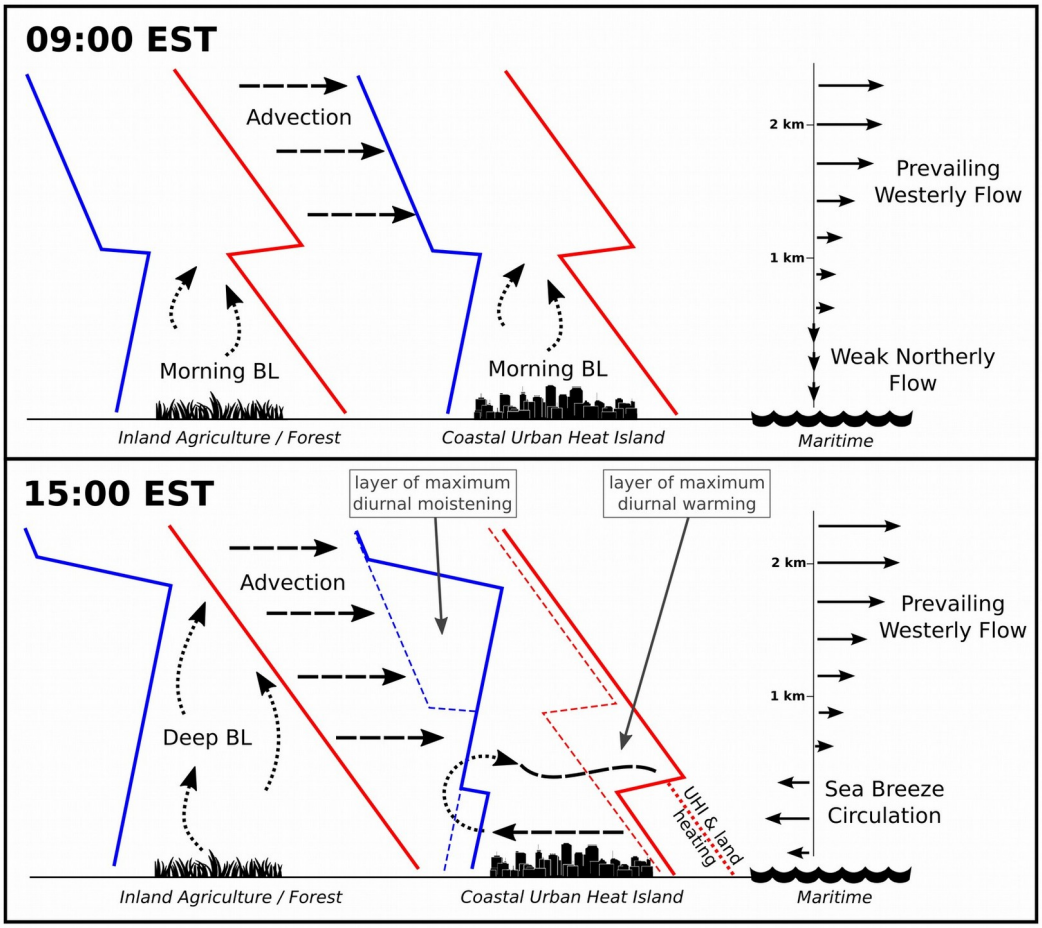

Figure 5.8: Conceptual schematic of diurnally forced preconditioning processes for deep moist convection in SEQ based on the soundings from Fig. 5.6. Idealised temperature (red) and dewpoint (blue) profiles are shown for inland agricultural / forested region and coastal urban region with solid lines. The 09:00 AEST profile is superimposed on the 15:00 AEST urban coastal profile with thin dashed lines for comparison. Hypothesised warming due to inland trajectories of the sea breeze over the coastal UHI and land shown with a thick red dotted line. Horizontal (vertical) flow shown with black dashed (dotted) lines. Idealised wind profiles are also provided on the right hand side.

Application of the concepts developed in Fig. 5.8 to the remaining cases of Fig. 5.6 highlights an elevated CBL air mass associated with warming and moistening above the sea breeze for all cases, excluding (b,l,n), where warming was accompanied by limited, or no moisture advection. This may be explained by the presence of a strong inversion for cases (l) and (n) which act to cap deep inland CBL development. For case (b), the morning free atmosphere above the CBL was considerably well-mixed and humid through to 3 km AGL, limiting the contribution of moisture by the advected continental CBL.

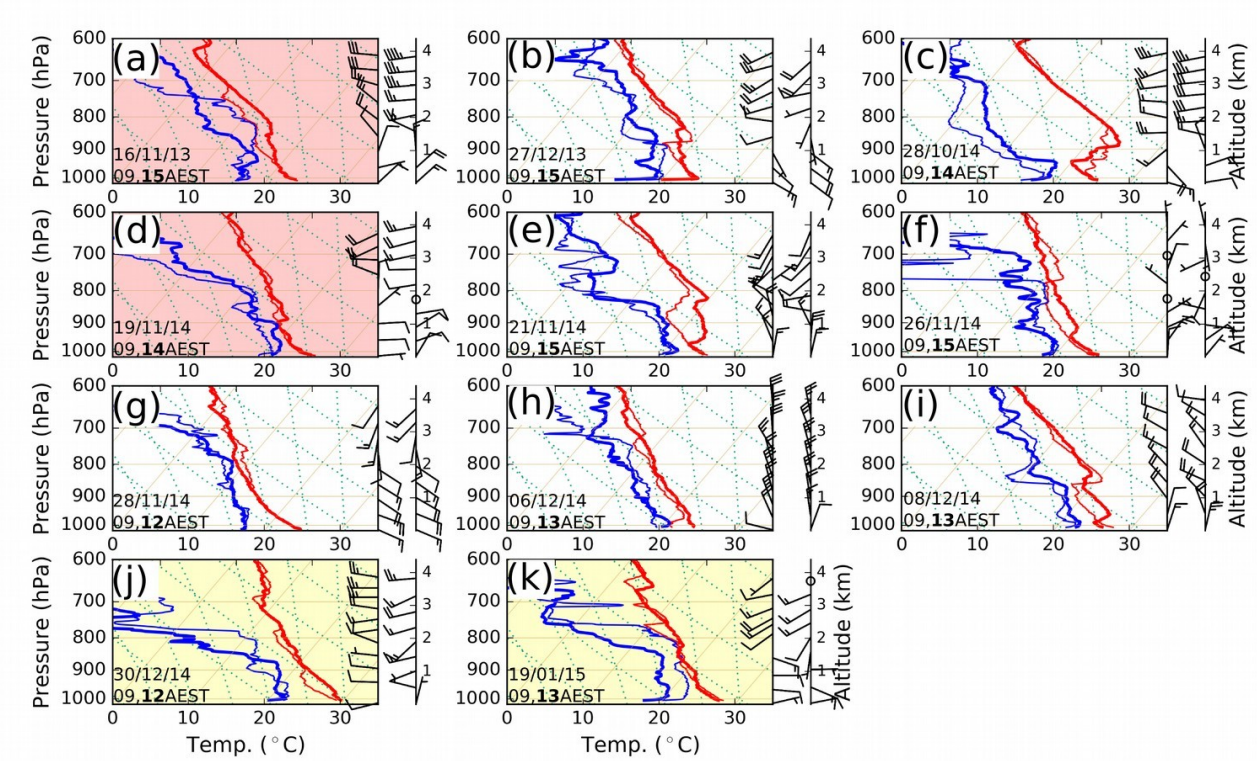

Figure 5.9: Morning (thin lines) and afternoon (bold lines) radiosonde profiles of temperature (red lines) and dewpoint (blue lines) from Brisbane Airport for non-sea breeze days. Dates (day/month/year, AEST) for each pair of profiles are shown in the bottom left corner of each panel, in addition to the time (hour, AEST) of the morning and afternoon profiles. Wind barbs for the morning and afternoon profiles are shown in the left and right columns, respectively, with half barbs for 2.5 ms^{-1} and full barbs for 5 ms^{-1}. Panel shading indicates thunderstorm mode within the Brisbane urban region, whereby white, yellow and red denotes null (no storms in SEQ), weakening (storms weaken near the coast) and convective (storms sustained/intensify near coast) modes, respectively.

To ascertain whether the eastward afternoon advection of a deep continental CBL is unique to the sea breeze days, an examination of 11 cases for which storms were anticipated but no sea breeze was detected is presented in Fig. 5.9. The mean wind profiles show limited diurnal variability through the first 1 km AGL in contrast to the afternoon veering seen on sea breeze days (Fig. 5.7c). Westerly advection starts from a higher altitude (1.5 km AGL) for non-sea breeze cases, resulting in an elevated but marginal mean afternoon warming maximum of 1.2 °C at 1.1 km AGL (Fig. 5.7a). Mean moisture advection in the north to north-westerly flow was also minimal (1.1 °C increase) and shallower (replaced by drying above 1.7 km AGL), suggesting the continental CBL was less developed than on sea breeze days. Analysis of the individual cases (Fig. 5.9)

indicates the presence of cloud layers (a,b,f,g,h,k) and strong synoptic flow (g,h) which may contribute to a less developed CBL inland. Furthermore, the absence of sea breeze return flow likely reduces the continental CBL mass flux for cases in Fig. 5.9.

5.4.3 Static Stability

Adaptive afternoon soundings from YBBN were released on 36 separate days during the CCIE when storms were forecast for SEQ; however storms only eventuated on 14 days, 10 of which had a sea breeze and 4 without a sea breeze. The higher occurrence of SEQ storm days during sea breeze conditions is consistent with Soderholm et al. (2016). Furthermore, convective storm activity varied markedly when it was present, with rapid intensification occurring for some cases over coastal plains (e.g., Brisbane), while other cases saw rapid dissipation when storms crossed the sea breeze front area This variability is summarised through the shaded backgrounds in Fig. 5.6 and 5.9, where white, yellow and red colours indicate null (no storms in SEQ), weakening (overall storm intensity decreased coastward) and convective (overall storm intensity sustained/increased coastward) modes, respectively.

To assess the stability characteristics of sea breeze convective environments, mean profiles of morning and afternoon θ_e are shown in Fig. 5.10. The stability of individual profiles appears related to the level of storm activity, with null modes occurring in the lowest energy environments, and convective modes in the highest energy environments. On sea breeze days, a shallow near-surface stable layer (increasing θ_e with height) is present for weakening and convective modes, while the lower θ_e profile for null modes may limit the energy difference to maritime air. Above approximately 750 m AGL (sea breeze depth, cf. Fig. 5.5), the decrease of θ_e with height apparent in the morning profiles is replaced with an afternoon layer of near-constant θ_e from the well-mixed continental CBL, resulting in steeper θ_e lapse rates (indicating stronger buoyancy) for all storm modes. The depth and magnitude of this warming also relate to storm activity, with the low energy shallow (~ 800 m), cool (335 K) CBL for null cases, and the high energy deep (~ 1.8 km AGL), warm (345 K) mixed-layer for convective days. Although the afternoon convective mode profile is the highest θ_e environment, it is also the only profile with a substantial stable layer below 1 km AGL, whereby afternoon θ_e is briefly lower than morning values around 450 m (7 K reduction).

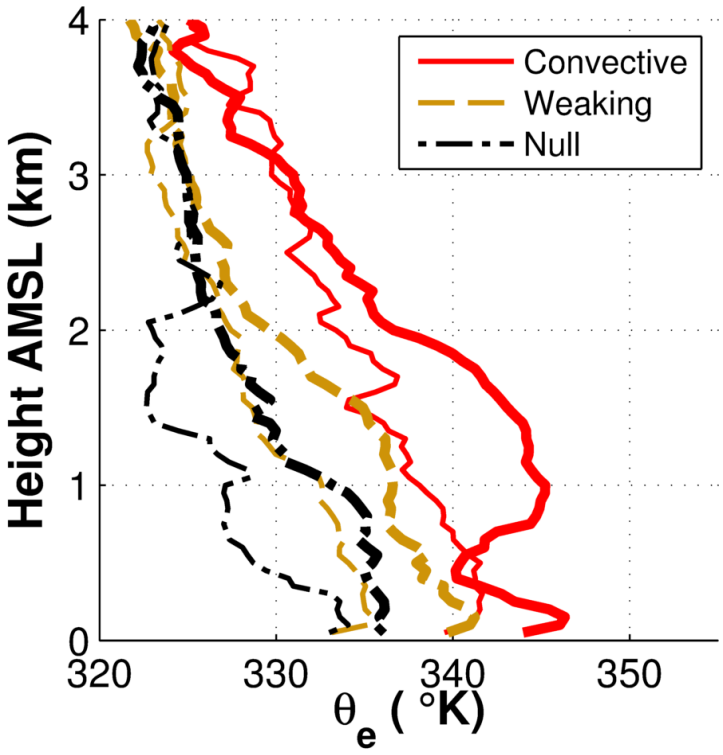

Figure 5.10: Mean equivalent potential temperature (θe) profiles derived from the morning (thin lines) and afternoon (bold lines) Brisbane Airport soundings (See Fig. 2.5 for location) shown in Fig. 5.6 on sea breeze days. Profiles have been classifed into the three thunderstorm modes described for Fig. 5.6: null convection (black lines; Fig. 5.6e,h,k,n,o), weakening convection (orange lines; Fig. 5.6a,d,f,g,I,l) and convective (red lines; Fig. 5.6b,c,j,m).

To diagnose the thermal and moisture driven contributions of the mean θ_e profile for convective cases, the mean difference between afternoon and morning profiles of temperature and dewpoint are shown in Fig. 5.11. The near-surface θ_e maximum of the convective mode profile in Fig. 5.11 is driven by both warming and moisture increase by afternoon, while the elevated θ_e maximum is mostly attributed to an increase in moisture. Maximum warming between 300-800 m is offset by substantial drying, leading to the noted stable θ_e layer. Analysis of individual cases (Fig. 5.6b,c,j,m) shows a reduction in afternoon dewpoint through a shallow layer at approximately 975-950 hPa, possibly associated with subsidence of westerly return/synoptic flow above the sea breeze (Finkele et al. 1995; Chiba et al. 1999). Mixing of this drier air into storm inflow would likely reduce parcel buoyancy; however the effect would be marginal due to the moisture aloft and near to the surface (Fig. 5.11).

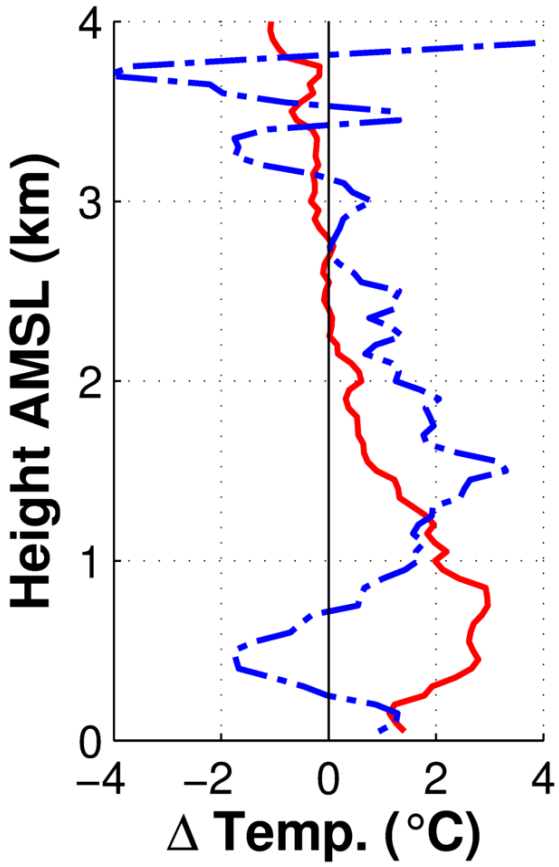

Figure 5.11: Mean difference between afternoon (variable time) and morning (09:00 AEST) temperature (red solid lines) and dewpoint (blue dash-dot lines) soundings from Brisbane Airport for 4 sea breeze days when convection was sustained/intensified on the coastal plains (Fig. 5.6b,c,j,m) between November 2013 and January 2015. Adaptive afternoon radiosondes released at times ranging from 14:00 to 16:00 AEST on forecast thunderstorm days, therefore limiting the availability of analysis days.

5.5 27 November 2014 Case Study

This section presents a severe thunderstorm event that illustrates how the boundary layer preconditioning concepts introduced above can influence the evolution of deep convection. On the 27 November 2014, a hailstorm producing 70-80 mm stones and a maximum wind gust of 39.2 ms^{-1} impacted Brisbane and the surrounding suburbs, resulting in insured losses exceeding $1.4 billion AUD (Insurance Council of Australia 2015). The synoptic environment was unremarkable, with a weak upper-level trough positioned over southeast Australia, a shallow southeasterly air mass change propagating into the region, and a continental dryline to the west (not shown). As a result, the 09:00 AEST Brisbane Airport sounding (Fig. 5.6b) lacks the steep lapse rates and deep layer wind shear commonly associated with a high-impact, organised convective storms (Weisman and Klemp 1982). A CCIE IOP was conducted during this event, providing the opportunity for an in-depth analysis of environmental preconditioning and storm evolution.

5.5.1 Radar and Environmental Analysis

Surface mesoanalyses were generated at four instances (12:00, 15:00, 16:12 and 16:24 AEST) prior to the storm's passage over Brisbane at 16:42 AEST using the BoM, EHP and CCIE AWS networks (Fig. 5.12). Characteristic features of the mean sea breeze mesoanalysis (Fig. 5.4) can be seen prior to the development of convection at 12:00 AEST (Fig. 5.12a), including the enhancement of moisture over Brisbane and the southwest region, and an axis of relatively dry, warm air running north-northwest to south-southeast through Amberley. Overall, near-surface temperature and dewpoint fields were 2-4 °C higher than the mean conditions (cf. Fig. 5.4a), increasing θ_e by approximately 10 K across SEQ. A 12:00 AEST sounding at Kalbar (Fig. 5.13) suggest that the developing continental CBL was advected towards Brisbane under weak southwesterly flow. The moisture depth (~ 850 hPa) and content of the CBL observed at Kalbar is comparable to the elevated CBL observed in the 14:00 AEST Brisbane Airport profile, 2 hours later (Fig. 5.13), therefore supporting the hypothesised mechanism for the observed warming and moistening over the coastal plains by the afternoon (Fig. 5.8). As the afternoon progresses, the near-surface dew point gradient (12 – 19 °C) sharpened as the continental dryline propagated into western SEQ at 15:00 AEST (Fig. 5.12b), decreasing the near-surface θ_e over western SEQ due to lower surface moisture. Two developing storms (reflectivity > 35 dBZ) were also present at this time, triggered near the elevated topography of the southern ranges

and the approaching southeasterly change.By 16:12 AEST, the eastern storm had strengthened into an east-west oriented multicell, while the western storm had dissipated following a period of strong outflow, despite interacting with a potentially favourable sea breeze triple point (Fig. 5.12c). In contrast to the dry, weakly sheared environment of central SEQ, the eastern storm was developing in a deep well-mixed CBL with rich near-surface moisture and favourable storm-relative inflow from the sea breeze while approaching the coastal θ_e maximum over Brisbane.

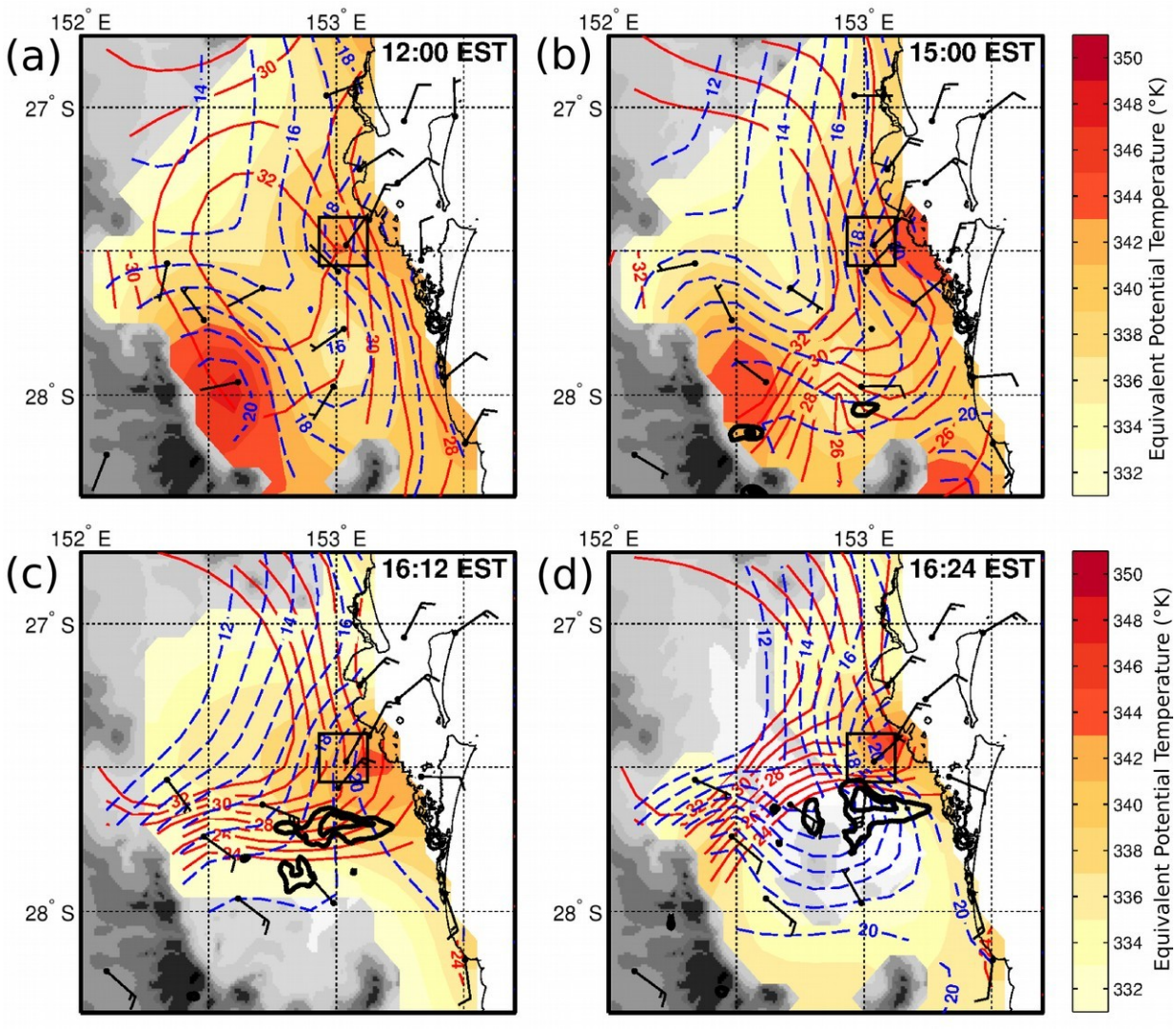

Figure 5.12: Contour plots of interpolated surface temperature (red solid lines), dewpoint (blue dashed lines) and equivalent potential temperature (shaded contours) at selected times on 27 November 2014. Contours of radar reflectivity from the CP-2 0.9° Plan Position Indicator (PPI) scans shown with bold black lines at 35 dBZ and 50 dBZ. Wind shown with half barbs for 2.5 ms^{-1} and full barbs for 5 ms^{-1}. Topography shaded in 250 m intervals and the box indicates the Brisbane urban region.

As the eastern storm propagated into the high θ_e near-surface environment, multiple concurrent bounded weak echo regions (BWERs; Phillips 1973; Markowski 2002) were observed on radar from 15:54 AEST, followed by a pronounced three body scatter spike (TBSS; Wilson and Reum 1988) associated with an elevated hail core from 16:18 AEST onward. Velocity couplets were also present; however, their short duration (6-12minutes) was likely insufficient to support a more steady-state updraft. A set of CP-2 PPI scans providing low (~500 m) and mid-level (~3.5 km) coverage of the storm are shown in Fig. 5.14, revealing the complex structure of the multicell, including the presence of concurrent BWERs. At 16:24 AEST, two mid-level BWERs can be identified in the 12.8° PPI scan (Fig. 5.14b) on the leading northern edge of the multicell, while 5 minutes later low-level outflow on the western flank produced a 39.2 ms^{-1} gust at Archerfield (16:29 AEST). By 16:42 AEST, the two previous BWERs were replaced with a single larger BWER as the system tracked north. A new BWER collocated with a broad mid-level mesocyclone (Fig. 5.14d) is also present above a surface inflow notch (Fig. 5.14c), indicating that an updraft was intensifying as the storm propagated over Brisbane. The continual development and replacement of large BWERs from 15:54 AEST onward is indicative of the storms potential to grow large hail. A broad region of high reflectivity > 65 dBZ (Fig. 5.14c,d) and low differential reflectivity (ZDR) (-1 to 0 dB; not shown) aloft and at the surface was associated with 70-80 mm hail stones reported south of Brisbane.

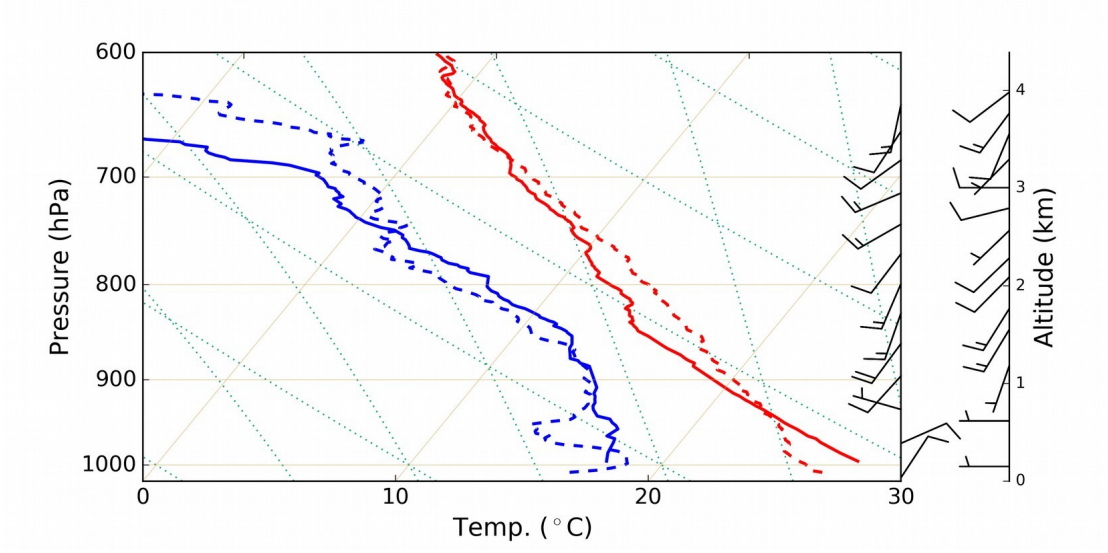

Figure 5.13: Afternoon soundings from Brisbane Airport at 14:00 AEST (dashed lines) and Kalbar 12:00 AEST (solid lines) of dewpoint (blue lines) and temperature (red lines) form 27 November 2014. Wind barbs for Brisbane Airport and Kalbar are shown in the left and right columns, respectively, with half barbs for 2.5 ms^{-1} and full barbs for 5 ms^{-1}.

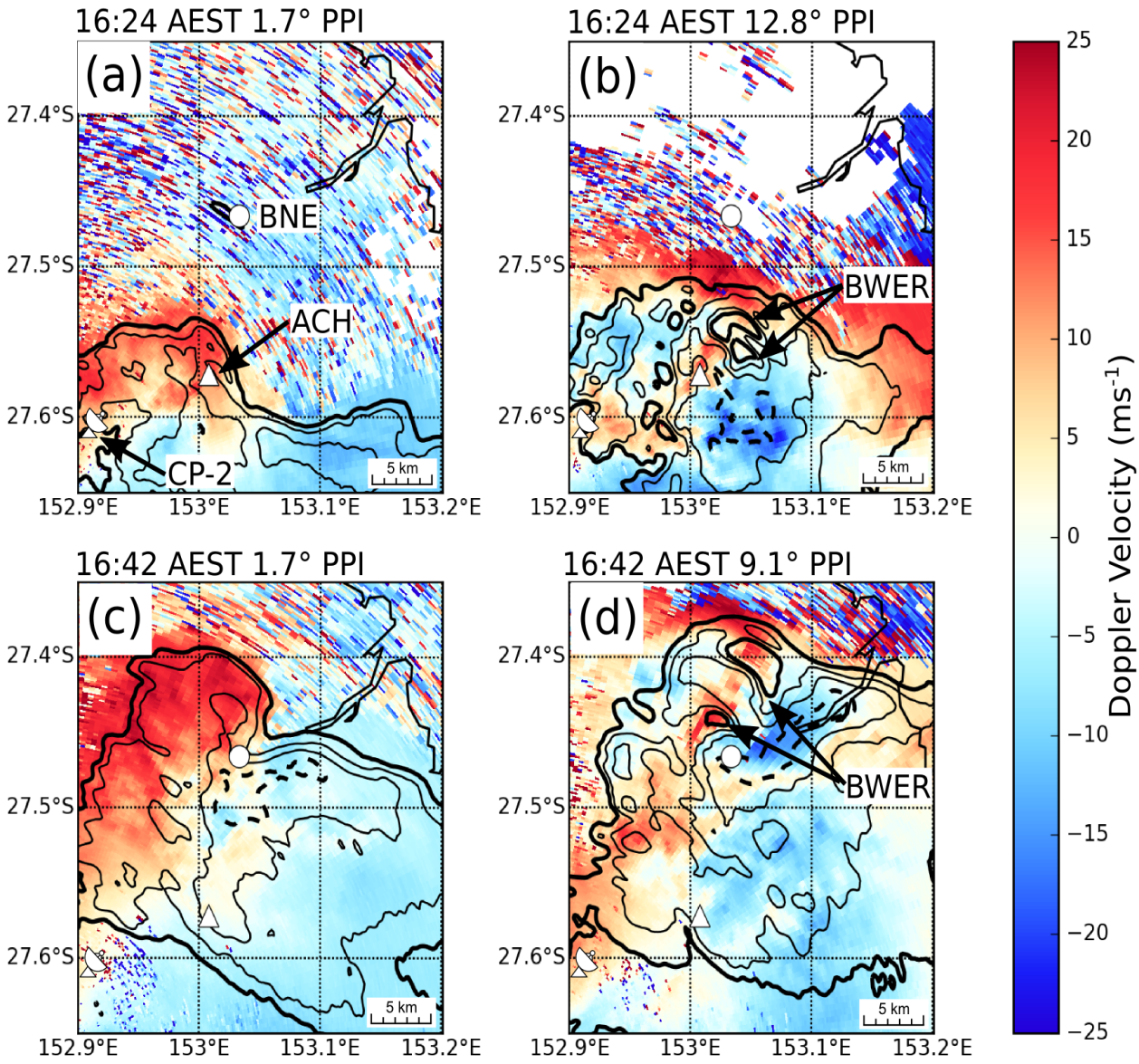

Figure 5.14: Plan Position Indicator (PPI) imagery of the 27 November 2014 hailstorm from CP-2 radar (location marked in lower left corner). PPI scans are shown at 16:24 AEST (a, b) and 16:42 AEST (c, d) for 1.7° (a, c) and 12.8° (b, d) tilts. Approximate height PPI surface cuts through storm updraft are 300 m (a), 3.3 km (b), 500 m (c) and 3.6 km (d). Doppler velocity is colour shaded and contours of smoothed reflectivity are shown in steps of 10 dBZ from 35 dBZ. The 35 dBZ contour is bold and the 65 dBZ contour is dashed. The location of Brisbane is marked with a white circle and Archerfield with a white triangle. Bounded weak echo regions (BWER) are labelled.

To estimate the convective potential of the near-surface airmass the storm was ingesting near Brisbane, the 16:30 AEST Brisbane AWS (BoM) observation of 28°/20° C (temperature/dewpoint) was inserted into the lowest level of the 14:00 AEST Brisbane Airport sounding. This sea-breeze - UHI influenced parcel was highly unstable, with 2120 J kg^{-1} of surface-based convective available potential energy (SBCAPE) and only 30 J kg^{-1} of convective inhibition (CIN). The environmental wind profile at 14:00 AEST was nevertheless marginal for organised storms; with 0 – 3 km storm-relative helicity (using a storm motion towards 14° at 14 m s^{-1}) of -23 m^2 s^{-2} and 7.7 m s^{-1} of 0 - 6 km bulk shear. The proximity of the southeasterly change to the multicell would have likely increased local shear further, particularly in the low levels. Prior to the storm's passage through Brisbane, intensification of the sea breeze was observed, with 16:00 AEST Brisbane Airport 10 m winds reaching 8 m s^{-1} from the north-northeast (10-minutes) and a 15:51 AEST Aircraft Meteorological Data Relay (AMDAR) observation of 11 m s^{-1} (northeast) at 600 m over Brisbane (not shown), increasing storm-relative inflow.

5.5.2 Environmental drivers of storm characteristics

The presence of intermittent high precipitation (HP) supercell features (e.g., large BWERs, > 65 dBZ reflectivity and brief mid-level mesocyclones) within a predominantly multicell storm system (concurrent updrafts, transience of the mesocyclones and lack of organisation), suggests the 27 November 2014 event was a multicell-HP supercell (Moller et al. 1990). This mode was also observed by Richter et al. (2014) for a wind storm which impacted northwest Brisbane on 16 November 2008. The convective environments from the 27 November 2014 and 16 November 2008 events are remarkably similar; including low 0-6 km bulk shear (< 10 ms^{-1}), 2000+ Jkg^{-1} of afternoon SBCAPE, an approaching southeasterly change and a sea breeze. Weisman and Klemp (1982) showed that for a given amount of buoyancy, a low-to-moderate shear noted for these events favours multicellular growth, rather than supercellular. The vorticity required to build a mesocyclone can potentially be sourced from the lifting and tilting of horizontal vorticity within the inflow layer along the boundaries (e.g., southeasterly change, sea breeze boundary; Markowski et al. 1998; Atkins et al. 1999). Sills et al. 2004 found that low-level boundaries were central to the enhancement and mesocyclone development of storms that produced tornadoes in Sydney under weak synoptic-scale forcing. Furthermore, without the sustained dynamical lifting promoted by a long-lived mesocyclone (Doswell

1996; Ziegler et al. 2010), multicell-HP supercells are consequently more sensitive to the stability of the inflow layer.

For the 27 November 2014 case where the storm's inflow layer included a deep well-mixed CBL, the heterogeneous near-surface moisture supply (e.g., sea breeze advection, irrigated areas) and heating (e.g., UHI, inland regions) potentially influenced the ultimate buoyancy of inflow parcels, and thus updraft intensity. The importance of land surface properties for storm evolution is widely recognised, including for urban settings (Chen et al. 2007; Haberlie et al. 2014; Ryu et al. 2015), reservoirs (Haberlie et al. 2015), sea breezes and irrigation/agriculture (Pielke and Zeng 1989; Carleton et al. 2001; Deangelis et al. 2010). Within the PBL, the availability of moisture also influences updraft intensity through the entrainment and drying of lifted parcels (James and Markowski 2010). The deep moisture from the advected CBL shown in Figure 14 suggests reduced potential for entrainment of dry ambient air and consequent buoyancy loss of updraft parcels. Furthermore, findings by Coniglio et al. (2011) and analysis by Richter et al. (2014) suggest that deep moisture, substantial hydrometeor loading and associated melting of hail stones may have contributed significantly towards the destructive surface gusts observed at Archerfield.

The weak deep-layer shear, high CAPE synoptic scale storm environments of the 2014 and 2008 Brisbane events are symptomatic of the subtropical climate in SEQ due to the poleward shift of the jet stream during the warm season. Synoptic scale convective parameters therefore provide limited diagnostic skill for forecasting multicell-HP supercell supporting environments. On the mesoscale, the southeasterly change and sea breeze noted in the 2008 and 2014 cases represent the dominant boundaries for SEQ hailstorms (Soderholm et al. 2016), including for the Brisbane region. Given both the synoptic conditions and mesoscale forcing of the 2008 and 2014 cases are not outliers within the climatology, it is not unexpected to find that these environmental conditions repeatedly occur for historical high-impact storm cases. This includes the 18 January 1985 hailstorm (Callaghan 1996), which incurred the largest single insured losses of any natural disaster for Brisbane ($2 billion AUD; Insurance Council of Australia 2015).

5.6 Discussion and Conclusions

The rapidly growing population of coastal regions benefit from an understanding of the processes which favour deep convection within the typically stable maritime atmosphere. A diverse range of diurnally forced planetary boundary layer (PBL) processes occur within the coastal settings (e.g., sea breezes, urban effects, terrain winds); yet, further research is required to understand their influence upon the convective storm environment. Observations from the Convective Coastal Interactions Experiment (CCIE) were analysed to identify and understand processes which provide favourable PBL preconditioning for convective storms in South East Queensland (SEQ), Australia.

The observational datasets were divided according to the presence or absence of the sea breeze, which is recognised as a dominant influence for coastal environments in chapters 3 and 4. The sea breeze and prevailing synoptic conditions were found to be associated with increased inland warming and coastal moisture (Fig. 5.1); however, modification by the near-surface and PBL processes were essential for favourable convective preconditioning. Earlier mean onset of the sea breeze was observed for Brisbane in contrast to the adjacent coastal rural environments, possibly due to the urban heat island (UHI) enhanced thermal gradient. Previous documentation of this interaction is limited to modelling studies (Khan and Simpson 2001; Ohashi and Kida 2002; Freitas et al. 2007). Furthermore, the enhanced moisture flow coupled with the UHI thermal contribution (Fig. 5.3) creates a notable near-surface instability maximum over Brisbane (Fig. 5.4), which may influence convective updraft intensity (e.g., Smith et al. 2000; Kunz et al. 2009; Mona et al. 2016).

Analysis of the inland surface environment showed increased near-surface moisture associated with agricultural areas in proximity to the areas of high hailstorm intensification documented by chapter 4. Coastward advection of this favourable inland convective boundary layer (CBL; Fig. 5.5) led to substantial afternoon warming and moistening of the coastal vertical profile (Fig. 5.7 and 5.8). An elevated convective boundary layer (CBL) was also noted by Muppa et al. (2015) for continental western Germany, suggesting this processes is not restricted to coastal settings. Coupled with the moisture rich sea breeze, the advected continental boundary layer substantially increases the depth of highly buoyant air available for storm updrafts (Fig. 5.10; Thompson et al. 2007). Furthermore,

maritime inversions were noted to be of marginal strength for the four most convectively active sea breeze days, indicating low convective inhibition (CIN) of the sea breeze air.

The potential importance of diurnally forced changes to the near-surface and PBL atmosphere was highlighted in the 27 November 2014 case study. The storm intensified as it approached an equivalent potential temperature maximum centred on Brisbane, induced by UHI enhanced sea breeze flow and warming (Fig. 5.12). Furthermore, an inland sounding confirmed the coastward advection of a deep inland CBL (Fig. 5.13), supporting the hypothesised mechanism for regular moistening and warming above the sea breeze. The afternoon sounding from Brisbane Airport indicates large SBCAPE and low CIN as a result of these preconditioning mechanisms. Although the broad-scale shear profile was unfavourable for storm organisation, intermittent mid-level supercell features were noted during the event, potentially due to low-level vorticity ingested from nearby surface boundaries and associated lifting/tilting suggested by Atkins et al. (1999). The predominantly multicellular features with occasional transient mesocyclones indicate a multicell-HP supercell mode (Moller et al. 1990), comparable to the 16 November 2008 windstorm event (Richter et al. 2014). Lacking the sustained dynamical lifting of a long-lived supercell, this mode is hypothesised to be more susceptible to the thermodynamic properties of the inflow. Numerous studies have identified the importance of heterogeneous surface features such as cities (Niyogi et al. 2011; Haberlie et al. 2014; Ryu et al. 2015), reservoirs (Haberlie et al. 2014), terrain (Banta and Schaaf 1987; Weckwerth et al. 2011; Nisi et al. 2016) and irrigated land (Pielke and Zeng 1989; Deangelis et al. 2010) for understanding convective response to the land surface properties.

Comparable storm-prone coastal environments can be found globally throughout the subtropical regions, including southern and southeastern United States (Blanchard and López 1985), Taiwan (Lin et al. 2011) and Brazil/Argentina (Pinto et al. 2013)); and for warmer temperate climates including Spain (Azorin-Molina et al. 2014b), Italy (Baldi et al. 2014), New Zealand (Steiner 1989) and Eastern USA (Cintineo et al. 2012). Findings of this study are applicable across these regions, particularly for coastal cities and synoptic conditions supporting the coastward advection of an inland CBL profile.

CHAPTER 6

CONCLUSIONS AND FUTURE RESEARCH

Explosive growth of a Hybrid multicell-HP Supercell over the climatological "hotspot" of southern Brisbane on the 7 November 2015 (Robert Skidmore, Mr "S" Photography).

Chapter 6. Conclusions and Future Research

This thesis represents the first comprehensive study of convective storm activity for a continental coastal setting. Significant knowledge gaps in the understanding of coastal storm environments have been addressed through the integration of a radar-derived climatology of convective storms, the longest published internationally, with Australia's first mobile convective storm experiment. Overall, this study addresses the primary research aim: to provide an understanding of atmospheric processes within the coastal setting which favour the intensification of convective storms. The following section provides a summary of the CCIE findings in relation to the objectives stated in section 1.3 and the overall significance of the study within an international context. Finally, priorities for future convective storm research in subtropical coastal settings are outlined.

6.1 Overview of Objectives and Major Findings

Objective 1: Develop a methodology for quantifying the drivers of frequent convective storm activity at climatological and meteorological scales for the SEQ region using observational datasets.

To investigate SEQ convective storms from temporal scales ranging from minutes to decades, this thesis developed the framework for integrating a long-term climatological analysis with an intensive field campaign in chapter 3. Firstly, climatology results from an 18-year radar dataset were analysed for the existence of hailstorm hotspots across the region. Major hotspots were identified in the vicinity of the Boonah and Esk townships of southwest and northwest SEQ, respectively, confirming anecdotal evidence provided by regional forecasters and the members of the public. Furthermore, hailstorm hotspots were found to be most pronounced on sea breeze days, confirming prior case study evidence documented by Callaghan (1996).

A field campaign strategy was designed to investigate convective storm hotspots in SEQ using the guidance provided by the long-term climatology (Soderholm et al. 2016). Specifically, the observation-sparse southwest region of SEQ was targeted for the deployment of weather stations and the operation of a mobile platform for polarised X-band radar and radiosonde observations. For the coastal region, the sea breeze activity was monitored using adaptive soundings, SODAR/RASS profilers and radar vertical cross

sections. An analysis of field observations highlighted the wealth of information available for analysing fine-scale variability sea breezes, convective storms and associated interactions from these field datasets.

Objective 2: Investigate the long-term climatologies of SEQ sea-breeze and convective storm activity for evidence of forcing on spatial scales ranging from local (< 10 km) to climate teleconnections.

An in-depth analysis of the radar-derived hailstorm and weather station-derived sea breeze datasets introduced by chapter 3 climatology was presented in chapter 4. The influence of atmospheric processes from the local/mesoscale (topography and sea breezes) to broad-scale (synoptic types and ENSO) were investigated. At inter-annual time-scales, hailstorm day frequency was found to be correlated (R = 0.76) with sea breeze day frequency, suggesting these processes share a similar response to large-scale forcing. Furthermore, significant autocorrelation was present for these time series, despite the limited influence sea breezes and hailstorms have upon the long-term weather. Given the robust evidence of ENSO influence upon eastern Australia rainfall, this climate oscillation was investigated as a possible mechanism for the significant autocorrelation and cross-correlation in the hailstorm and sea breeze time series. A statistically significant relationship was found whereby El Niño ENSO events increase the frequency of annual hailstorm (R = -0.52) and sea breeze (R = -0.69) days. It was hypothesised that the suppressed trade wind flow during El Niño events promotes diurnal heating, providing more buoyancy for convective storms and a stronger and-sea gradient for sea breezes, while enhanced trade wind flow during La Niña events suppresses activity.

Spatial analysis of hailstorm tracks identified that convectivie initiation was most frequent on the coastward aspect of the inland Great Dividing Range, suggesting lee slope convergence forced by thermotopographic winds and prevailing westerly flow was a dominant trigger mechanism of convective storms in SEQ. These storms developed hail (MESH ≥ 21 mm) most frequently over the inland valleys of SEQ in proximity to the Boonah and Esk townships. Investigation of average sea breeze arrival time through this region indicates that HD activity peaks within the post sea breeze airmass (0600 - 0700 UTC). It is hypothesised that the inland trajectory of sea breeze over a warming land surface modified the typically stable maritime air mass sufficiently to promote storm

intensification. Out of the six synoptic – sea breeze scenarios investigated, the southeasterly change type coupled with a sea breeze was found to be most favourable for hailstorms, accounting for 30% of all events. MESH distribution under southeasterly changes were found to be skewed towards larger hail sizes, confirming preliminary work by Callaghan (1996), which suggested that this scenario accounts for the majority of significant hailstorm events in SEQ

Objective 3: Explore the influence of local processes upon the preconditioning and the evolution of convective storms through observations obtained by the CCIE.

In chapter 5, field campaign measurements from the CCIE were investigated to identify PBL processes which provided favourable preconditioning for storms over the hotspots regions of SEQ analysed by chapters 3 and 4, and for the coastal plains. Concepts developed in this chapter were also applied to investigate a severe hailstorm case study event. Spatial analysis of near-surface conditions indicated substantial variability of buoyancy associated with land types and usage. In particular, irrigated agriculture across the southwest hailstorm hotspot region identified in chapter 3 was associated with enhanced near-surface moisture, increasing the favourability for convection. For Brisbane, comparison of morning (09:00 AEST) temperature measurements within urban environment to those from rural coastal areas showed a mean increase of 2.7 °C associated with the UHI, indicating a substantial contribution to near-surface parcel warming. The enhanced land-sea gradient from the UHI likely contributed to the earlier arrival of the sea breeze in contrast to adjacent rural areas, leading to enhanced maritime moisture over the city landscape. The combination of enhanced sensible heating and moisture advection produced an θ_e maximum over Brisbane 4-6 K warmer than the surrounding coastal plains. Above the sea breeze, substantial afternoon warming (> 3 °C) and moistening (> 4 °C dew point) was also observed at the coast, providing a deep layer of high θ_e air within the boundary layer. Weather radar and radiosonde measurements suggest this instability increase was attributed to the coastward advection of the deep afternoon convective boundary layer from western regions of SEQ.

The 27 November 2014 hailstorm event was investigated for the influence of the PBL preconditioning processes introduced above. Large BWERs and associated hailstone growth developed as the storm approached the convectively favourable θ_e maximum of Brisbane. Inland radiosonde releases suggested the advection of a deep CBL above the

coastal plains sea breeze, leading to large SBCAPE and low CIN over the city environment. The presence of intermittent mid-level mesocyclones in the absence of a supportive ambient deep-layer shear suggested the contribution of low-level shear lifted from boundaries within the southeasterly change – sea breeze environment. These mechanisms likely contribute to the climatological favourability of this environment for hailstorms shown by chapter 4.

6.2 Study Significance

The Coastal Convective Interaction Experiment represents the first comprehensive observational study of a continental coastline setting globally, providing a foundation for understanding the atmospheric processes which influence storms in this landscape. Prior studies of coastal storm environments are rare in the literature, in spite of this narrow landscape setting containing more than 50% of the global population in high density urbanised areas. The Convective and Precipitation/Electrification (CaPE) experiment conducted in Florida, United States, represents the only comparable observational study of a sub-tropical coastal storm environment (Wakimoto and Atkins 1994; Atkins et al. 1995). However, the opposing sea breeze scenario investigated by CaPE can only be found in a peninsular setting, in contrast to single sea breezes across continental coastlines. Furthermore, the contemporary understanding of global convective storm environments is primarily derived from the wealth of measurement and simulation studies conducted for the tornado-prone Great Plains of the United States, which have a less pronounced maritime and topographical influence.

Previous observational studies of convective storms focus upon developing either a long-term climatological analysis at broad scales or short-term meteorological analysis at fine spatial scales. Both approaches have enabled us to develop considerable understanding of these processes, but they remain limited to their respective atmospheric scale of analysis. In chapter 3 it was shown that these two approaches are complementary for developing a long-term study at fine-spatial scales of convective storm characteristics. Climatological evidence of hailstorm hotspots and sea breeze influence was targeted by a field program to understanding the meteorological forcing of long-term trends, while field measurements were applied to guide further investigation of mesoscale processes in the climatology. The CCIE field campaign included the first application of mobile Doppler scanning lidar and mobile polarised radar in a sub-tropical coastal environment for the

study of convective storms. Results presented in chapter 3 are particularly encouraging for the application of the CCIE methodology for understanding the PBL and associated storms in coastal environments globally.

This thesis provides a significant contribution to our understanding of long-term influences upon convective storm trends. Previous studies of long-term radar-derived climatologies focus either upon mesoscale (e.g., UHIs, lakes) or large-scale (synoptic regimes, topography, land-use) influences. In chapter 4 this study presents the longest (18-year) radar-derived climatology of hailstorms published internationally, and the first to incorporate an analysis of both mesoscale (sea breeze occurrence) and large-scale (ERA-Interim reanalysis, SOI) datasets. Results from the mesoscale analysis not only confirm the importance of the sea breeze front as a trigger for convective storms, but also highlights the potential role of the associated inland maritime air mass for the intensification of convection. Comparable findings regarding the climatological significance of convective activity within an inland sea breeze flow are absent from the literature, promoting further investigation using field campaign datasets in chapter 5. The likely applicability of SEQ to sub-tropical coastlines worldwide suggests inland modification of sea breeze is likely important for storm prone regions. At synoptic scales, the southeasterly change type in combination with a sea breeze was found to be the optimal scenario for hailstorms, confirming previous case-study derived hypotheses of Callaghan (1996).

In addition to a mesoscale and broad-scale analysis, chapter 4 provides the an inter-annual analysis of a radar-derived hailstorm climatology. A negative correlation was found between the frequency of annual hailstorm and sea breeze days with the SOI, indicating ENSO contributes to the inter-annual variability. This finding is inconsistent with previous multi-decadal studies using reanalysis derived storm environments (Allen and Karoly 2014) and severe storm reports (Yeo 2005); however these studies do not apply explicit observations of convective storms. The radar derived climatology dataset provides both uniform sampling and storm-resolving observations, highlighting its robustness. The inter-annual correlation with ENSO is encouraging for the seasonal storm prediction using climate models.

This thesis investigates the PBL preconditioning processes of a continental coastal storm environment using datasets from an intensive field campaign. The Brisbane urban setting was found to generate a substantial increase in near-surface instability through increased sensible heat flux and modified sea breeze flow. This finding is supported by the first observational evidence of earlier sea breeze arrival at a coastal city environment associated with the UHI enhanced land-sea gradient, confirming prior modelling studies. The importance of small changes in parcel stability for deep convection is well documented by previous studies, suggesting storm inflow parcels sourced from Brisbane likely contribute to updraft instability. This hypothesis has significant implications for the vulnerability of rapidly growing coastal urban regions globally. Above the sea breeze, a substantial increase in afternoon instability was attributed to the coastward advection of the deep afternoon CBL from western regions of SEQ. This processes in combination with inland warming of the sea breeze produced the most favourable environments for severe storms during the CCIE, highlighting the misconception that the sea breeze is a stable airmass and unfavourable for convective storms.

Examination of 27 November 2014 severe hailstorm environment identified the presence of favourable near-surface and PBL processes associated with the occurrence of the rarely documented multicell-HP supercell mode. There is a significant lack of knowledge regarding the relationship between this storm mode and its environment. It is hypothesised that in the absence of dynamical lifting from a persistent mesocyclone, inflow buoyancy is the dominant mechanism for determining storm intensity, highlighting the potential significance of increased near-surface buoyancy associated with anthropogenic land use. Furthermore, previous studies have shown the multicell-HP mode (Richter et al. 2014) and associated environmental conditions (Callaghan 1996) are attributed to the highest impact storms in SEQ over the last 30 years, further emphasises the value in improving the prediction of this storm mode and the potential significance for sub-tropical coastal storm environments globally.

6.3 Limitations and Priorities for Future Research

Results from chapters 4 and hailstorm case study of chapter 5 identify the favourability of southeasterly changes for hailstorms; however, this boundary was not targeted during the field campaign due to limited resources. Detailed observations of the southeasterly change kinematic and thermodynamic structure through future field campaigns are required to

quantify its influence upon convective storms and interactions with the sea breeze air mass. Expansion of the mobile instrumentation is also required to provide more continuous observations of convective storms as they propagate across the complex surface environment. In particular, radiosonde and remote sensing equipment require separate mobile platforms as these instruments are most effectively applied in different areas of the convective storm environment. Multiple mobile platforms also increase the field campaigns capacity to observe storm-scale interactions with the sea breeze and southeasterly change. Furthermore, collaboration with mesoscale modelling using the rich observational datasets is encouraged for future research to quantify the influence of land surface types (e.g., urban area and agriculture) on different background states of the atmosphere.

In chapter 5 it was shown how the land use in SEQ (e.g., urban, irrigated agriculture and cleared areas) modifies the near-surface parcel stability. Direct measurement of the vertical and horizontal extent of this instability using eddy-covariance instrumentation and radar refractivity retrieval techniques is recommended to quantify the influence upon the PBL and storm inflow layer. Previous studies have shown an increase in convective initiation in proximity to urban settings using radar-derived climatologies (e.g., Niyogi et al. 2011; Haberlie et al. 2014). It is recommended that the climatology results from chapter 4 be expanded to include all storm events in an effort to identify similar signatures for the city of Brisbane. Recent work has also shown that large shallow lakes are associated with an increased frequency of convective initiation (Haberlie et al. 2015). It is therefore recommended that further research is required to determine the influence of Lake Wivenhoe in central SEQ using both the climatological datasets and the collection of in-situ observations.

Climatological analysis of storm attributes on sea breeze days was limited by the indiscriminate sampling of hailstorms on either side of the maritime boundary. It is recommended that the inland transect developed for chapter 4 be applied to estimate the location of hailstorm cells in relation to the sea breeze front in an effort to better resolve possible changes in vertical reflectivity profiles. The continual growth of operational radar datasets is encouraging for the ongoing investigation of inter-annual processes which influence convective storms. It is recommended that future research considers the influence of local SST gradients, land use changes and short-scale climate modes (e.g., Madden Julian Oscillation) in addition to ENSO. Furthermore, the CCIE climatological

algorithms can be readily applied across Australia (e.g., Sydney and Melbourne) and internationally where sufficiently long radar datasets exist to explore spatial and temporal drivers of hailstorm variability.

This thesis and previous studies have identified the multicell-HP supercell mode and associated environment in association with severe hailstorm events in SEQ. It is also apparent that an understanding of the synoptic and mesoscale processes which support this storm mode are lacking. It is recommended that the multicell-HP mode be the focus of a long-term case study analysis to analyse the spatial occurrence, evolution and synoptic environments in SEQ and globally. For effective nowcasting of future hybrid-HP systems, it is essential to improve the detection of precursor signatures for large hail growth and the accurate detection of hail using polarimetric radar. There is also a need for more extensive analysis of how PBL variability in complex physical settings influences this storm mode, in particular for urbanised landscapes.

References

Abbs, D., 1986: Sea-breeze interactions along a concave coastline in southern Australia: Observations and numerical modeling study. *Mon. Weather Rev.*, **114**, 831–848, doi:10.1175/1520-0493(1986)114<0831:SBIAAC>2.0.CO;2.

Abbs, D., and W. Physick, 1992: Sea-breeze observations and modelling- A review. *Wea*, **41**, 7–19.

Allen, J., and D. Karoly, 2014: A climatology of Australian severe thunderstorm environments 1979-2011: inter-annual variability and ENSO influence. *Int. J. Climatol.*, **34**, 81–97, doi:10.1002/joc.3667.

Allen, J., D. Karoly, and G. Mills, 2011: A severe thunderstorm climatology for Australia and associated thunderstorm environments. *Aust. Meteorol. Oceanogr. J.*, **61**, 143–158.

Allen, J. T., and E. R. Allen, 2016: A review of severe thunderstorms in Australia. *Atmos. Res.*, **178**–**179**, 347–366, doi:10.1016/j.atmosres.2016.03.011.

Atkins, N., and R. Wakimoto, 1997: Influence of the synoptic-scale flow on sea breezes observed during CaPE. *Mon. Weather Rev.*, **125**, 2112–2130, doi:10.1175/1520-0493(1997)125<2112:IOTSSF>2.0.CO;2.

Atkins, N., R. Wakimoto, and T. Weckwerth, 1995: Observations of the sea-breeze front during CaPE. Part II: Dual-Doppler and aircraft analysis. *Mon. Weather Rev.*, **123**, 944–969, doi:10.1175/1520-0493.

Atkins, N., M. Weisman, and L. Wicker, 1999: The influence of preexisting boundaries on supercell evolution. *Mon. Weather Rev.*, **127**, 2910–2927, doi:10.1175/1520-0493(1999)127<2910:TIOPBO>2.0.CO;2.

Australian Bureau of Statistics, 2013: Queensland state summary. *3218.0 - Reg. Popul. Growth, Aust. 2011-12*,. http://www.abs.gov.au/ausstats/abs@.nsf/Products/3218.0~2011-12~Main+Features~Queensland?OpenDocument#PARALINK3 (Accessed June 26, 2013).

Australian Emergency Management Insitute, 2014: Australian Emergy Management Disaster Reports. *Aust. Emerg. Manag. Knowl. HUB*,. http://www.emknowledge.gov.au/disaster-information/ (Accessed January 12, 2014).

Azorin-Molina, C., B. H. Connell, and R. Baena-Calatrava, 2009: Sea-breeze convergence zones from AVHRR over the Iberian Mediterranean area and the Isle of Mallorca, Spain. *J. Appl. Meteorol. Climatol.*, **48**, 2069–2085, doi:10.1175/2009JAMC2141.1.

Azorin-Molina, C., S. Tijm, and D. Chen, 2011: Development of selection algorithms and databases for sea breeze studies. *Theor. Appl. Climatol.*, **106**, 531–546, doi:10.1007/s00704-011-0454-4.

Azorin-Molina, C., S. Tijm, E. E. Ebert, S. M. Vicente-Serrano, and M. J. Estrela, 2014a: Sea breeze thunderstorms in the eastern Iberian Peninsula. Neighborhood verification of HIRLAM and HARMONIE precipitation forecasts. *Atmos. Res.*, **139**, 101–115, doi:10.1016/j.atmosres.2014.01.010.

Azorin-Molina, C., S. M. Vicente-Serrano, D. Chen, B. H. Connell, M. Á. Domínguez-Durán, J. Revuelto, and J. I. López-Moreno, 2014b: AVHRR warm-season cloud climatologies under various synoptic regimes across the Iberian Peninsula and the Balearic Islands. *Int. J. Climatol.*, **35**, 1984–2002, doi:10.1002/joc.4102.

Baldi, M., V. Ciardini, J. D. Dalu, T. De Filippis, G. Maracchi, and G. Dalu, 2014: Hail occurrence in Italy: Towards a national database and climatology. *Atmos. Res.*, **138**, 268–277, doi:10.1016/j.atmosres.2013.11.012.

Banta, R., 1995: Sea breezes shallow and deep on the California coast. *Mon. Weather Rev.*, **123**, 3614–3622, doi:10.1175/1520-0493(1995)123<3614:SBSADO>2.0.CO;2.

Banta, R., and C. B. Schaaf, 1987: Thunderstorm genesis zones in the Colorado Rocky Mountains as determined by traceback of geosynchronous satellite images. *Mon. Weather Rev.*, **115**, 463–467, doi:10.1175/1520-0493(1987)115<0463:TGZITC>2.0.CO;2.

Banta, R., L. Olivier, and D. Levinson, 1993: Evolution of the Monterey Bay sea-breeze layer as observed by pulsed Doppler lidar. *J. Atmos. Sci.*, **50**, 3959–3982, doi:10.1175/1520-0469(1993)050<3959:EOTMBS>2.0.CO;2.

Banta, R. M., 1984: Daytime boundary-layer evolution over mountainous terrain. Part 1: observations of the dry circulations. *Mon. Weather Rev.*, **112**, 340–356, doi:10.1175/1520-0493(1984)112<0340:DBLEOM>2.0.CO;2.

Banta, R. M., and W. Blumen, 1990: *Atmospheric processes over complex terrain*. American Meteorological Society, Boston, MA., 323 pp.

Basara, J. B., D. W. Mitchell, D. R. Cheresnick, and B. G. Illston, 2007: An analysis of severe hail swaths in the southern plains of the United States. *Trans. GIS*, **11**, 531–554, doi:10.1111/j.1467-9671.2007.01059.x.

Bastin, S., P. Drobinski, A. Dabas, P. Delville, O. Reitebuch, and C. Werner, 2005: Impact of the Rhône and Durance valleys on sea-breeze circulation in the Marseille area. *Atmos. Res.*, **74**, 303–328, doi:10.1016/j.atmosres.2004.04.014.

Bates, B., R. Chandler, and A. Dowdy, 2015: Estimating trends and seasonality in Australian monthly lightning flash counts. *J. Geophys. Res. Atmos.*, **120**, 3973–3983, doi:10.1002/ 2014JD023011.

Bennett, L. J., T. M. Weckwerth, A. M. Blyth, B. Geerts, Q. Miao, and Y. P. Richardson, 2010: Observations of the evolution of the nocturnal and convective boundary layers

and the structure of open-celled convection on 14 June 2002. *Mon. Weather Rev.*, **138**, 2589–2607, doi:10.1175/2010MWR3200.1.

Biggs, W., and M. Graves, 1962: A lake breeze index. *J. Appl. Meteorol.*, **1**, 474–480, doi:10.1175/1520-0450(1962)001<0474:ALBI>2.0.CO;2.

Blanchard, D. O., and R. E. López, 1985: Spatial patterns of convection in south Florida. *Mon. Weather Rev.*, **113**, 1282–1299, doi:10.1175/1520-0493(1985)113<1282:SPOCIS>2.0.CO;2.

Bluestein, H. B., J. B. Houser, M. M. French, J. C. Snyder, G. D. Emmitt, I. Popstefanija, C. Baldi, and R. T. Bluth, 2014: Observations of the boundary layer near tornadoes and in supercells using a mobile, collocated, pulsed doppler lidar and radar. *J. Atmos. Ocean. Technol.*, **31**, 302–325, doi:10.1175/JTECH-D-13-00112.1.

Boer, E. P. J., K. M. de Beurs, and A. D. Hartkamp, 2001: Kriging and thin plate splines for mapping climate variables. *Int. J. Appl. Earth Obs. Geoinf.*, **3**, 146–154, doi:10.1016/S0303-2434(01)85006-6.

Brimelow, J. C., J. M. Hanesiak, and W. R. Burrows, 2011: Impacts of land-atmosphere feedbacks on deep, moist convection on the Canadian prairies. *Earth Interact.*, **15**, 1–29, doi:10.1175/2011EI407.1.

Brooks, H., and N. Dotzek, 2008: The spatial distribution of severe convective storms and an analysis of their secular changes. *Climate Extremes and Society*, H.F. Diaz and J. Murnane, Eds., Cambridge University Press, Cambridge, UK, 35–53.

Brooks, H. E., 2009: Proximity soundings for severe convection for Europe and the United States from reanalysis data. *Atmos. Res.*, **93**, 546–553, doi:10.1016/j.atmosres.2008.10.005.

Browning, K. A., 1977: The structure and mechanism of hailstorms; Hail: A Review of Hail Science and Hail Suppression. *Meteorological Monographs 16*, American Meteorological Society, Boston, MA., 1–43.

Bryan, G., and M. D. Parker, 2010: Observations of a Squall Line and Its Near Environment Using High-Frequency Rawinsonde Launches during VORTEX2. *Mon. Weather Rev.*, **138**, 4076–4097, doi:10.1175/2010MWR3359.1.

Bryan, G., R. Rotunno, and M. Weisman, 2004: What is RKW theory? *26th Conference on Severe Local Storms*, Nashville, TN, American Meteorological Society, 4B.6.

Byers, H. R., and H. R. Rodebush, 1948: Causes of thunderstorms of the Florida peninsula. *J. Meteorol.*, **5**, 275–280, doi:10.1175/1520-0469(1948)005<0275:COTOTF>2.0.CO;2.

Byers, H. R., and R. R. Braham, 1949: *The Thunderstorm*. Washington, DC., 287 pp.

Cai, W., and P. van Rensch, 2012: The 2011 southeast Queensland extreme summer rainfall: A confirmation of a negative Pacific Decadal Oscillation phase? *Geophys. Res. Lett.*, **39**, doi:10.1029/2011GL050820.

Callaghan, J., 1996: Review of severe thunderstorm forecasting and the severe thunderstorm warning service in the southeast coast district of Queensland. *5th Australian Severe Thunderstorm Conference*, Avoca Beach, New South Wales, 178.

Carleton, A., J. Adegoke, J. Allard, D. Arnold, and D. Travis, 2001: Summer season land cover – convective cloud associations for the Midwest US “Corn Belt.” *Geophys. Res. Lett.*, **28**, 1679–1682, doi:10.1029/2000GL012635.

Changnon, S. A., 2001: Thunderstorm rainfall in the conterminous United States. *Bull. Am. Meteorol. Soc.*, **82**, 1925–1940, doi:10.1175/1520-0477(2001)082<1925:TRITCU>2.3.CO;2.

Chemel, C., and R. S. Sokhi, 2012: Response of London’s urban heat island to a marine air intrusion in an easterly wind regime. *Boundary-Layer Meteorol.*, **144**, 65–81, doi:10.1007/s10546-012-9705-x.

Chen, T. C., S. Y. Wang, and M. C. Yen, 2007: Enhancement of afternoon thunderstorm activity by urbanization in a valley: Taipei. *J. Appl. Meteorol. Climatol.*, **46**, 1324–1340, doi:10.1175/JAM2526.1.

Chiba, O., 1997: Variability of the sea-breeze front from SODAR measurements. *Boundary-layer Meteorol.*, **82**, 165–174, doi:10.1023/A:1000216406527.

Chiba, O., K. Fumiaki, G. Naito, and K. Sassa, 1999: Helicopter Observations of the Sea Breeze over a Coastal Area. *J. Appl. Meteorol.*, **38**, 481–492, doi:10.1175/1520-0450(1999)038<0481:HOOTSB>2.0.CO;2.

Cintineo, J. L., T. M. Smith, V. Lakshmanan, H. E. Brooks, and K. L. Ortega, 2012: An objective high-resolution hail climatology of the contiguous United States. *Weather Forecast.*, **27**, 1235–1248, doi:10.1175/WAF-D-11-00151.1.

Clark, A. J., S. J. Weiss, J. S. Kain, I. L. Jirak, M. Coniglio, C. J. Melick, C. Siewert, R. A. Sobash, P. T. Marsh, A. R. Dean, M. Xue, F. Kong, K. W. Thomas, Y. Wang, K. Brewster, J. Gao, X. Wang, J. Du, D. R. Novak, F. E. Barthold, M. J. Bodner, J. J. Levit, C. B. Entwistle, T. L. Jensen, and J. Correia, 2012: An overview of the 2010 Hazardous Weather Testbed experimental forecast program spring experiment. *Bull. Am. Meteorol. Soc.*, **93**, 55–74, doi:10.1175/bAms-d-11-00040.1.

Clark, C. A., and R. W. Arritt, 1995: Numerical simulations of the effect of soil moisture and vegetation cover on the development of deep convection. *J. Appl. Meteorol.*, **34**, 2029–2045, doi:10.1175/1520-0450(1995)034<2029:NSOTEO>2.0.CO;2.

Coniglio, M. C., S. F. Corfidi, and J. S. Kain, 2011: Environment and early evolution of the 8 May 2009 derecho-producing convective system. *Mon. Weather Rev.*, **139**, 1083–1102, doi:10.1175/2010MWR3413.1.

Corfidi, S. F., S. J. Corfidi, and D. M. Schultz, 2008: Elevated convection and castellanus: ambiguities, significance, and questions. *Weather Forecast.*, **23**, 1280–1303, doi:10.1175/2008WAF2222118.1.

Cotton, W., G. Bryan, and S. C. van den Heever, 2011: Cumulonimbus Clouds and Severe Convective Storms. *Storm and Cloud Dynamics*, Elsevier, USA, 315–454.

Crook, N. A., 1996: Sensitivity of moist convection forced by boundary layer processes to low-level thermodynamic fields. *Mon. Weather Rev.*, **124**, 1767–1785, doi:10.1175/1520-0493(1996)124<1767:SOMCFB>2.0.CO;2.

Dandou, A., M. Tombrou, and N. Soulakellis, 2009: The influence of the City of Athens on the evolution of the sea-breeze front. *Boundary-Layer Meteorol.*, **131**, 35–51, doi:10.1007/s10546-008-9306-x.

Darby, L., R. Banta, and R. A. Pielke, 2002: Comparisons between mesoscale model terrain sensitivity studies and Doppler lidar measurements of the sea breeze at Monterey Bay. *Mon. Weather Rev.*, **130**, 2813–2838.

Davini, P., R. Bechini, R. Cremonini, and C. Cassardo, 2012: Radar-based analysis of convective storms over Northwestern Italy. *Atmosphere (Basel).*, **3**, 33–58, doi:10.3390/atmos3010033.

Dawdy, D. R., and N. C. Matalas, 1964: Statistical and Probability Analysis of Hydrologic Data, Part III: Analysis of Variance. *Handbook of Applied Hydrology, A Compendium of Water-Resources Technology*, V.T. Chow, Ed., McGraw-Hill Book Company: New York, New York, 68–90.

Deangelis, A., F. Dominguez, Y. Fan, A. Robock, M. D. Kustu, and D. Robinson, 2010: Evidence of enhanced precipitation due to irrigation over the Great Plains of the United States. *J. Geophys. Res. Atmos.*, **115**, 1–14, doi:10.1029/2010JD013892.

Dee, D. P., S. M. Uppala, a. J. Simmons, P. Berrisford, P. Poli, S. Kobayashi, U. Andrae, M. a. Balmaseda, G. Balsamo, P. Bauer, P. Bechtold, a. C. M. Beljaars, L. van de Berg, J. Bidlot, N. Bormann, C. Delsol, R. Dragani, M. Fuentes, a. J. Geer, L. Haimberger, S. B. Healy, H. Hersbach, E. V. Hólm, L. Isaksen, P. Kållberg, M. Köhler, M. Matricardi, a. P. McNally, B. M. Monge-Sanz, J.-J. Morcrette, B.-K. Park, C. Peubey, P. de Rosnay, C. Tavolato, J.-N. Thépaut, and F. Vitart, 2011: The ERA-Interim reanalysis: configuration and performance of the data assimilation system. *Q. J. R. Meteorol. Soc.*, **137**, 553–597, doi:10.1002/qj.828.

Dixon, P. G., and T. L. Mote, 2003: Patterns and causes of Atlanta's urban heat island–initiated precipitation. *J. Appl. Meteorol.*, **42**, 1273–1284, doi:10.1175/1520-0450(2003)042<1273:PACOAU>2.0.CO;2.

Doswell, C., 1996: What is a supercell? *18 th AMS Conf. Severe Local Storms*, San Francisco, CA, Amer. Meteor. Soc., 641.

Doswell, C., 2001: Severe Convective Storms - An Overview. *Severe Convective Storms*, C.A. Doswell, Ed., American Meteorological Society, Boston, 1–26.

Doswell, C. A., 2003: Societal impacts of severe thunderstorms and tornadoes: Lessons learned and implications for Europe. *Atmos. Res.*, **67**–**68**, 135–152, doi:10.1016/S0169-8095(03)00048-6.

Dowdy, A. J., 2016: Seasonal forecasting of lightning and thunderstorm activity in tropical and temperate regions of the world. *Sci. Rep.*, **6**, 20874, doi:10.1038/srep20874.

Dowdy, a J., and Y. Kuleshov, 2014: Climatology of lightning activity in Australia: Spatial and seasonal variability. *Aust. Meteorol. Oceanogr. J.*, **64**, 103–108.

Fabry, F., Q. Cazenave, and R. Basivi, 2013: New horizons opended using 17 years of conterminous US radar composites. *36th Conference on Radar Meteorology*, Breckenridge, CO, American Meteorological Society.

Feng, Y.-C., F. Fabry, and T. M. Weckwerth, 2016: Improving radar refractivity retrieval by considering the change in the refractivity profile and the varying altitudes of ground targets. *J. Atmos. Ocean. Technol.*, 160309141059002, doi:10.1175/JTECH-D-15-0224.1.

Finkele, K., J. Hacker, H. Kraus, and B.-S. R, 1995: A complete sea-breeze circulation cell derived from aircraft observations. *Boundary-Layer Meteorol.*, **3**, 299–317, doi:10.1007/BF00711261.

Fovell, R., 2005: Convective initiation ahead of the sea-breeze front. *Mon. Weather Rev.*, **133**, 264–278, doi:10.1175/MWR-2852.1.

Fovell, R. G., and Y. Ogura, 1989: Effect of Vertical Wind Shear on Numerically Simulated Multicell Storm Structure. *J. Atmos. Sci.*, **46**, 3144–3176, doi:10.1175/1520-0469(1989)046<3144:EOVWSO>2.0.CO;2.

Fovell, R. G., and P. S. Dailey, 1999: Numerical simulation of the interaction between the sea-breeze front and horizontal convective rolls. Part I: Offshore ambient flow. *Mon. Weather Rev.*, **127**, 858–878, doi:10.1175/1520-0493(1999)127<0858:NSOTIB>2.0.CO;2.

Frame, J., and P. Markowski, 2013: Dynamical Influences of Anvil Shading on Simulated Supercell Thunderstorms. *Mon. Weather Rev.*, **141**, 2802–2820, doi:10.1175/MWR-D-12-00146.1.

Freitas, E. D., C. M. Rozoff, W. R. Cotton, and P. L. Silva Dias, 2007: Interactions of an urban heat island and sea-breeze circulations during winter over the metropolitan area of São Paulo, Brazil. *Boundary-Layer Meteorol.*, **122**, 43–65, doi:10.1007/s10546-006-9091-3.

Frye, J. D., and T. L. Mote, 2010: Convection initiation along soil moisture boundaries in the southern Great Plains. *Mon. Weather Rev.*, **138**, 1140–1151, doi:10.1175/2009MWR2865.1.

Gal, T., and Z. Sumeghi, 2007: Mapping the roughness parameters in a large urban area for urban climate applications. *Acta Climatol. Chorol.*, **40**–**41**, 27–36.

Gao, X., C. A. Schlosser, P. Xie, E. Monier, and D. Entekhabi, 2014: An analogue approach to identify heavy precipitation events: evaluation and application to CMIP5 climate models in the United States. *J. Clim.*, **27**, 5941–5963, doi:10.1175/JCLI-D-13-00598.1.

Garcia, S. R., and M. T. Kayano, 2007: Climatological aspects of Hadley, Walker and monsoon circulations in two phases of the Pacific Decadal Oscillation. *Theor. Appl. Climatol.*, **91**, 117–127, doi:10.1007/s00704-007-0301-9.

Gartland, L., 2011: *Heat islands: understanding and mitigating heat in urban areas*. Earthscan, London, UK, 192 pp.

Gasperoni, N. A., M. Xue, R. D. Palmer, and J. Gao, 2013: Sensitivity of convective initiation prediction to near-surface moisture when assimilating radar refractivity: Impact tests using OSSEs. *J. Atmos. Ocean. Technol.*, **30**, 2281–2302, doi:10.1175/JTECH-D-12-00038.1.

Gedzelman, S. D., S. Austin, R. Cermak, N. Stefano, and S. Partridge, 2003: Mesoscale aspects of the Urban Heat Island around New York City. *Theor. Appl. Climatol.*, **42**, 29–42, doi:10.1007/s00704-002-0724-2.

Geerts, B., M. Parker, D. B. Parsons, T. M. Weckwerth, J. Wurman, and C. Ziegler, 2013: *Plains Elevated Convection at Night (PECAN) Experimental Design Overview*. 37 pp.

Goff, R. C., 1975: *Thunderstorm Outflow Kinematics and Dynamics*. Volume 75. U.S. Department of Commerce, National Oceanic and Atmospheric Administration, Environmental Research Laboratories, National Severe Storms Laboratory, Norman, OK, 63 pp.

Haberlie, A. M., W. S. Ashley, and T. J. Pingel, 2014: The effect of urbanisation on the climatology of thunderstorm initiation. *Q. J. R. Meteorol. Soc.*, **141**, 663–675, doi:10.1002/qj.2499.

Haberlie, A. M., W. S. Ashley, A. J. Fultz, and S. M. Eagan, 2015: The effect of reservoirs on the climatology of warm-season thunderstorms in Southeast Texas, USA. *Int. J. Climatol.*, **1820**, 1808–1820, doi:10.1002/joc.4461.

Halbert, K. T., G. W. Blumberg, and P. T. March, 2015: SHARPpy: Fueling the Python Cult. *95th American Meteorological Soceity Annual Meeting*, Phoenix, AZ, 1.402.

Harper, B., and J. Callaghan, 1998: Modelling of severe thunderstorms in south east Queensland. *Proc. Sixth Australian Severe Storms Conference*, Bardon, QLD, Australian Bureau of Meteorology, 152.

Hart, M., R. de Dear, and R. Hyde, 2006: A synoptic climatology of tropospheric ozone episodes in Sydney, Australia. *Int. J. Climatol.*, **26**, 1635–1649, doi:10.1002/joc.1332.

Hartigan, J. a., and M. a. Wong, 1979: Algorithm AS 136: A k-means clustering algorithm. *J. R. Stat. Soc. C*, **28**, 100–108, doi:10.2307/2346830.

Helmus, J. J., and S. M. Collis, 2016: The Python ARM Radar Toolkit (Py-ART), a Library for Working with Weather Radar Data in the Python Programming Language. *J. Open Res. Softw.*, **4**, e25.

Holcombe, G and Moynihan, G., 1978: *An investigation of the Brisbane tornado of 4 November 1973*.

Insurance Council of Australia, 2015: Catastrophe Database. http://www.tiki-toki.com/timeline/entry/568110/Ten-Years-of-Catastrophe/ (Accessed April 10, 2016).

James, R. P., and P. M. Markowski, 2010: A numerical investigation of the effects of dry air aloft on deep convection. *Mon. Weather Rev.*, **138**, 140–161, doi:10.1175/2009MWR3018.1.

Johnson, R. H., and B. E. Mapes, 2001: Mesoscale Processes and Severe Convective Weather. *Severe Convective Storms*, C.A. Doswell, Ed., American Meteorological Society, Boston, 71–122.

Jorgensen, D., and T. Weckwerth, 2003: Forcing and Organization of Convective Systems. *Radar and Atmospheric Science: A Collection of Essays in Jonor of David Atlas*, R. Wakimoto and R. Srivastva, Eds., American Meteorological Society, Boston, 75–104.

Kanda, M., 2007: Progress in urban meteorology: A review. *J. Meteorol. Soc. Japan*, **85B**, 363–383, doi:10.2151/jmsj.85B.363.

Karan, H., and K. Knupp, 2009: Radar and profiler analysis of colliding boundaries: a case study. *Mon. Weather Rev.*, **137**, 2203–2222, doi:10.1175/2008MWR2763.1.

Khan, S. M., and R. W. Simpson, 2001: Effect of heat island on the meteorology of a complex urban airshed. *Boundary-Layer Meteorol.*, **100**, 487–506, doi:10.1023/A:1019284332306.

King, A. D., N. P. Klingaman, L. V. Alexander, M. G. Donat, N. C. Jourdain, and P. Maher, 2014: Extreme rainfall variability in Australia: Patterns, drivers, and predictability. *J. Clim.*, **27**, 6035–6050, doi:10.1175/JCLI-D-13-00715.1.

King, P. W. S., M. J. Leduc, D. M. L. Sills, N. R. Donaldson, D. R. Hudak, P. Joe, and B. P. Murphy, 2003: Lake breezes in southern Ontario and their relation to tornado

climatology. *Weather Forecast.*, **18**, 795–807, doi:10.1175/1520-0434(2003)018<0795:LBISOA>2.0.CO;2.

Kingsmill, D. E., 1995: Convection initiation associated with a sea-breeze front, a gust front, and their collision. *Mon. Weather Rev.*, **123**, 2913–2933, doi:10.1175/1520-0493(1995)123<2913:CIAWAS>2.0.CO;2.

Klemp, J., 1987: Dynamics of tornadic thunderstorms. *Annu. Rev. Fluid Mech.*, **19**, 1–33, doi:10.1146/annurev.fluid.19.1.369.

Knight, C. A., and N. C. Knight, 2001: Hailstorms. *Severe Convective Storms*, C.A. Doswell, Ed., American Meteorological Society, Boston, 223–254.

Koch, S., and C. Ray, 1997: Mesoanalysis of summertime convergence zones in central and eastern North Carolina. *Weather Forecast.*, **12**, 56–77, doi:10.1175/1520-0434(1997)012<0056:MOSCZI>2.0.CO;2.

Kumar, V. V., C. Jakob, A. Protat, P. T. May, and L. Davies, 2013: The four cumulus cloud modes and their progression during rainfall events: A C-band polarimetric radar perspective. *J. Geophys. Res. Atmos.*, **118**, 8375–8389, doi:10.1002/jgrd.50640.

Kunz, M., J. Sander, and C. Kottmeier, 2009: Recent trends of thunderstorm and hailstorm frequency and their relation to atmospheric characteristics in southwest Germany. *Int. J. Climatol.*, **29**, 2283–2297, doi:10.1002/joc.1865.

Lakshmanan, V., and T. Smith, 2007: The warning decision support system-integrated information. *Weather Forecast.*, **22**, 596–612, doi:10.1175/WAF1009.1.

Lakshmanan, V., and T. Smith, 2010: An Objective Method of Evaluating and Devising Storm-Tracking Algorithms. *Weather Forecast.*, **25**, 701–709, doi:10.1175/2009WAF2222330.1.

Lakshmanan, V., K. Hondl, and R. Rabin, 2009: An Efficient, General-Purpose Technique for Identifying Storm Cells in Geospatial Images. *J. Atmos. Ocean. Technol.*, **26**, 523–537, doi:10.1175/2008JTECHA1153.1.

Lakshmanan, V., K. Hondl, C. K. Potvin, and D. Preignitz, 2013: An Improved Method for Estimating Radar Echo-Top Height. *Weather Forecast.*, **28**, 481–488, doi:10.1175/WAF-D-12-00084.1.

Lemon, L., and C. Doswell, 1979: Severe thunderstorm evolution and mesocyclone structure as related to tornadogenesis. *Mon. Weather Rev.*, **107**, 1184–1197, doi:10.1175/1520-0493(1979)107<1184:STEAMS>2.0.CO;2.

Lemonsu, A., S. Bastin, V. Masson, and P. Drobinski, 2006a: Vertical structure of the urban boundary layer over Marseille under sea-breeze conditions. *Boundary-Layer Meteorol.*, **118**, 477–501, doi:10.1007/s10546-005-7772-y.

Lemonsu, A., G. Pigeon, V. Masson, and C. Moppert, 2006b: Sea-town interactions over Marseille : 3D urban boundary layer and thermodynamic fields near the surface. **178**, 171–178, doi:10.1007/s00704-005-0155-y.

Lima, M. A., and J. W. Wilson, 2008: Convective Storm Initiation in a Moist Tropical Environment. *Mon. Weather Rev.*, **136**, 1847–1864, doi:10.1175/2007MWR2279.1.

Lin, P.-F., P.-L. Chang, B. J.-D. Jou, J. W. Wilson, and R. D. Roberts, 2011: Warm season afternoon thunderstorm characteristics under weak synoptic-scale forcing over Taiwan island. *Weather Forecast.*, **26**, 44–60, doi:10.1175/2010WAF2222386.1.

Markowski, P. M., 2002: Hook echoes and rear-flank downdrafts: A review. *Mon. Weather Rev.*, **130**, 852–876, doi:10.1175/1520-0493(2002)130<0852:HEARFD>2.0.CO;2.

Markowski, P. M., E. N. Rasmussen, and J. M. Straka, 1998: The cccurrence of tornadoes in supercells interacting with boundaries during VORTEX-95. *Weather Forecast.*, **13**, 852–859, doi:10.1175/1520-0434(1998)013<0852:TOOTIS>2.0.CO;2.

May, P. T., 1999: Thermodynamic and vertical velocity structure of two gust fronts observed with a wind profiler/RASS during MCTEX. *Mon. Weather Rev.*, **127**, 1796–1807, doi:10.1175/1520-0493(1999)127<1796:TAVVSO>2.0.CO;2.

May, P. T., A. R. Jameson, T. D. Keenan, P. E. Johnston, and C. Lucas, 2002: Combined wind profiler/polarimetric radar studies of the vertical motion and microphysical characteristics of tropical sea-breeze thunderstorms. *Mon. Weather Rev.*, **130**, 2228–2239.

McCaul, E., and M. Weisman, 2001: The sensitivity of simulated supercell structure and intensity to variations in the shapes of environmental buoyancy and shear profiles. *Mon. Weather Rev.*, **129**, 664–687.

McJannet, D., F. Cook, J. Knight, and S. Burn, 2008: *Evaporation Reduction by Monolayers : Overview , Modelling and Effectiveness*. Brisbane, 32 pp.

Melas, D., A. Lavagnini, and A. Sempreviva, 2000: An investigation of the boundary layer dynamics of Sardinia Island under sea-breeze conditions. *J. Appl. Meteorol.*, **39**, 516–524.

Mezher, R. N., M. Doyle, and V. Barros, 2012: Climatology of hail in Argentina. *Atmos. Res.*, **114**–**115**, 70–82, doi:10.1016/j.atmosres.2012.05.020.

Miller, S., 2003: Sea breeze: Structure, forecasting, and impacts. *Rev. Geophys.*, **41**, 1011, doi:10.1029/2003RG000124.

Miller, S., and B. Keim, 2003: Synoptic-scale controls on the sea breeze of the central New England coast. *Weather Forecast.*, **18**, 236–248.

Moller, A. R., C. A. Doswell, and R. Przybylinski, 1990: High-precipitation supercells: A conceptual model and documentation. *16th Conf. Sev. Local Storms*, 52–57.

Mona, T., Á. Horváth, and F. Ács, 2016: A thunderstorm cell-lightning activity analysis: The new concept of air mass catchment. *Atmos. Res.*, **169**, 340–344, doi:10.1016/j.atmosres.2015.10.017.

Moncrieff, M. W., and M. J. Miller, 1976: The dynamics and simulation of tropical cumulonimbus and squall lines. *Q. J. R. Meteorol. Soc.*, **102**, 373–394, doi:10.1002/qj.49710243208.

Mueller, C. K., J. W. Wilson, and N. A. Crook, 1993: The utility of sounding and mesonet data to nowcast thunderstorm initiation. *Weather Forecast.*, **8**, 132–146, doi:10.1175/1520-0434(1993)008<0132:TUOSAM>2.0.CO;2.

Muppa, S. K., A. Behrendt, F. Späth, V. Wulfmeyer, S. Metzendorf, and A. Riede, 2015: Turbulent humidity fluctuations in the convective boundary layer: case studies using water vapour differential absorption lidar measurements. *Boundary-Layer Meteorol.*, **158**, 43–66, doi:10.1007/s10546-015-0078-9.

Nicholls, M., R. A. Pielke, and W. Cotton, 1991: A two-dimensional numerical investigation of the interaction between sea breezes and deep convection over the Florida peninsula. *Mon. Weather Rev.*, **119**, 298–323, doi:10.1175/1520-0493(1991)119<0298:ATDNIO>2.0.CO;2.

Nicholls, N., W. Drosdowsky, and B. Lavery, 1997: Australian rainfall variability and change. *Weather*, **52**, 66–72, doi:10.1002/j.1477-8696.1997.tb06274.x.

Nisi, L., O. Martius, A. Hering, M. Kunz, and U. Germann, 2016: Spatial and temporal distribution of hailstorms in the Alpine region: a long-term , high resolution , radar-based analysis. *Q. J. R. Meteorol. Soc.*, **142**, 1590–1604, doi:10.1002/qj.2771.

Niyogi, D., P. Pyle, M. Lei, S. P. Arya, C. M. Kishtawal, M. Shepherd, F. Chen, and B. Wolfe, 2011: Urban modification of thunderstorms: An observational storm climatology and model case study for the Indianapolis urban region. *J. Appl. Meteorol. Climatol.*, **50**, 1129–1144, doi:10.1175/2010JAMC1836.1.

Novak, D. R., and B. a. Colle, 2006: Observations of multiple sea breeze boundaries during an unseasonably warm day in metropolitan New York City. *Bull. Am. Meteorol. Soc.*, **87**, 169–174, doi:10.1175/BAMS-87-2-169.

Ohashi, Y., and H. Kida, 2002: Local circulations developed in the vicinity of both coastal and inland urban areas: A numerical study with a mesoscale atmospheric model. *J. Appl. Meteorol.*, **41**, 30–45, doi:10.1175/1520-0450(2002)041<0030:LCDITV>2.0.CO;2.

Oort, A. H., and J. J. Yienger, 1996: Observed interannual variability in the Hadley circulation and its connection to ENSO. *J. Clim.*, **9**, 2751–2767, doi:10.1175/1520-0442(1996)009<2751:OIVITH>2.0.CO;2.

Orlanski, I., 1975: A rational subdivision of scales for atmospheric processes. *Bull. Am. Meteorol. Soc.*, **56**, 527–530.

Parackal, K. I., M. S. Mason, D. J. Henderson, D. J. Smith, and J. D. Ginger, 2015: *Investigation of Damage : Brisbane 27 November 2014*. Townsville, 47 pp.

Peter, J. R., M. J. Manton, R. J. Potts, P. T. May, S. M. Collis, and L. Wilson, 2015: Radar-derived statistics of convective storms in southeast Queensland. *J. Appl. Meteorol. Climatol.*, **54**, 1985–2008, doi:10.1175/JAMC-D-13-0347.1.

Phillips, B. B., 1973: Precipitation characteristics of a sheared, moderate intensity, supercell-type Colorado thunderstorm. *J. Appl. Meteorol.*, **12**, 1354–1363, doi:10.1175/1520-0450(1973)012<1354:PCOASM>2.0.CO;2.

Physick, W., 1993: *Brisbane Windfield Study: Part 1*. Brisbane, 66 pp.

Pielke, R. A., 1974: A three-dimensional numerical model of the sea breezes over south Florida. *Mon. Weather Rev.*, **102**, 115–139, doi:10.1175/1520-0493(1974)102<0115:ATDNMO>2.0.CO;2.

Pielke, R. A., and X. Zeng, 1989: Influence on severe storm development of irrigated land. *Natl. Weather Dig.*, **14**, 16–17, doi:10.1.1.258.5806.

Pinto, O., I. R. C. A. Pinto, and M. A. S. Ferro, 2013: A study of the long-term variability of thunderstorm days in southeast Brazil. *J. Geophys. Res. Atmos.*, **118**, 5231–5246, doi:10.1002/jgrd.50282.

Plant, R. S., and G. J. Keith, 2006: Occurrence of Kelvin-Helmholtz billows in sea-breeze circulations. *Boundary-Layer Meteorol.*, **122**, 1–15, doi:10.1007/s10546-006-9089-x.

Potts, R. J., T. D. Keenan, and P. T. May, 2000: Radar characteristics of storms in the sydney area. *Mon. Weather Rev.*, **128**, 3308–3319, doi:10.1175/1520-0493(2000)128<3308:RCOSIT>2.0.CO;2.

Potvin, C. K., K. L. Elmore, and S. J. Weiss, 2010: Assessing the impacts of proximity sounding criteria on the climatology of significant tornado environments. *Weather Forecast.*, **25**, 921–930, doi:10.1175/2010WAF2222368.1.

Power, S., T. Casey, C. Folland, A. Colman, and V. Mehta, 1999: Inter-decadal modulation of the impact of ENSO on Australia. *Clim. Dyn.*, **15**, 319–324, doi:10.1007/s003820050284.

Puygrenier, V., F. Lohou, B. Campistron, F. Saïd, G. Pigeon, B. Bénech, and D. Serça, 2005: Investigation on the fine structure of sea-breeze during ESCOMPTE experiment. *Atmos. Res.*, **74**, 329–353, doi:10.1016/j.atmosres.2004.06.011.

Richter, H., J. Peter, and S. Collis, 2014: Analysis of a destructive wind storm on 16 November 2008 in Brisbane, Australia. *Mon. Weather Rev.*, **142**, 3038–3060, doi:10.1175/MWR-D-13-00405.1.

Riebsame, W. E., M. Price, H. F. Diaz, and T. Moses, 1986: The social burden of weather and climate hazards. *Bull. Am. Meteorol. Soc.*, **67**, 1378–1388, doi:10.1175/1520-0477(1986)067<1378:TSBOWA>2.0.CO;2.

Rotunno, R., J. Klemp, and M. Weisman, 1988: A theory for strong, long-lived squall lines. *J. Atmos. Sci.*, **45**, 463–483, doi:10.1175/1520-0469(1988)045<0463:ATFSLL>2.0.CO;2.

Rozoff, C. M., W. R. Cotton, and J. O. Adegoke, 2003: Simulation of St . Louis, Missouri, land use impacts on thunderstorms. *J. Appl. Meteorol. Climatol.*, **42**, 716–738, doi:10.1175/1520-0450(2003)042<0716:SOSLML>2.0.CO;2.

Ryu, Y.-H., J. A. Smith, E. Bou-Zeid, and M. L. Baeck, 2015: The influence of land-surface heterogeneities on heavy convective rainfall in the Baltimore-Washington metropolitan area. *Mon. Weather Rev.*, **144**, 553–573, doi:10.1175/MWR-D-15-0192.1.

Santamouris, M., 2015: Analyzing the heat island magnitude and characteristics in one hundred Asian and Australian cities and regions. *Sci. Total Environ.*, **512**–**513**, 582–598, doi:10.1016/j.scitotenv.2015.01.060.

Schatz, J., and C. J. Kucharik, 2014: Seasonality of the urban heat island effect in Madison, Wisconsin. *J. Appl. Meteorol. Climatol.*, **53**, 2371–2386, doi:10.1175/JAMC-D-14-0107.1.

Segal, M., R. W. Arritt, C. Clark, R. Rabin, and J. Brown, 1995: Scaling evaluation of the effect of surface characteristics on potential for deep convection over uniform terrain. *Mon. Weather Rev.*, **123**, 383–400, doi:10.1175/1520-0493(1995)123<0383:SEOTEO>2.0.CO;2.

Shem, W., and M. Shepherd, 2009: On the impact of urbanization on summertime thunderstorms in Atlanta: Two numerical model case studies. *Atmos. Res.*, **92**, 172–189, doi:10.1016/j.atmosres.2008.09.013.

Shin, S., R. Smith, and J. Callaghan, 2005: Severe thunderstorms over northeastern Queensland on 19 January 2001: the influence of an upper-level trough on the convective destabilisation of the atmosphere. *Aust. Meteorol. Mag.*, **54**, 333–346.

Sills, D. M. L., J. Wilson, J. I. Paul, D. W. Burgess, R. M. Webb, and N. I. Fox, 2004: The 3 November tornadic event during Sydney 2000: Storm evolution and the role of low-level boundaries. *Weather Forecast.*, **19**, 22–42, doi:10.1175/1520-0434(2004)019<0022:TNTEDS>2.0.CO;2.

Simpson, J., D. Mansfield, and J. Milford, 1977: Inland penetration of sea-breeze fronts. *Q. J. R. Meteorol. Soc.*, **103**, 47–76, doi:10.1002/qj.49710343504.

Small, C., and R. J. Nicolls, 2003: A global analysis of human settlement in coastal zones. *J. Coast. Res.*, **19**, 584–599.

Smith, S. B., J. G. LaDue, and D. R. MacGorman, 2000: The relationship between cloud-to-ground lightning polarity and surface equivalent potential temperature during three tornadic outbreaks. *Mon. Weather Rev.*, **128**, 3320–3328, doi:10.1175/1520-0493(2000)128<3320:TRBCTG>2.0.CO;2.

Soderholm, J., H. A. McGowan, H. Richter, K. Walsh, T. M. Weckwerth, and M. Coleman, 2016: The Coastal Convective Interactions Experiment (CCIE): Understanding the role of sea breezes for hailstorm hotspots in Eastern Australia. *Bull. Am. Meteorol. Soc.*, **97**, 1687–1698, doi:10.1175/BAMS-D-14-00212.1.

Steiner, J. T., 1989: New Zealand hailstorms. *New Zeal. J. Geol. Geophys.*, **32**, 279–291, doi:10.1080/00288306.1989.10427589.

Stensrud, D. J., M. C. Coniglio, R. P. Davies-Jones, and J. S. Evans, 2005: Comments on "'A Theory for Strong Long-Lived Squall Lines' Revisited." *J. Atmos. Sci.*, **62**, 2989–2996, doi:10.1175/JAS3514.1.

Sun, J., M. Xue, J. W. Wilson, I. Zawadzki, S. P. Ballard, J. Onvlee-Hooimeyer, P. Joe, D. M. Barker, P. W. Li, B. Golding, M. Xu, and J. Pinto, 2014: Use of NWP for nowcasting convective precipitation: Recent progress and challenges. *Bull. Am. Meteorol. Soc.*, **95**, 409–426, doi:10.1175/BAMS-D-11-00263.1.

Tait, A., and R. Woods, 2007: Spatial interpolation of daily potential evapotranspiration for new zealand using a spline model. *J. Hydrometeorol.*, **8**, 430–438, doi:10.1175/JHM572.1.

Taylor, N. M., D. M. L. Sills, J. M. Hanesiak, J. a. Milbrandt, C. D. Smith, G. S. Strong, S. H. Skone, P. J. McCarthy, and J. C. Brimelow, 2011: The Understanding Severe Thunderstorms and Alberta Boundary Layers Experiment (UNSTABLE) 2008. *Bull. Am. Meteorol. Soc.*, **92**, 739–763, doi:10.1175/2011BAMS2994.1.

The National Severe Storms Labratory, 2015: Thunderstorm Basics. *Sev. Weather 101*,. http://www.nssl.noaa.gov/education/svrwx101/thunderstorms/ (Accessed May 18, 2016).

Theobald, A., H. McGowan, J. Speirs, and N. Callow, 2015: A synoptic classification of inflow-generating precipitation in the Snowy Mountains, Australia. *J. Appl. Meteorol. Climatol.*, **54**, 1713–1732, doi:10.1175/JAMC-D-14-0278.1.

Thompson, R. L., C. M. Mead, and R. Edwards, 2007: Effective storm-relative helicity and bulk shear in supercell thunderstorm environments. *Weather Forecast.*, **22**, 102–115, doi:10.1175/WAF969.1.

Thorpe, A. J., M. Miller, and M. W. Moncrieff, 1982: Two-dimensional convection in non-constant shear: A model of mid-latitude squall lines. *Q. J. R. Meteorol. Soc.*, **108**, 739–762, doi:10.1002/qj.49710845802.

Trainor, J. E., D. Nagele, B. Philips, and B. Scott, 2015: Tornadoes, social science, and the false alarm effect. *Weather. Clim. Soc.*, **7**, 333–352, doi:10.1175/WCAS-D-14-00052.1.

Tsunematsu, N., and K. Kai, 2004: Time variation of cloud distribution near surface wind convergence zone in the Nobi Plain during daytime on summer sunny days. *J. Meteorol. Soc. Japan*, **82**, 1505–1520, doi:10.2151/jmsj.82.1505.

United Nations, 2010: Human Settlements on the Coast. *UN Atlas Ocean.*,. http://www.oceansatlas.org/servlet/CDSServlet?status=ND0xODc3JjY9ZW4mMzM9KiYzNz1rb3M~ (Accessed April 10, 2016).

Vinet, F., 2000: Climatology of hail in France. *Atmos. Res.*, **56**, 309–323, doi:10.1016/S0169-8095(00)00082-X.

Wakimoto, R., 1982: The life cycle of thunderstorm gust fronts as viewed with Doppler radar and rawinsonde data. *Mon. Weather Rev.*, **110**, 1060–1082, doi:10.1175/1520-0493(1982)110<1060:TLCOTG>2.0.CO;2.

Wakimoto, R., and N. Atkins, 1994: Observations of the sea-breeze front during CaPE. Part I: Single-Doppler, satellite, and cloud photogrammetry analysis. *Mon. Weather Rev.*, **122**, 1092–1114, doi:10.1175/1520-0493(1994)122<1092:OOTSBF>2.0.CO;2.

Wakimoto, R., and H. V. Murphey, 2009: Analysis of a dryline during IHOP: Implications for convection initiation. *Mon. Weather Rev.*, **137**, 912–936, doi:10.1175/2008MWR2584.1.

Weckwerth, T., 1997: Horizontal convective rolls: Determining the environmental conditions supporting their existence and characteristics. *Mon. Weather Rev.*, **125**, 505–526, doi:10.1175/1520-0493(1997)125<0505:HCRDTE>2.0.CO;2.

Weckwerth, T., 2000: The effect of small-scale moisture variability on thunderstorm initiation. *Mon. Weather Rev.*, **128**, 4017–4030, doi:10.1175/1520-0493(2000)129<4017:TEOSSM>2.0.CO;2.

Weckwerth, T., J. Wilson, and R. Wakimoto, 1996: Thermodynamic variability within the convective boundary layer due to horizontal convective rolls. *Mon. Weather Rev.*, **124**, 769–784, doi:10.1175/1520-0493(1996)124<0769:TVWTCB>2.0.CO;2.

Weckwerth, T., D. B. Parsons, S. E. Koch, J. A. Moore, M. A. LeMone, B. B. Demoz, C. Flamant, B. Geerts, J. Wang, and W. F. Feltz, 2004: An overview of the International H2O Project (IHOP_2002) and some preliminary highlights. *Bull. Am. Meteorol. Soc.*, **85**, 253–277, doi:10.1175/BAMS-85-2-253.

Weckwerth, T., H. V. Murphey, C. Flamant, J. Goldstein, and C. R. Pettet, 2008: An observational study of convection initiation on 12 June 2002 during IHOP_2002. *Mon. Weather Rev.*, **136**, 2283–2304, doi:10.1175/2007MWR2128.1.

Weckwerth, T. M., and R. M. Wakimoto, 1992: The Initiation and Organization of Convective Cells atop a Cold-Air Outflow Boundary. *Mon. Weather Rev.*, **120**, 2169–2187, doi:10.1175/1520-0493(1992)120<2169:TIAOOC>2.0.CO;2.

Weckwerth, T. M., J. W. Wilson, M. Hagen, T. J. Emerson, J. O. Pinto, D. L. Rife, and L. Grebe, 2011: Radar climatology of the COPS region. *Q. J. R. Meteorol. Soc.*, **137**, 31–41, doi:10.1002/qj.747.

Weisman, M., 1990a: An observational study of warm season southern Appalachian lee troughs. Part I: boundary layer circulation. *Mon. Weather Rev.*, **118**, 950–963, doi:10.1175/1520-0493(1990)118<0950:AOSOWS>2.0.CO;2.

Weisman, M., 1990b: An observational study of warm season southern Appalachian lee troughs. Part II: Thunderstorm genesis zones. *Mon. Weather Rev.*, **118**, 2020–2041, doi:10.1175/1520-0493(1990)118<2020:AOSOWS>2.0.CO;2.

Weisman, M., and J. Klemp, 1982: The dependence of numerically simulated convective storms on vertical wind shear and buoyancy. *Mon. Weather Rev.*, **110**, 504–520, doi:10.1175/1520-0493(1982)110<0504:TDONSC>2.0.CO;2.

Weisman, M., and J. Klemp, 1984: The Structure and Classification of Numerically Simulated Convective Stormsin Directionally Varying Wind Shears. *Mon. Weather Rev.*, **112**, 2479–2498, doi:10.1175/1520-0493(1984)112<2479:TSACON>2.0.CO;2.

Weisman, M., and J. Klemp, 1986: Characteristics of isolated convective storms. *Mesoscale Meteorology and Forecasting*, P. Ray, Ed., Amer. Meteor. Soc., 331–358.

Weisman, M. L., R. J. Trapp, G. S. Romine, C. Davis, R. Torn, M. Baldwin, L. Bosart, J. Brown, M. Coniglio, D. Dowell, A. C. Evans, T. J. Galarneau, J. Haggerty, T. Hock, K. Manning, P. Roebber, P. Romashkin, R. Schumacher, C. S. Schwartz, R. Sobash, D. Stensrud, and S. B. Trier, 2015: The Mesoscale Predictability Experiment (MPEX). *Bull. Am. Meteorol. Soc.*, **96**, 2127–2149, doi:10.1175/BAMS-D-13-00281.1.

Wilson, C., K. Ortega, and V. Lakshmanan, 2009: Evaluating multi-radar, multi-sensor hail diagnosis with high resolution hail reports. *Preprints, 25th Conference on IIPS*, Seattle, WA, American Meteorological Society, P2.9.

Wilson, J., and W. Schreiber, 1986: Initiation of convective storms at radar-observed boundary-layer convergence lines. *Mon. Weather Rev.*, **114**, 2516–2536.

Wilson, J., and D. Megenhardt, 1997: Thunderstorm initiation, organization, and lifetime associated with Florida boundary layer convergence lines. *Mon. Weather Rev.*, **125**, 1507–1525, doi:10.1175/1520-0493(1997)125<1507:TIOALA>2.0.CO;2.

Wilson, J., G. B. Foote, N. A. Crook, J. Fankhauser, C. G. Wade, J. D. Tuttle, C. K. Mueller, and S. K. Krueger, 1992: The role of boundary-layer convergence zones and horizontal rolls in the initiation of thunderstorms: A case study. *Mon. Weather Rev.*, **120**, 1785–1815, doi:10.1175/1520-0493(1992)120<1785:TROBLC>2.0.CO;2.

Wilson, J., T. Weckwerth, J. Vivekanandan, R. Wakimoto, and R. W. Russell, 1994: Boundary layer clear-air radar echoes: Origin of echoes and accuracy of derived winds. *J. Atmos. Ocean. Technol.*, **11**, 1184–1206, doi:10.1175/1520-0426(1994)011<1184:BLCARE>2.0.CO;2.

Wilson, J. W., and D. Reum, 1988: The Flare Echo: Reflectivity and velocity signature. *J. Atmos. Ocean. Technol.*, **5**, 197–205.

Wilson, J. W., N. A. Crook, C. K. Mueller, J. Sun, and M. Dixon, 1998: Nowcasting thunderstorms: A status report. *Bull. Am. Meteorol. Soc.*, **79**, 2079–2099, doi:10.1175/1520-0477(1998)079<2079:NTASR>2.0.CO;2.

Wilson, L., M. J. Manton, and S. T. Siems, 2013: Relationship between rainfall and weather regimes in south-eastern Queensland, Australia. *Int. J. Climatol.*, **33**, 979–991, doi:10.1002/joc.3484.

Witt, A., M. Eilts, and G. Stumpf, 1998: An enhanced hail detection algorithm for the WSR-88D. *Weather Forecast.*, **13**, 286–303, doi:10.1175/1520-0434(1998)013<0286:AEHDAF>2.0.CO;2.

Wurman, J., D. Dowell, Y. Richardson, P. Markowski, E. Rasmussen, D. Burgess, L. Wicker, and H. B. Bluestein, 2012: The Second Verification of the Origins of Rotation in Tornadoes Experiment: VORTEX2. *Bull. Am. Meteorol. Soc.*, **93**, 1147–1170, doi:10.1175/BAMS-D-11-00010.1.

Yeo, C., 2005: Severe thunderstorms in the Brisbane region and a relationship to the El Niño Southern Oscillation. *Aust. Meteorol. Mag.*, **54**, 197–202.

Ziegler, C. L., E. R. Mansell, J. M. Straka, D. R. MacGorman, and D. W. Burgess, 2010: The impact of spatial variations of low-level stability on the life cycle of a simulated supercell storm. *Mon. Weather Rev.*, **138**, 1738–1766, doi:10.1175/2009MWR3010.1.